Interim Report 69-1

AD

RCS OSD-1366

Research and Development Technical Report
ECOM 2-68 1-4

THE ENERGY BUDGET AT THE EARTH'S SURFACE: EFFECTS OF AIR TURBULENCE UPON GAS EXCHANGE FROM SOIL

Contribution by:

B. A. Kimball, E. R. Lemon

MICROCLIMATE INVESTIGATIONS
INTERIM REPORT 69-1

E. R. Lemon — Investigations Leader
U. S. DEPT. OF AGRICULTURE and
CORNELL UNIVERSITY

NOVEMBER 1969

OM
ELECTRONICS COMMAN
ICES LABORATORY
ARIZONA
ions, U. S. Department of Agriculture
Ithaca, New York 14850

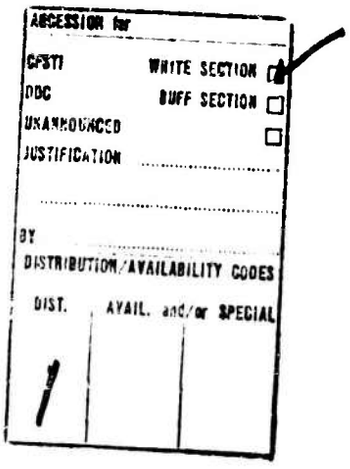

NOTICES

Citation of trade names and names of manufacturers in this report is not to be construed as official Government indorsement or approval of commercial products or services referenced.

The findings of this report are not to be construed as an official Department of Army position unless so designated by other authorized documents.

Destroy this report when it is no longer needed. Do not return it to the originator.

Technical Report ECOM 2-68I-4
November 1969

Reports Control Symbol
OSD - 1366

THE ENERGY BUDGET AT THE EARTH'S SURFACE:

EFFECTS OF AIR TURBULENCE UPON GAS EXCHANGE FROM SOIL

INTERIM REPORT 69-1

Cross Service Order 2 - 68
Task 1TO-61102-B53A-17

Prepared by

B. A. Kimball, E. R. Lemon

of

Northeast Branch
Soil and Water Conservation Research Division
Agricultural Research Service
U. S. Department of Agriculture
Ithaca, New York

Report No. 405

In Cooperation With

N. Y. State College of Agriculture
Cornell University
Ithaca, New York

Research Report No. 870

For

U. S. Army Electronics Command
Atmospheric Sciences Laboratory
Fort Huachuca, Arizona

PREFACE

This publication (Interim Report 69-1) forms the first part of two reports dealing with gas exchange from soil. Included here are pages 1-124 of the work while the second part (Interim Report 69-2) forms an appendix of pages 125-188. The latter is entitled "Basic Concepts of Spectral Analysis by Digital Means." We have chosen to make two reports because of the anticipated diversity of interest in them.

E. R. Lemon

TABLE OF CONTENTS

LIST OF TABLES

LIST OF ILLUSTRATIONS

INTRODUCTION

Both the evaporation rate from soil during the second stage of drying and the soil aeration status depend upon the rate at which soil gases are exchanged with the atmosphere. For many years, it has been generally believed that the most important mechanism determining the rate of soil gas exchange is molecular diffusion. However, the basis for such belief has not been experimental evidence; rather, it has been logical speculation. Since recent experimental evidence has indicated that a mass flow mechanism caused by turbulent air flow over the ground might also be important, this study was initiated to evaluate the effects of air turbulence upon soil gas exchange.

In Chapter I, field measurements of a liquid's evaporation rate from beneath surface coverings of soil and other porous media are described. The measurements were made using a new instrument, christened vapor exchange meter (VEM), which could be buried beneath the soil surface so that disturbance of air turbulence characteristics at the soil surface would be minimal.

It has been shown in laboratory studies that an oscillatory mass flow can cause an increase in mixing of soil gases. Since mass flows are caused by pressure gradients, measurements of natural pressure fluctuations at the soil surface, described in Chapter II, were made for various conditions. The pressure fluctuations were characterized using spectral analysis, a technique described in the Appendix, which is more familiar to meteorologists than to agronomists.

In order to be able to predict quantitatively the influence of air turbulence upon soil gas exchange, equations are needed which relate soil gas movement to air turbulence parameters. In Chapter III, two equations are derived from which an average velocity and displacement of mass flow can be calculated given the spectra of air pressure fluctuations obtained in Chapter II. Using the two equations and the results of previous workers, an attempt is made to calculate the total amount of gas movement which could be expected from both diffusion and mass flow.

Chapter I

MEASUREMENTS OF SOIL GAS EXCHANGE WITH AIR TURBULENCE

Soil aeration and the loss of water by evaporation in the later stages of drying are important processes in which gases are exchanged between the soil and the atmosphere. To understand fully soil aeration and evaporation, one must first understand the mechanisms by which this exchange occurs. Romell (1922) [as described by Keen (1931)] published the first study of these mechanisms. He calculated how much exchange could occur from wetting and drying of soil, from temperature gradients, from barometric pressure changes, from wind, and from diffusion. He concluded diffusion was the most important mechanism, and, although he had no direct measurements, his arguments appeared sound. Recently, however, evidence has appeared which suggests that air turbulence may also have an important influence, at least, under some conditions.

The possible importance of air turbulence is illustrated by the work of Hanks and Woodruff (1958) who observed that evaporation through soil, gravel, and straw mulches increased with wind velocity in their wind tunnel. Also, Holmes, Graecen, and Gurr (1960), using a wind tunnel, found that evaporation was affected by surface tilth (and, hence, from inference also by surface roughness and by the subsequent nature of air turbulence). Benoit and Kirkham (1963) observed an increase in evaporation rate when they increased the air movement over soil columns having a soil mulch. Evans, Kraner, and Schroeder (1962) state that a high wind (>313 cm/sec at a height of 168 cm) caused a decrease of about 10% in the Rn^{222} concentration at the 61 cm depth in the field. Their Rn^{222} flux

measurements from the soil surface were somewhat higher for unstable atmospheric conditions than for stable for the same concentration gradient below the surface, but they had few observations.

Although Pearson (1965) found no significant correlation of Rn^{222} flux with wind speed at 50 cm above the ground, he did observe a large increase in flux when he increased the air velocity inside his bottomless sampling box. Scotter, Thurtell, and Raats, (1967) found an increase in "dispersion" of gas in columns of soil and other porous media as they increased the velocity and displacement amplitude of sinusoidal gas flow in their columns. Also, the theoretical work of Covey (1965. Air movement and gaseous diffusion in the soil in relation to drainage: I. Physical principles. Talk presented before the Conference on Drainage Requirements of Crops, Weslaco, Texas, Feb. 24. Mimeograph copy.), Farrel, Greacen and Gurr (1966), and Scotter and Raats (1968, 1969) indicates that air turbulence can affect soil gas exchange, particularly at shallow depths and in materials with large pores. Thus, since there were several indications of turbulence effects in the literature, a re-examination of mechanisms of exchange from porous media was deemed necessary and was initiated.

Materials and Methods

To study the mechanisms of gas exchange from soil or other porous media, a vapor exchange meter (VEM) was built which could measure changes in the rate of soil gas exchange in the field as they occur with changes in the turbulence pattern above the soil. The VEM, shown schematically in Fig. 1.1, consisted of a two-chambered plate which could be buried beneath the soil surface. The upper chamber contained liquid heptane and the lower chamber contained two heater wires. When some of the heptane had evaporated, more liquid was drawn into the upper chamber from a tube to the outside. The outside end of the tube dipped into a little pail, and the evaporation rate of the heptane could be obtained by measuring the rate of weight loss from the pail. Evaporation from the pail itself was insignificant. Since the concentration of heptane vapor in the air above the soil could usually be assumed to be zero, the VEM was not affected by changes in the composition of the air above the soil. Since the plate was buried, the turbulence pattern above the soil was not affected, although there may have been some effects on gas movement within the soil. The VEM had a time response constant of about 15 sec, so the rate of heptane evaporation could be correlated against turbulence parameters obtained for time periods as short as one minute.

The plate for the VEM was made from a 91.5 cm length of 3.81 cm diameter, hard-drawn brass tubing which was softened by heating and shaped into a hollow, flattened "U" with a steel mold. The hollow inside the "U" held the heating wires. The liquid heptane chamber was formed by soldering across the top of the "U" a porous stainless steel strip (Haddam Manufacturing Co.), which was 4.45 cm wide, 0.152 cm thick,

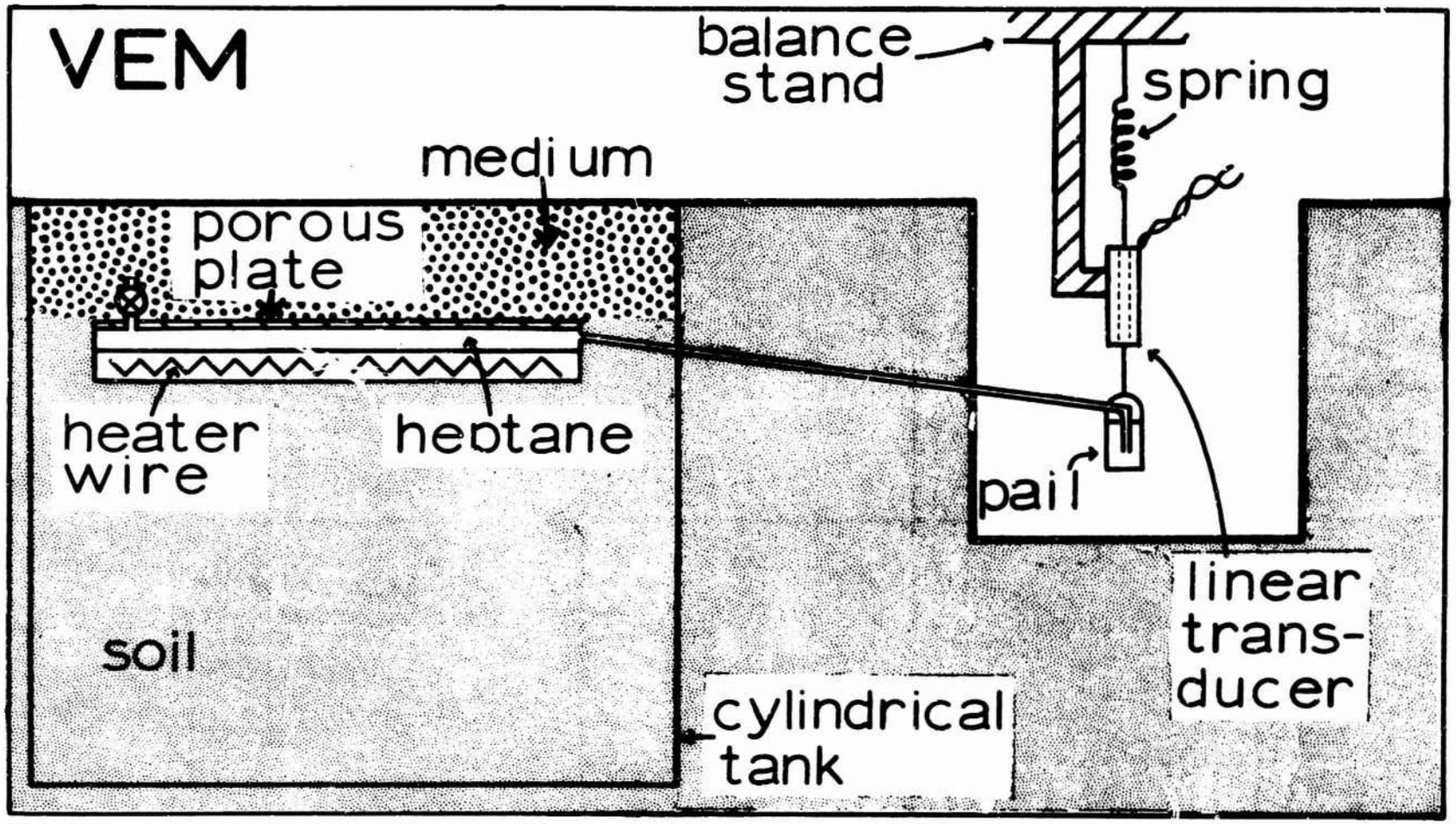

Figure 1.1 Schematic diagram of the VEM

25 micron pore size. The ends were sealed with brass strips; short lengths of 0.635 cm O.D. copper tubing soldered near the ends provided access to the internal chamber. Aluminum screen over the porous stainless steel provided an air gap between soil and the plate surface. Polyethylene tubing (0.635 cm O.D.) with short connecting lengths of teflon-lined rubber tubing (0.635 cm I.D.) was used to connect the heptane chamber to a small glass spout that dipped into the weighing pail. A valve system not shown in Fig. 1.1 permitted the plate to be switched from the pail to a large heptane supply reservoir. The plate would be switched to the reservoir when the pail was being refilled and when no evaporation runs were being made. The pail was weighed on a recording balance like the one described by Kunze and Peters (1964). A spring was connected to the top of the magnetic core of a linear displacement transducer, and the bottom of the core was connected to the pail. As the weight of the pail changed, the spring contracted or expanded, and the voltage from the transducer changed in proportion to the change in core displacement. The balance was placed in a small excavation about 150 cm from the plate to permit the pail to be below the plate surface and thus provide a slight capillary tension. To prevent the heptane evaporation rate from being dependent upon the rate at which the soil supplied heat to the surface, a temperature controller was used to supply a heating current proportional to the difference between the plate temperature and the soil temperature several cm away at the same depth. The temperatures were sensed by 9 thermocouples on the plate surface and 9 thermocouples in the soil. The temperatures of the plate could be maintained within 0.5°C of the soil temperature, except when the "soil" was coarse gravel or straw.

Heptane was chosen for the evaporating liquid in the VEM because it is insoluble in water, not toxic to handle, and not prohibitively expensive. From Handbook (1963) figures, the heptane vapor pressure under field temperatures was never more than 60 mm Hg. Thus, errors due to the mass flow effect of slow vapor molecules diffusing into faster counter-diffusing O_2 and N_2 molecules were not more than 3% according to the analysis of Evans (1952. Effect of combined pressure and concentration gradients on pressure flow through soils. Unpublished Ph.D. Thesis. Ames, Iowa, Iowa State University Library.). The density of heptane-saturated air is greater than normal air, however, so buoyancy effects had to be minimized. This was accomplished by burying vertically a large steel cylinder (180 cm diameter x 250 cm deep) in the experimental field with the VEM plate always in or on the soil near the open top of the cylindrical tank. Except when a coarse gravel was being studied, heptane evaporation measurements were not started until the soil air in the cylinder below the plate had had time to saturate with heptane vapor. Plaster of Paris disks cemented over small access holes in the bottom of the tank permitted water to move in and out of the tank.

Air turbulence over the ground was measured with two instruments. A capacitive manometer-type absolute pressure transducer (Datametrics Corp., Model 511A) sensed the air pressure at the soil surface directly over the VEM plate through a 120 cm long by 0.635 cm O.D. copper tube. Mean wind was measured at a height of 270 cm or 475 cm on a mast located about 10 m from the VEM plate by cup anemometers.

The measurements were taken at field site in Ellis Hollow near Ithaca, New York. During the first stage in data acquisition, the VEM plate was

placed over the Chenango silt loam in the large tank and filled with heptane. The entire area of the tank was then covered with soil or one of several other porous media. A "run" would be made by recording the voltage output from the VEM, the VEM plate thermocouples, and the absolute pressure transducer with a multi-channel data logger. The voltages with accompanying clock data were printed on paper tape at 1 sec intervals. The counters for the cup anemometers were automatically photographed at 1 min intervals. Runs usually lasted about 2 hr including interruptions to refill the VEM pail with heptane. The runs were made for each porous medium under both unstable daytime and stable nighttime conditions so that a range of natural turbulent conditions would be observed. Between runs the plate was allowed to evaporate heptane continuously from the supply reservoir. A fan, which was directed toward the porous media surface over the VEM plate, provided particularly high levels of turbulence during portions of each run. The permeability of each porous medium was measured by filling a 7.7 cm diameter by 17.0 cm long copper tube with the porous medium and then measuring the pressure drop across the tube with a differential pressure transducer (Datametrics Corp., Model 511), as N_2 gas was passed through the tube. The volume flow rate was measured using a stop watch to determine the rate of movement of a soap film through a second glass tube in series with the sample tube. The high sensitivity of the transducer permitted differential pressures of only a few μbar to be used.

The flux and accompanying data were analyzed using consecutive 1 min intervals for averaging periods. An average heptane flux for a particular minute was computed from the weight of heptane lost from the pail during

the minute. Plate temperature was taken as the average of the temperature at the end and beginning of each minute. The plate temperature measurement was used to adjust the heptane flux measurements to a standard temperature so that the effect of having a higher vapor pressure at higher temperature would not be confused with turbulence effects on the flux measurements. The change in plate temperature from the beginning to the end of each minute was also computed in order to correct the flux measurements for the error due to differences in thermal expansion between liquid heptane and the solid plate and tubing. The root mean square (rms) amplitude of pressure fluctuation was taken as the standard deviation of the pressure measurements for each minute after being corrected for linear trend. A rms frequency of pressure oscillation was also computed by dividing the standard deviation of numerical derivative of pressure by the rms amplitude. Mean wind speed was computed from the change in count.

Multiple regressions were run with heptane evaporation flux as the dependent variable, and VEM plate temperature change, average VEM plate temperature, wind speed, rms amplitude of pressure oscillation, and rms frequency of fluctuation as independent variables.

Results and Discussion

In Fig. 1.2, 1.3, 1.4, 1.5, 1.6, and 1.7 are plotted the values of heptane flux against the rms amplitude of pressure fluctuation which were obtained when the VEM plate rested on silt loam and was covered with 2 cm of straw, coarse gravel, fine gravel, very coarse sand, medium sand, and Chenango silt loam. Some physical properties of the media are listed in Table 1.1. All of the flux values in the graphs have been corrected to zero change in temperature and adjusted to a 20°C VEM plate temperature from the partial regression coefficient for flux on these two variables. As indicated on the graphs, the data were obtained under nighttime stable and daytime unstable atmospheric conditions, with and without a fan. In spite of a large amount of scatter in the data, it is apparent that the pressure fluctuations definitely affected the heptane evaporation rate, and that the effect became less pronounced as particle size decreased, particularly when going from medium sand to silt loam. The partial regression coefficients listed in Table 1.2 substantiate these conclusions. All are significantly different from zero, and there is somewhat of a decrease with particle size particularly when going from medium sand to silt loam. The regression lines along with their 5% standard error confidence limits are also plotted on the graphs.

If attention is concentrated only on those points obtained from natural turbulence using no fan, the effects of turbulence are far less apparent. The statistics given in Table 1.3 show that the regression coefficients for heptane flux on pressure amplitude were significantly different from zero only when the plate was covered with straw and coarse

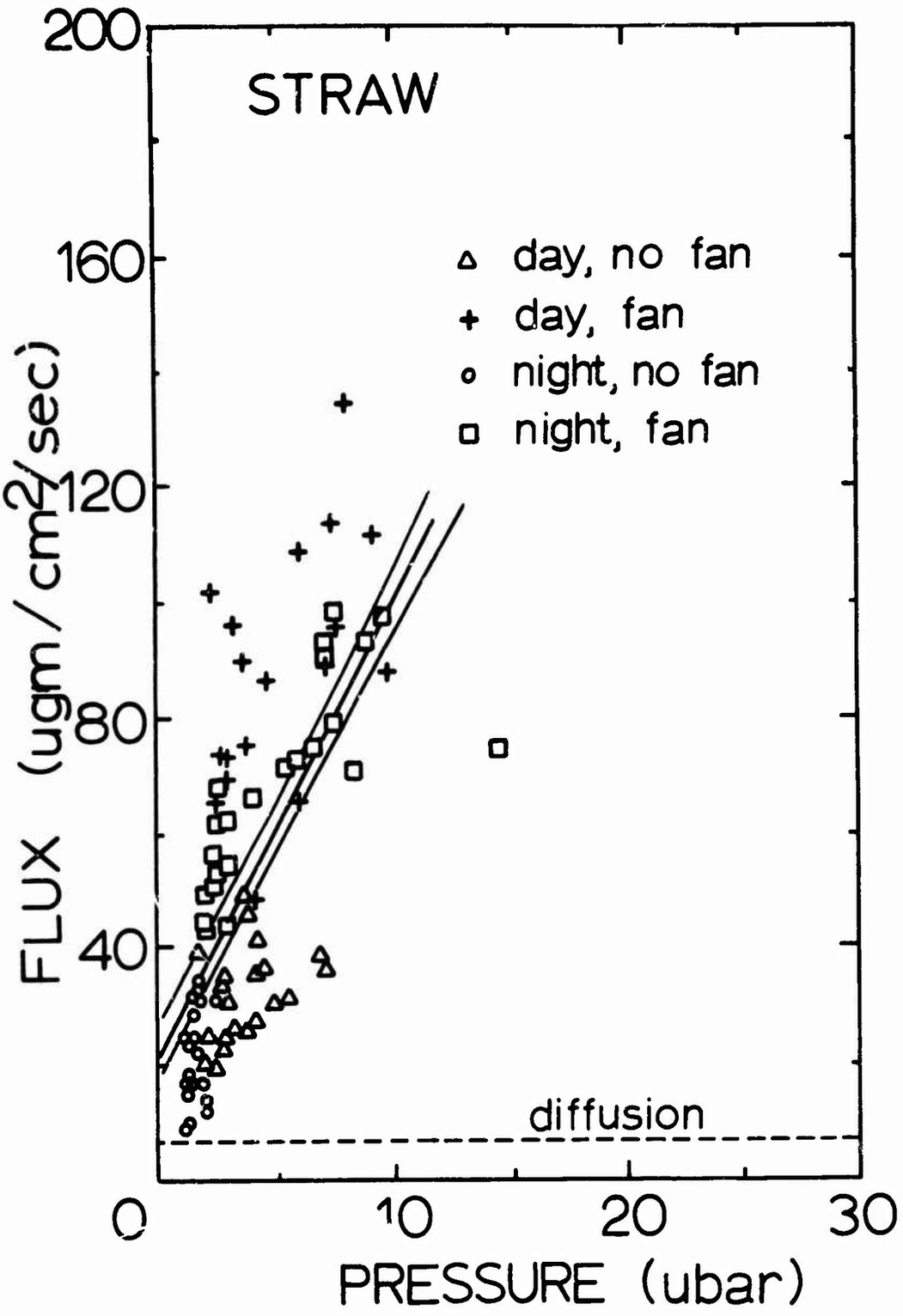

Figure 1.2 Flux of heptane evaporation from beneath 2 cm of straw plotted against root mean square pressure fluctuation for 1 min time periods

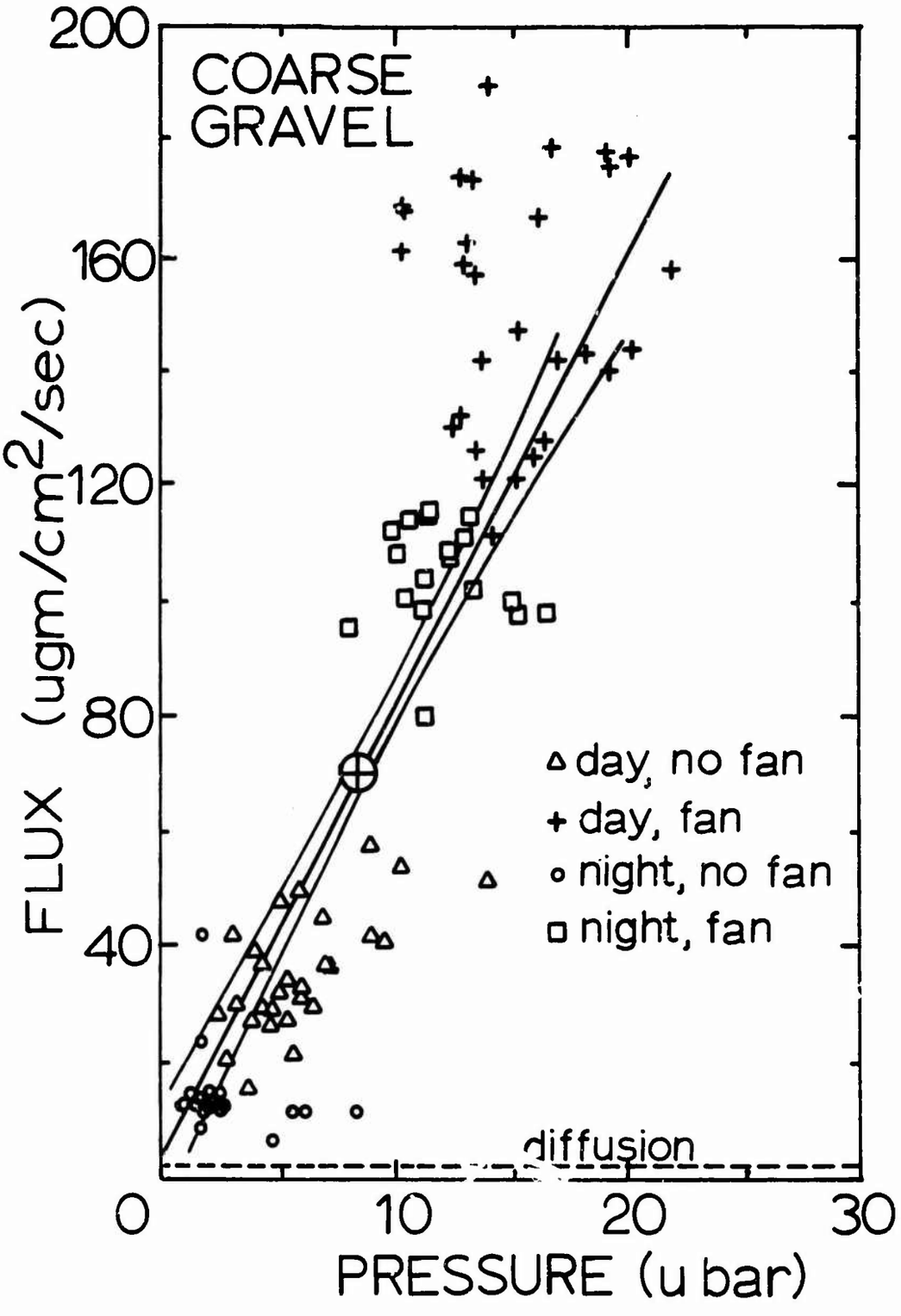

Figure 1.3 Flux of heptane evaporation from beneath 2 cm of coarse gravel plotted against root mean square pressure fluctuation for 1 min time periods

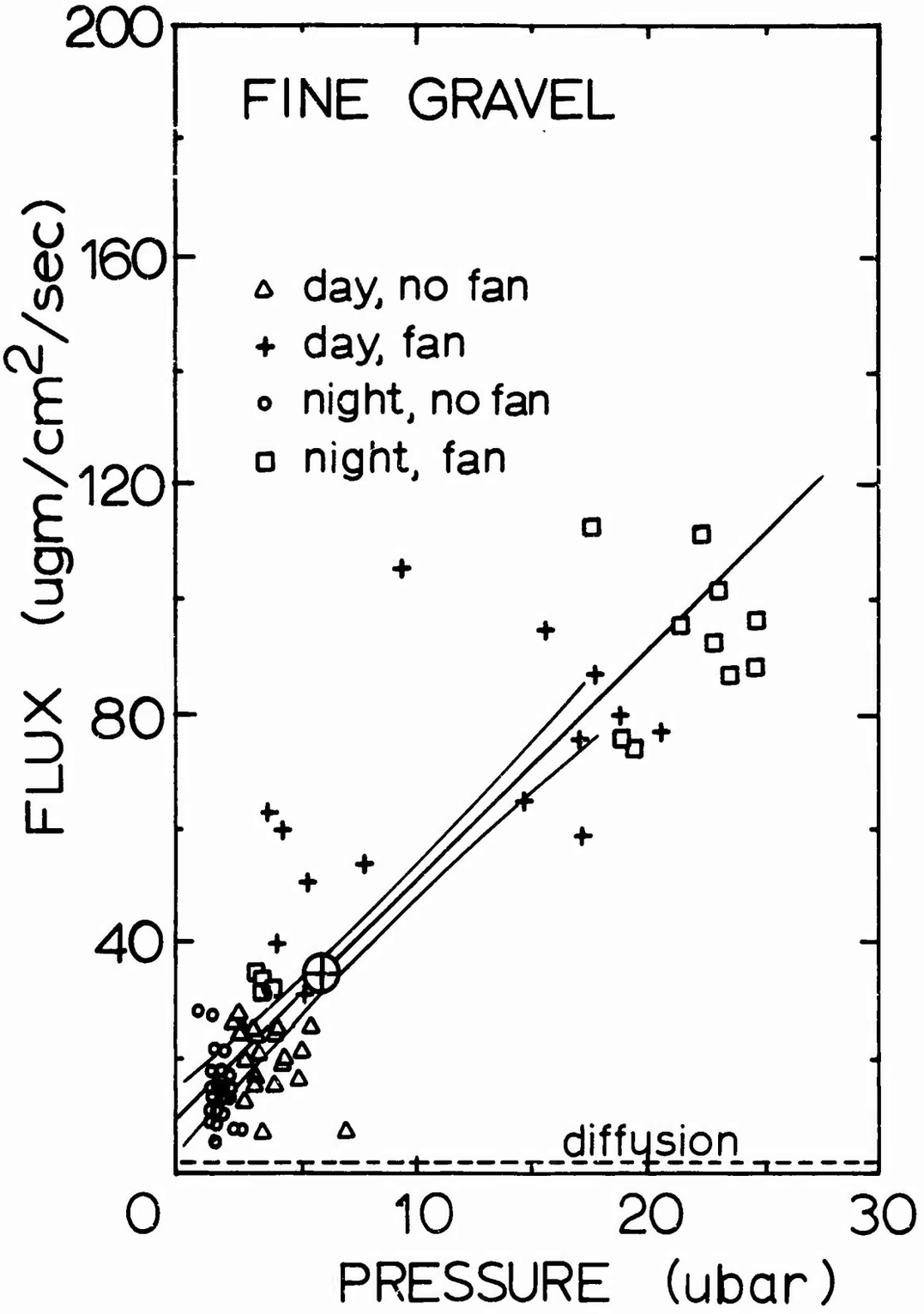

Figure 1.4 Flux of heptane evaporation from beneath 2 cm of fine gravel plotted against root mean square pressure fluctuation for 1 min time periods

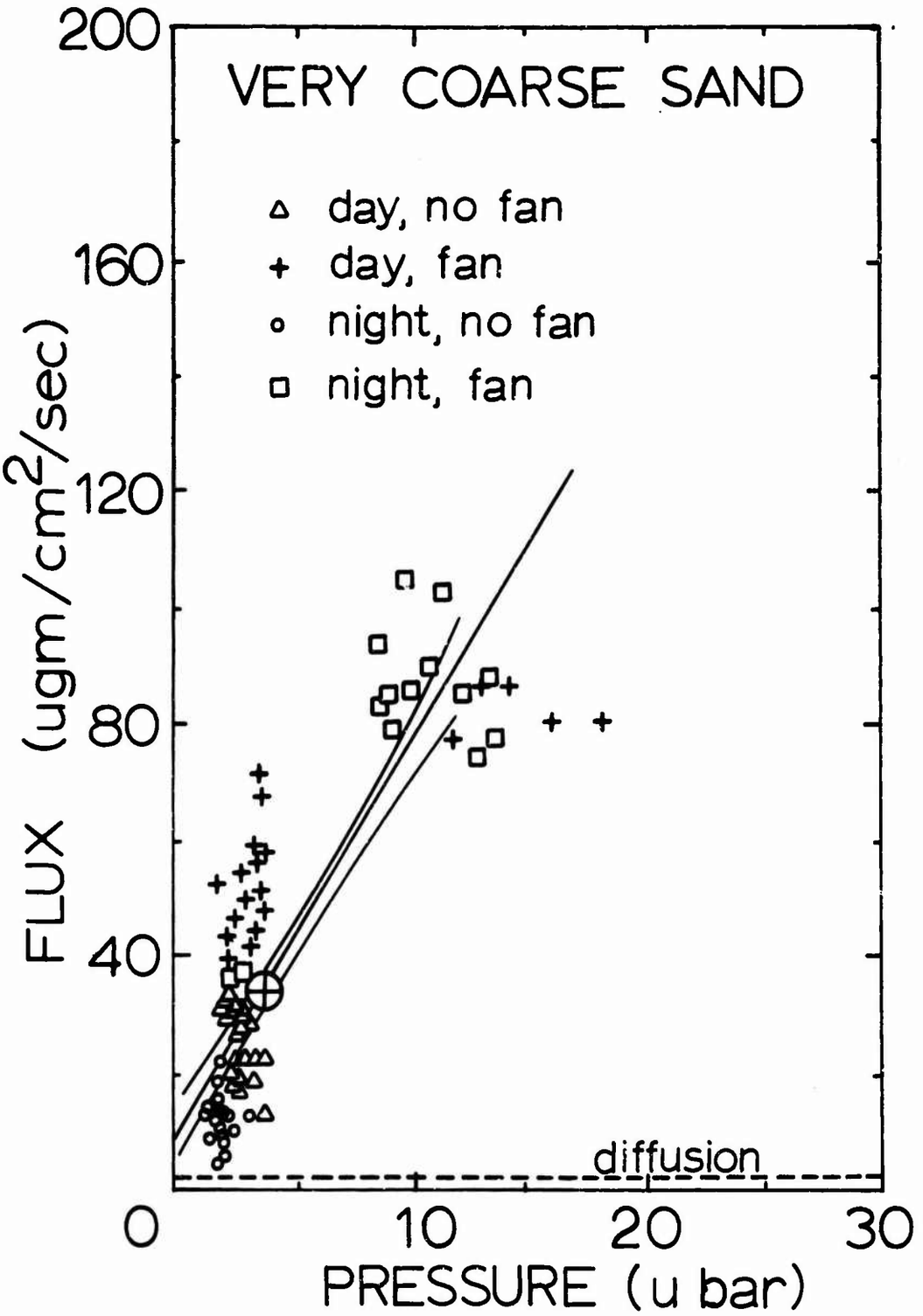

Figure 1.5 Flux of heptane evaporation from beneath 2 cm of very coarse sand plotted against root mean square pressure fluctuation for 1 min time periods

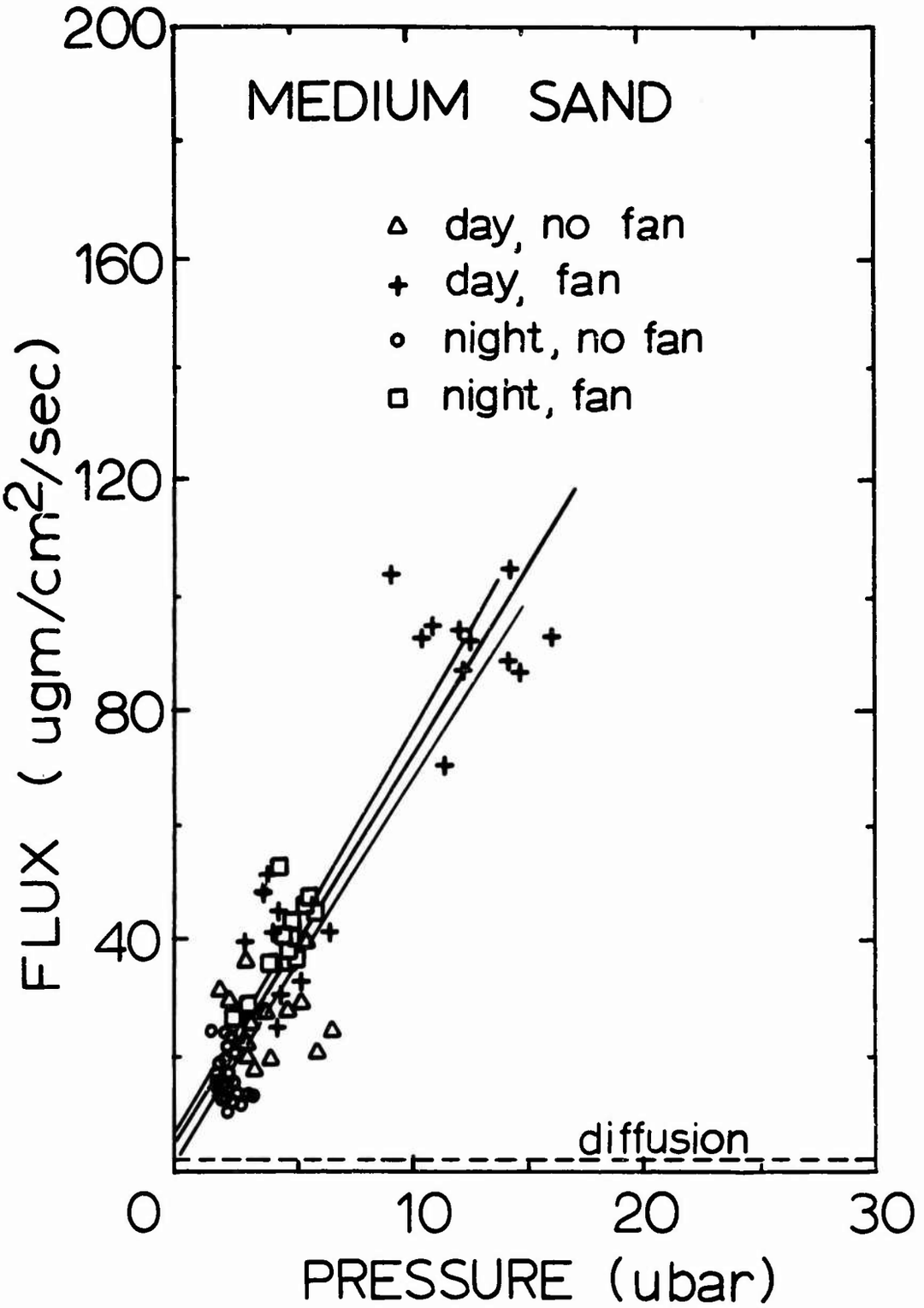

Figure 1.6 Flux of heptane evaporation from beneath 2 cm of medium sand plotted against root mean square pressure fluctuation for 1 min time periods

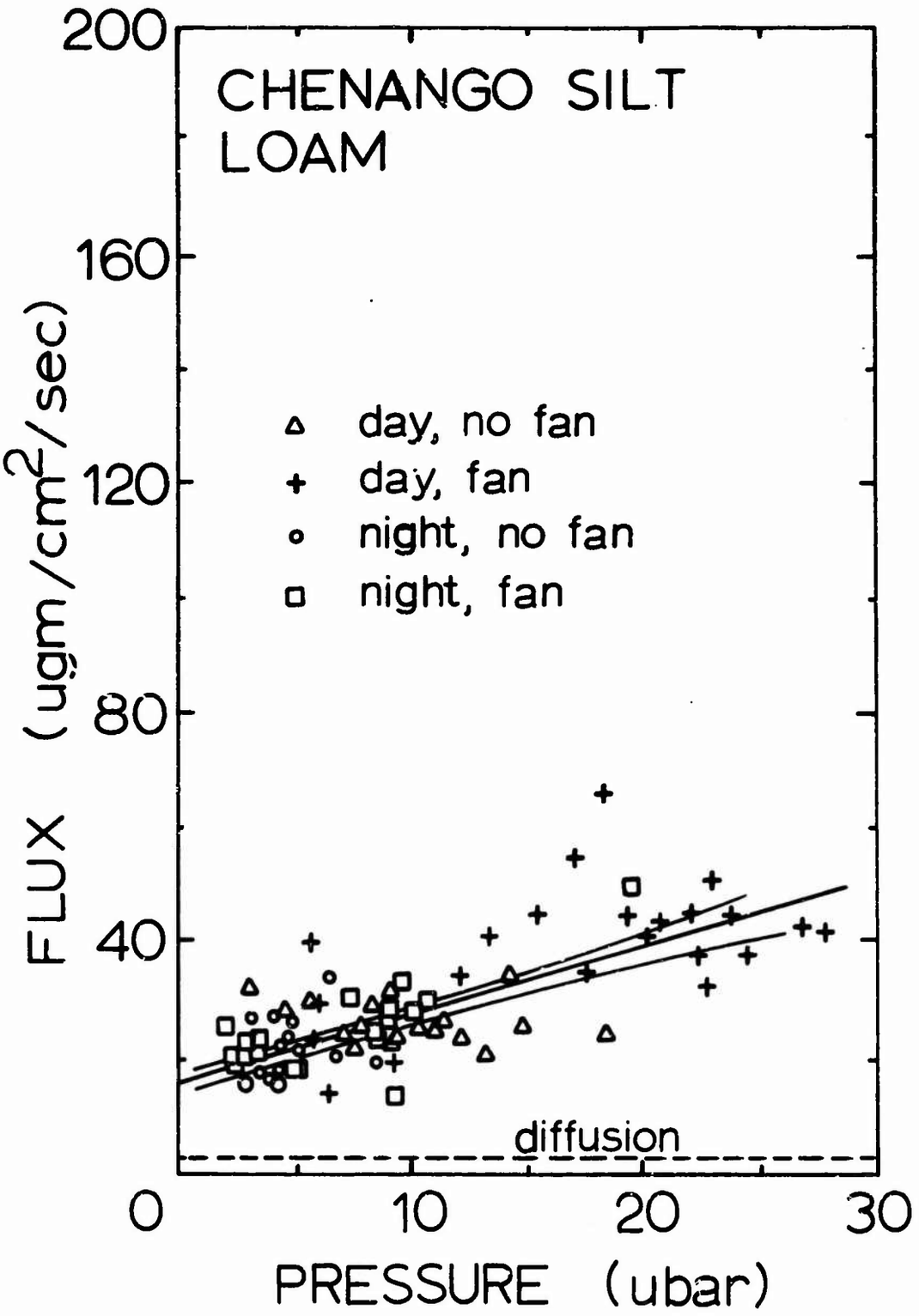

Figure 1.7 Flux of heptane evapcration from beneath 2 cm of Chenango silt loam plotted against root mean square pressure fluctuation for 1 min time periods

Table 1.1 Properties of the porous media used in the VEM experiments

Medium	Property			
	Permeability (μ^2)	Particle diameter* (cm)	Air porosity+	Moisture content (%)
Straw	540,000		0.97	- dry
Coarse gravel	320,000	1.8	0.36	- dry
Fine gravel	67,000	0.90	0.33	- dry
Very coarse sand	2,800	0.11	0.39	2.0
Medium sand	1,600	0.030	0.40	2.3
Chenango silt loam	10,000		0.42	4.5
Coarse white sand	4,200	0.10	0.40	0.2

* Taken from sieve size at which 50% of sample was retained

+ Particle density assumed to be 2.65 gm/cm^2 except for straw assumed to be 0.8 gm/cm^3

Table 1.2 Regression statistics for heptane flux on rms amplitude of pressure fluctuation when fan was on from multiple regressions of heptane flux on rms amplitude, VEM plate temperature, and change in VEM plate temperature for several porous media

	Porous material					
Statistic+	Straw	Coarse gravel	Fine gravel	Very coarse sand	Medium sand	Chenango silt loam
Intercept‡	18.8	4.7	11.6	12.5	8.7	16.3
Regression coefficient	8.39	8.04	3.91	5.9	6.42	1.09
SE of Reg. coef.	0.87	0.50	0.24	0.42	0.31	0.12
T value	9.68**	15.9**	16.5**	14.1**	20.5**	9.29**
Multiple corr. coef.	0.80	0.85	0.91	0.87	0.90	0.74

+ Heptane flux in $\mu gm/cm^2/sec$ and rms pressure amplitude in μbar

‡ Adjusted to 20°C from regression on VEM plate temperature

** Significant at 1%

Table 1.3 Regression statistics for heptane flux on rms amplitude of pressure fluctuation from multiple regressions of heptane flux on rms amplitude, VEM plate temperature, and change in VEM plate temperature for several porous media

	Porous material					
Statistic+	Straw	Coarse gravel	Fine gravel	Very coarse sand	Medium sand	Chenango silt loam
Intercept‡	10.1	13.4	13.8	6.8	9.5	17.8
Regression coefficient	2.06	1.64	-0.82	1.23	0.205	0.179
SE of reg. coef.	0.63	0.36	0.78	1.13	0.61	0.18
T value	3.26**	4.52**	-1.05	1.09	0.34	0.99
Multiple corr. coef.	0.94	0.95	0.72	0.77	0.65	0.49

+ Heptane flux in $\mu gm/cm^2/sec$ and rms pressure amplitude in μbar

‡ Adjusted to 20°C from regression on VEM plate temperature

** Significant at 1.0%

gravel, and that the natural pressure fluctuations had no significant effect on evaporation from the other media.

In Figures 1.8, 1.9, 1.10, 1.11, 1.12 and 1.13, the heptane flux is plotted against wind speed for times when the fan was not on, again adjusted to zero temperature change and to 20°C. The statistics in Table 1.4 show that wind had significant effects on heptane evaporation through straw and coarse gravel and also through very coarse sand. However, the range of wind speeds was not very large when the data with very coarse sand were taken. The correlation of rms pressure amplitude with wind speed was about 0.65, thus indicative that the two parameters were not equivalent. However, the regressions in Table 1.3 and Table 1.4 were quite similar. Both indicate little influence of natural air turbulence upon gas exchange through media of small particle size. They contrast with the regressions in Table 1.2 which show that air turbulence caused by a fan can significantly influence gas exchange through media whose particle size is as small as silt loam.

The effects of depth of one porous medium upon the regression of heptane flux on wind speed is indicated in Table 1.5. The regression coefficient for the 8 cm depth is much smaller than those for the 1 and 2 cm depths, but the wind may still be having an effect since the T value indicates that the null hypothesis cannot be completely accepted.

One can conclude from the data presented that air turbulence can indeed affect heptane evaporation at shallow depths when the particle size of the material is large enough. The scatter of the data, however, prevents one from concluding that natural air turbulence has no effect on gas exchange in fine textured media. Since the effects of air turbulence on gas exchange did decrease with pore size, and since the pore sizes in soils containing enough water to support plant growth are much smaller

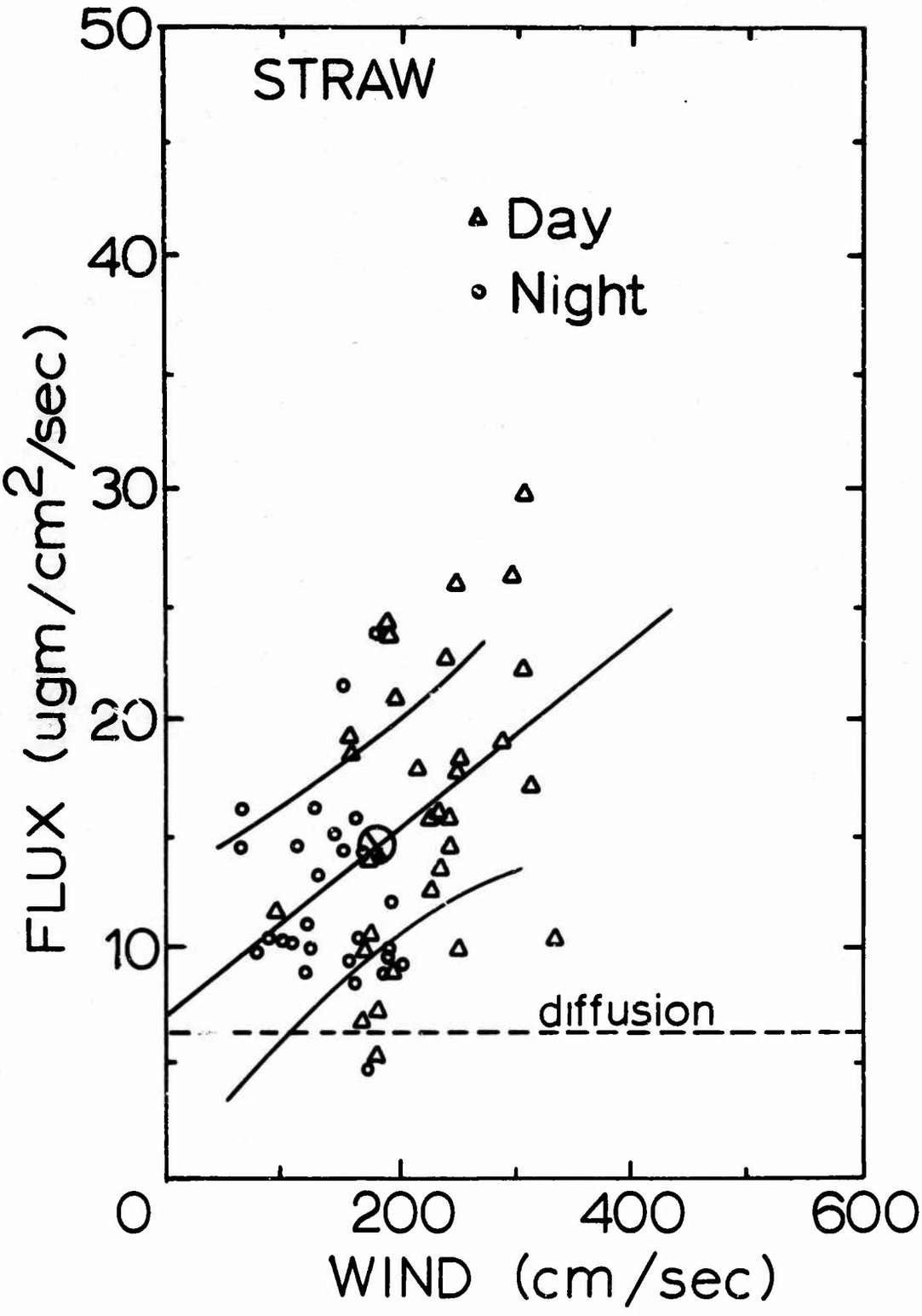

Figure 1.8 Flux of heptane evaporation from beneath 2 cm of straw plotted against mean wind speed for 1 min time periods

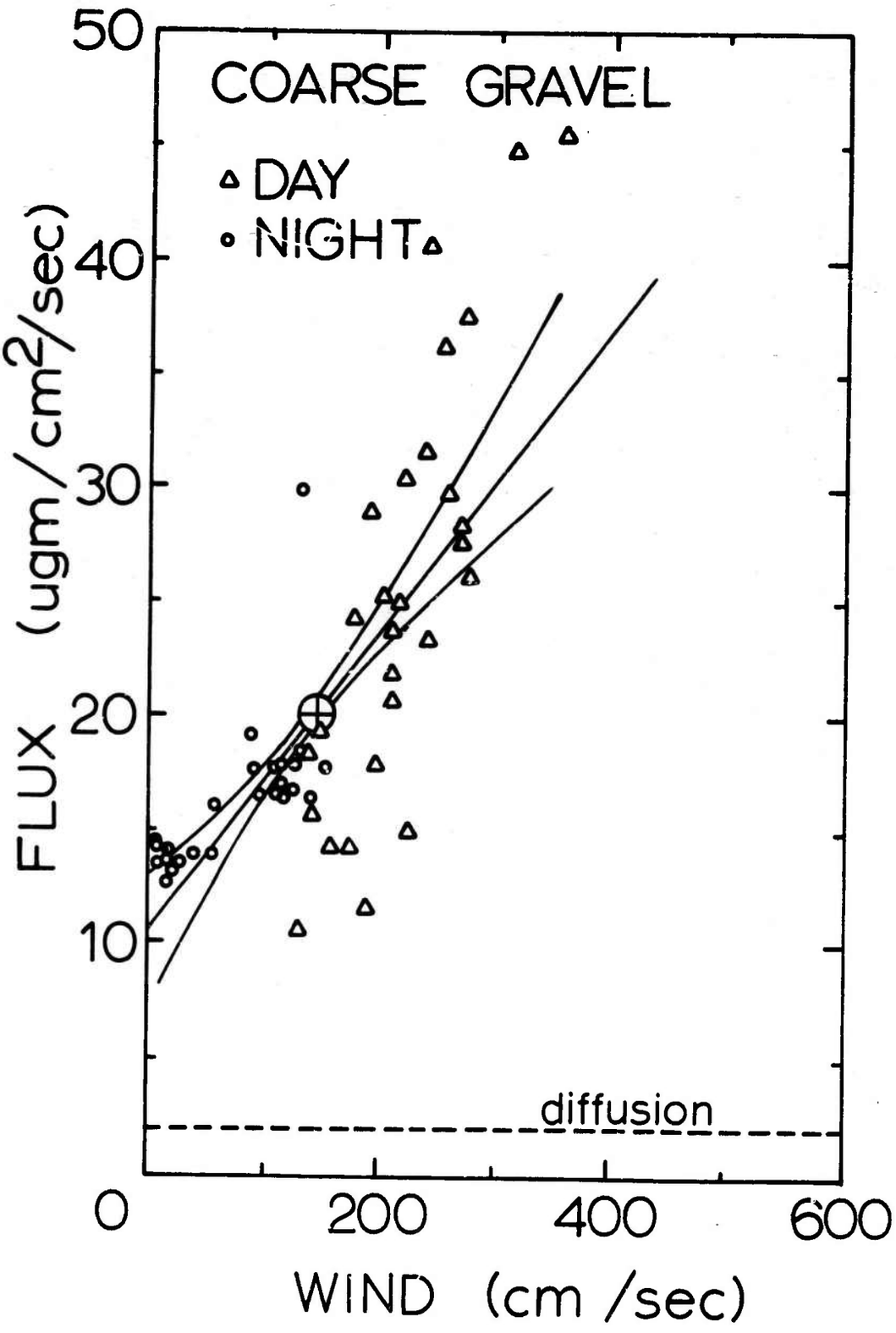

Figure 1.9 Flux of heptane evaporation from beneath 2 cm of coarse gravel plotted against mean wind speed for 1 min time periods

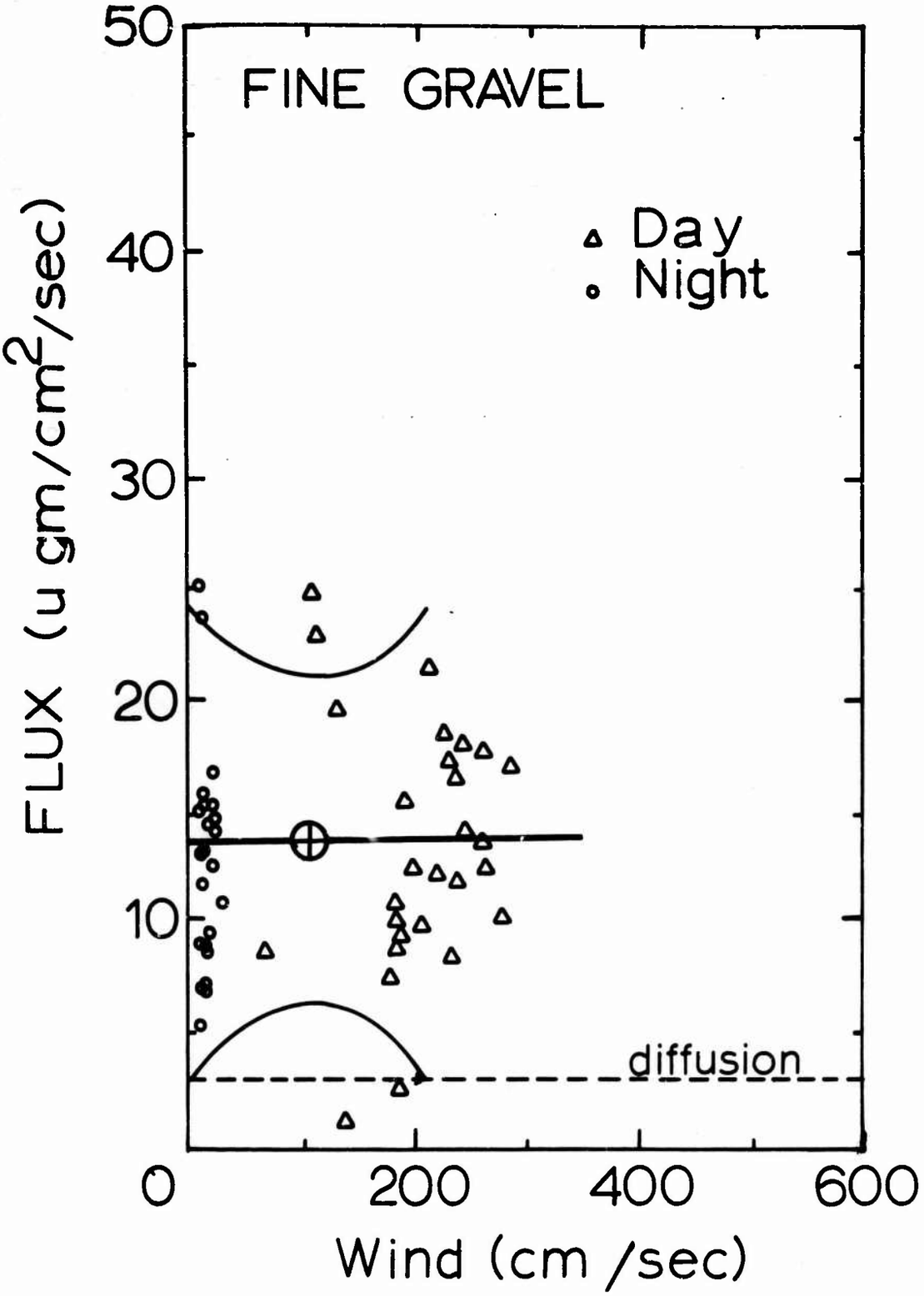

Figure 1.10 Flux of heptane evaporation from beneath 2 cm of fine gravel plotted against mean wind speed for 1 min time periods

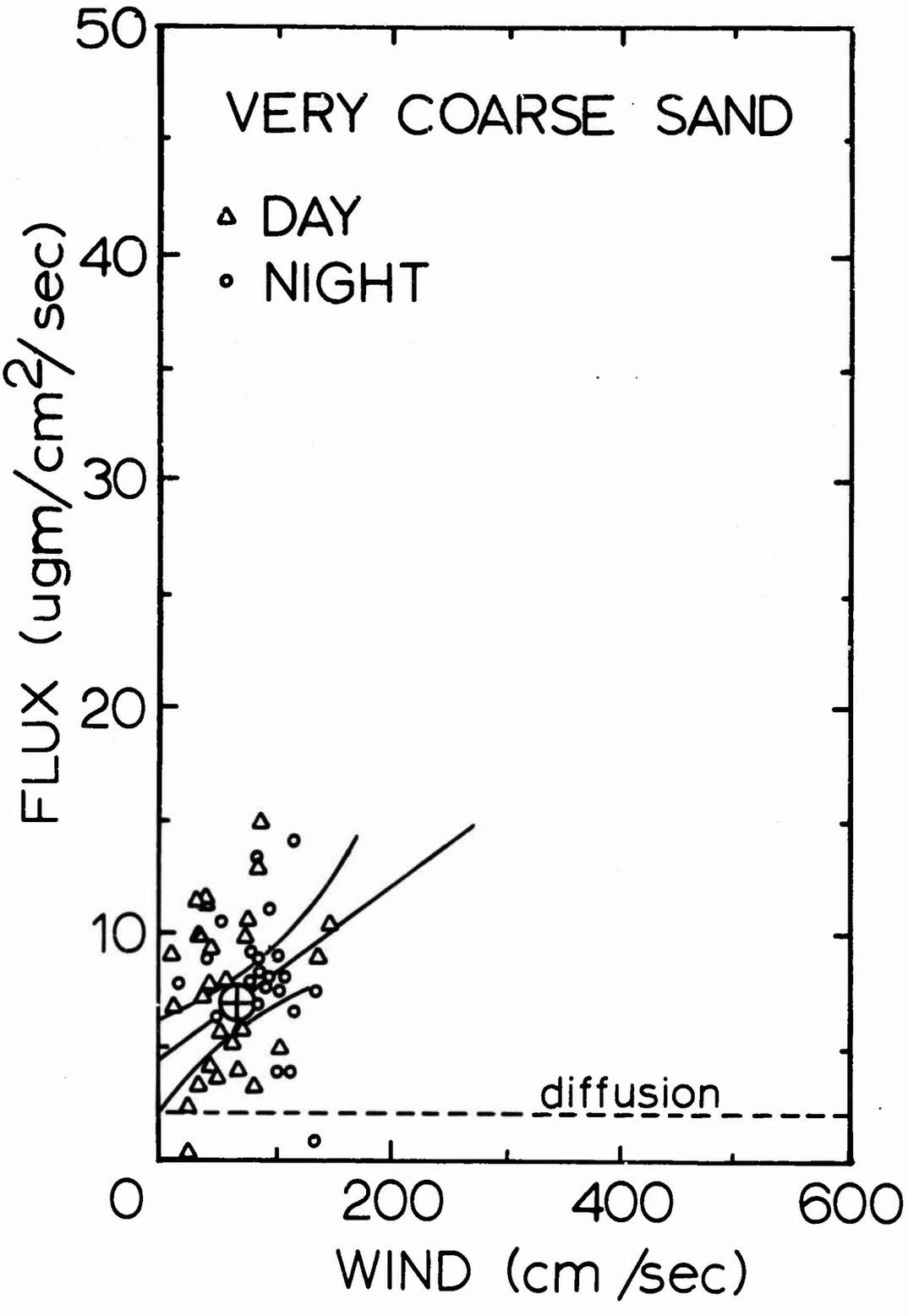

Figure 1.11 Flux of heptane evaporation from beneath 2 cm of very coarse sand plotted against mean wind speed for 1 min time periods

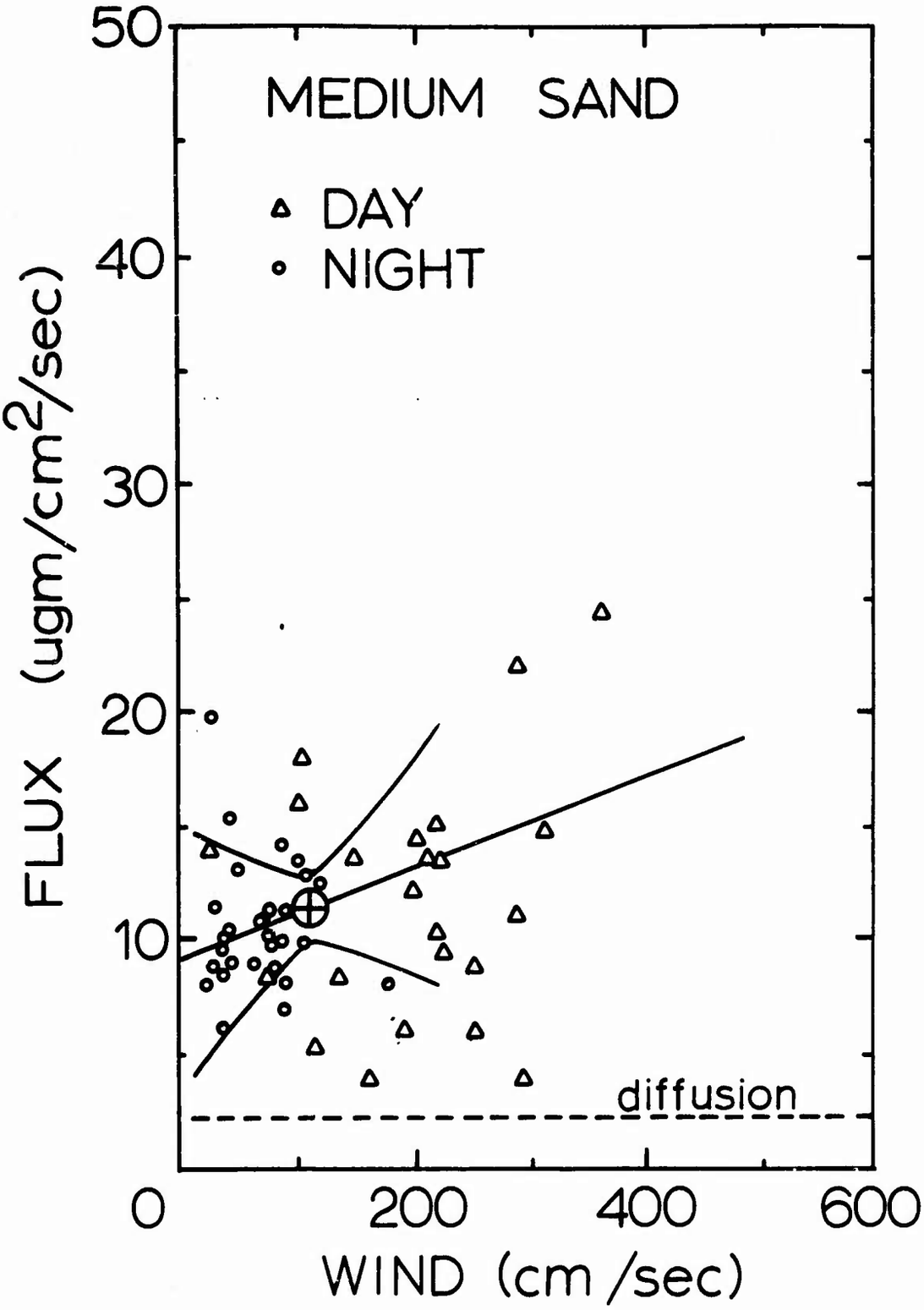

Figure 1.12 Flux of heptane evaporation from beneath 2 cm of medium sand plotted against mean wind speed for 1 min time periods

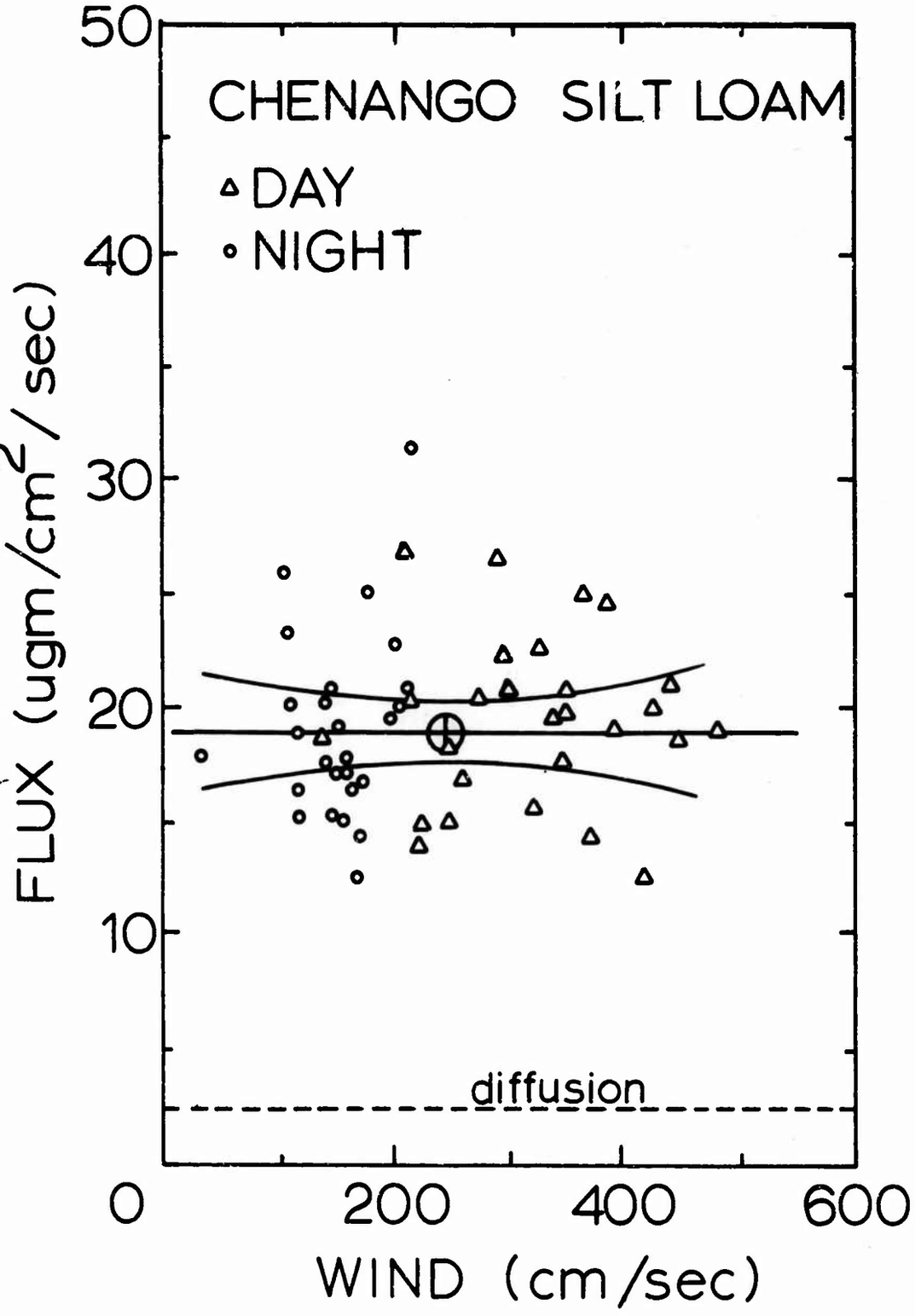

Figure 1.13 Flux of heptane evaporation from beneath 2 cm of Chenango silt loam plotted against mean wind speed for 1 min time periods

Table 1.4 Regression statistics for heptane flux on wind speed from multiple regressions of heptane flux on wind speed, VEM plate temperature, and change in VEM plate temperature for several porous media

	Porous material					
Statistic+	Straw	Coarse gravel	Fine gravel	Very coarse sand	Medium sand	Chenango silt loam
Intercept‡	7.5	10.5	12.8	4.7	9.5	17.5
Regression coefficient	0.0355	0.0713	0.00100	0.0362	0.0103	0.0688
SE of reg. coef.	0.0154	0.0111	0.0133	0.0158	0.00988	0.00652
T value	2.30*	6.44**	0.08	2.28**	1.05	1.06
Multiple corr. coef.	0.93	0.96	0.71	0.79	0.66	0.49

+ Heptane flux in $\mu gm/cm^2/sec$ and wind in cm/sec

‡ Adjusted to 20°C from regression on VEM plate temperature

* Significant at 5%

** Significant at 1%

Table 1.5 Regression statistics for heptane flux on wind speed from multiple regressions of heptane flux on wind speed, VEM plate temperature, and change in VEM plate temperatures for several depths of coarse white sand

	Depth (cm)			
Statistic+	1	2	4	8
Intercept‡	7.5	5.0	4.7	4. 5
Regression coefficient	0.00627	0.00665	0.00211	0.00058
SE of reg. coef.	0.00388	0.00182	0.00262	0.00040
T value	1.62*	3.65**	0.807	1.44*
Multiple corr. coef.	0.61	0.68	0.32	0.50

+ Heptane flux in $gm/cm^2/sec$ and wind speed in cm/sec

‡ Adjusted to 27°C from regression on VEM plate temperature

* Significant at 10%

** Significant at 1%

than the materials used in this study, it seems likely that Romell (1922) was correct in his conclusion that diffusion is the main process contributing to soil aeration. Nonetheless, air turbulence definitely contributes to evaporation of water through coarse textured mulches and probably also through very shallow depths of soils during the second stage of drying. In regions which have high wind speeds, the effects of natural air turbulence probably would be larger and more like the effects of the fan used in the study because winds in Ellis Hollow, New York, are comparatively light.

The reasons the data are so scattered in this study are unknown. The multiple correlation coefficients given in Tables 1.3 and 1.4 for natural turbulence show that about 95% of the variance in heptane flux through corase material was explained by a regression on change in plate temperature, average plate temperature, wind or air pressure fluctuation amplitude, but only about 50% for silt loam. No significant effects of the frequency of fluctuation were found for natural turbulence, although frequency of fluctuation when the fan was on had significant effects on all media.

The intercepts for the regression lines also are all substantially larger than predicted by molecular diffusion. Using Wesseling's (1962) linear equation relating diffusion coefficient to soil porosity and inferring the vapor pressure at the plate surface from plate temperature (Handbook, 1963), diffusion fluxes were calculated, and they are plotted in Fig. 1.2 - 1.13. The value of this computed diffusion flux is in error no more than 60%. This error comes from possible errors in a) Wesseling's relationship, b) the vapor pressure curve, c) the measured porosity, and d) the measured soil depth. The flux at the intercept thus must be due to something other than diffusion.

Since most of the data points near the intercept for very low wind speed and pressure amplitude were obtained at night, the possibility exists that nighttime thermal gradients were causing mixing of the soil air. Since the soil temperature at a depth of 2 cm was 5°C cooler than the temperature at 7 cm every night data was obtained, cooler, heavier air was over warmer, lighter air. Elder (1967) has studied convection of heat in a porous medium heated from below, and his results apply here. Elder found that there was no contribution by convection to heat transfer when the Rayleigh number was less than 40. The Rayleigh number is given by

$$A = \frac{k\gamma g \Delta T H \rho^2 c}{K_m \mu}$$

where

H = thickness of material (2 cm)

k = permeability (10^{-2} cm^2)

γ = coefficient of cubical expansion (0.003670/°C)

g = acceleration of gravity (980 cm/sec^2)

ΔT = temperature difference (10°C)

ρ = density of fluid (0.0011 gm/cm^3)

c = heat capacity of fluid (0.2404 cal/gm°C)

K_m = thermal conductivity of saturated medium (0.001 (cal/cm^2/sec)/°C/cm))

μ = viscosity of fluid (1.8×10^{-4} poise)

Assuming very large values for k and ΔT, and obtaining the values shown in parenthesis for the other variables from the Handbook (1963),

the A for a thickness of 2 cm is 1.60. This is much below 40 so one must conclude there was no transfer of heat by convection. If there was no convection, there was no mass flow of air due to a thermal gradient and consequently no mixing of the soil air beyond diffusion due to a thermal gradient either.

It may be possible that buoyancy effects of heavy heptane vapor could have caused the scatter and the flux intercept values to be so much larger than diffusion, but it seems unlikely. Since the heptane vapor is heavier than air, one would presume that it would settle to the bottom of the tank until the tank became nearly saturated. Since the vapor is heavy, the air in the tank should be quite stable. Assuming a low flux rate of 10 $\mu gm/cm^2/sec$ from the plate, and not counting the rather liberal addition of heptane to the tank from spillage when the plate was filled, 56 hours would be required to fill the tank with saturated heptane vapor. Only with the coarse gravel were measurements taken less than this amount of time after filling. The data for the Chenango silt loam were obtained after the plate had been evaporating almost continuously for 10 days. These data show the highest, and not the lowest, flux of heptane at low wind speeds, so it is improbable that the high flux rates at zero wind were caused by a settling of heptane vapor down into the soil.

It is also puzzling why the permeability values given in Table 1.1 are not more closely related to particle size, and also why the flux regression coefficients are more closely related to the particle size than to the permeability measurements. Since in the permeability determinations, the measurements of volume flow rate and pressure drop across soil columns were accurate and precise, the permeability values should

be quite reliable. However, it was necessary to transfer the porous material from its experimental position over the VEM plate and pack it in the column so the difference could be due to the differences in bulk density of the material over the VEM plate and in the permeability column.

Summary

A VEM(vapor exchange meter) was built which could measure the exchange of a gas between soil or other porous medium and the atmosphere. The device measures the rate of evaporation of liquid heptane from a porous stainless steel plate buried beneath the surface of the porous medium. Natural air turbulence as indicated by both mean wind speed and root mean square air pressure fluctuations significantly affected the heptane evaporation rate through 2 cm of straw and coarse gravel but not through fine gravel, medium sand, or Chenango silt loam. The regression coefficients for wind decreased from 0.0713 to 0.00688 ($\mu gm/cm^2/sec$)/(cm/sec) with a decrease in particle size from that of the coarse gravel to that of the Chenango silt loam. When a fan was used to provide higher turbulence levels than the comparatively low turbulence level in Ellis Hollow, New York, the rms air pressure fluctuations significantly increased heptane evaporation through 2 cm of all of the porous media tested. Increasing depth from 1 to 8 cm in coarse sand caused a decrease from 0.00627 to 0.00058 in the regression coefficient for wind speed. It is inferred from the data that soil aeration is mostly a diffusive process, as has been thought previously, but that natural air turbulence can significantly increase the transport of water vapor through coarse mu[illegible]nes and through very shallow depths of soil. However, heptane flux values are quite scattered and are larger than those predicted from diffusion theory even at zero levels of turbulence. Neither the magnitude nor the scatter are fully explained.

Literature Cited

Benoit, G. R. and Kirkham, D. 1963. The effect of soil surface conditions on evaporation of water. Soil Sci. Soc. Amer. Proc. 27:495-498.

Elder, J. W. 1967. Steady free convection in a porous medium heated from below. J. Fluid Mech. 27:29-48.

Evans, R. D., Kraner, H. W., and Schroeder, G. L. 1962. On site Radon in surface soils - Project Vela, Final report AFTAC Project No. Vela T/2031/S/OSR, Edgerton, Germeshausen, and Grier, Inc., Boston, 93 pp.

Farrel, D. A., Greacen, E. L., and Gurr, C. G. 1966. Vapor transfer in soil due to air turbulence, Soil Sci. 102:305-313.

Handbook of Chemistry and Physics. 1963. 44th edition, Chemical Rubber Publishing Co., Cleveland, Ohio, 3604 pp.

Hanks, R. J. and Woodruff, N. P. 1958. Influence of wind on water vapor transfer through soil, gravel, and straw mulches. Soil Science 86:160-164.

Holmes, J. W., Greacen, E. L., and Gurr, C. G. 1960. The evaporation of water from bare soils with different tilths. Trans. Int. Congr. Soil Sci., 7th Congr. Madison 1:188-194.

Keen, B. A. 1931. The Physical Properties of Soil. Longmans, Green and Co., New York, 380 pp.

Kunze, R. J. and Peters, D. B. 1964. A recording balance for measuring moisture flow in soil. Soil Sci. Soc. Amer. Proc. 28:130.

Pearson, J. E. 1965. Radon-222: A study of its emanation from soil, source strength, and use as a tracer. Final Res. Rept. Dept. of General Engineering, Univ. of Illinois, Urbana, Ill. 73 pp.

Romell, L. G. 1922. Luftvaxlingen i marken s. ekol. faktor. Medd. J. Stat. Skogsforsoki 19:125-127.

Scotter, D. R. and Raats, P. A. C. 1968. Dispersion in porous mediums due to oscillating flow. Water Resources Res. 4:1201-1206.

Scotter, D. R. and Raats, P. A. C. 1969. Dispersion of water vapor in soil due to air turbulence. Soil Sci. 108:170-176.

Scotter, D. R., Thurtell, G. W., and Raats, P. A. C. 1967. Dispersion resulting from sinusoidal gas flow in porous materials. Soil Sci. 104:306-308.

Wesseling, J. 1962. Some solutions of the steady state diffusion of carbon dioxide through soils. Netherlands J. Agric. Sci. 10:109-117.

Chapter II

SPECTRA OF AIR PRESSURE FLUCTUATIONS AT THE SOIL SURFACE

A theoretical explanation of the effects of air turbulence upon gas exchange from soil depends upon an adequate evaluation of the air turbulence which exists at the soil surface in the field. The work of Rolston, Kirkham, and Nielsen (1969) and Scotter and Raats (1968) shows that there is an increase in the effective diffusion coefficient or "dispersivity" of the soil air when there is an increase in soil air velocity. Therefore, since pressure gradients cause soil air velocities, attention here is focused upon the fluctuations of air pressure associated with turbulence.

For their theoretical analysis of soil air velocity, Farrel, Graecen, and Gurr (1966) considered the air pressure to be a one space dimensional, traveling cosine wave, and they used a differential pressure transducer to try to measure the amplitudes, periods, and wave lengths of waves which exist in the field. However, as the recording in Fig. 2.1 of air pressure obtained with an absolute pressure transducer indicates, the pressure at a point in the field appears to be as random as it is sinusoidal. Because of this, it is necessary to consider methods for dealing with seemingly random variables.

One technique which has contributed to the understanding of such seemingly random variables in other fields than agronomy is spectral analysis, which is discussed in detail in the Appendix. With this technique the contribution to the statistical variance of a variable is determined for each of a whole series or "spectrum" of sinusoidal waves.

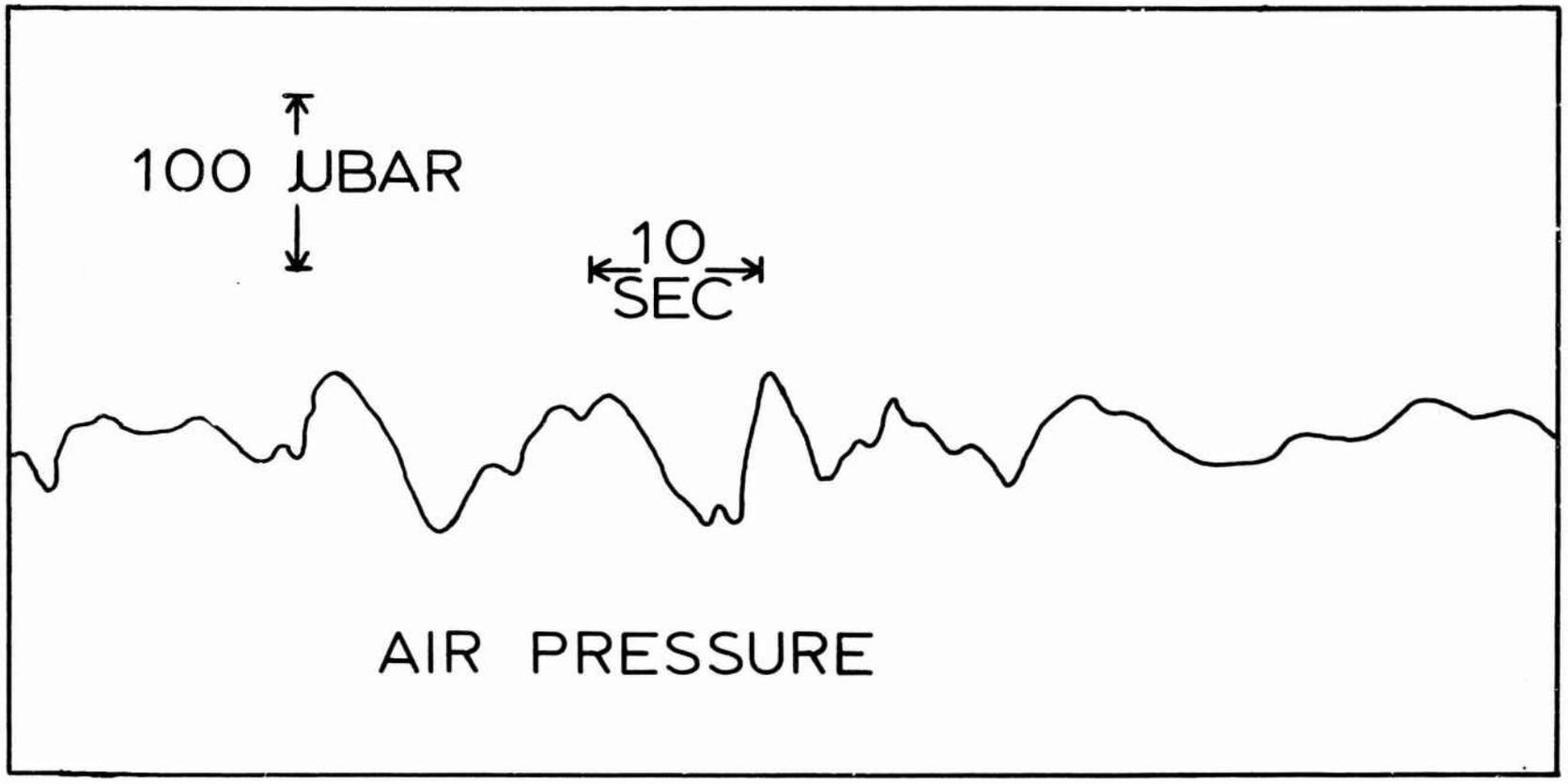

Figure 2.1 Absolute pressure at soil surface, Ellis Hollow, New York, October 24, 1967. The wind was 90 cm/sec at a height of 60 cm.

As will be shown in Chapter III, it is possible to extend the theory of Farrel et al. to consider the air pressure at the soil to be a series of superimposed, traveling waves whose amplitudes can be determined from spectra. Therefore, spectra of air pressure at the soil surface were determined for various conditions.

Methods

Measurements of air pressure using a Datametrics absolute pressure transducer model 511A equipped with a null offset adapter were obtained at a 10 hectare field site in Ellis Hollow near Ithaca, New York, at various times between June 11 and July 31, 1968. The transducer was placed on the soil surface about 30 m from air-conditioned trailers which housed signal conditioning and recording equipment. On any runs which lasted more than 5 min, the transducer was mounted inside a Styrofoam container on a thermal base which maintained the transducer temperature at 49°C.

During the day and night of June 11, 1968, when the soil surface was nearly bare, and during the night and following day of July 30, 1968, when a 200 cm corn crop was present, the pressure data for four different but overlapping ranges in frequency spectra were obtained. The frequency ranges and other supplementary information are given in Table 2.1. A simultaneous recording of wind speed was obtained using a Hastings-Raydist heated thermocouple anemometer mounted at a height of 50 cm on June 20 and a height of 250 cm on July 30.

During both time periods, a low pressure system was moving into the area, and the wind blew rather steadily from the southeast both day and night. Generally, the sky was partly cloudy to lightly overcast. Unfortunately, rain started before run number 5 could be completed, and it had to be cancelled.

The pressure for the two higher frequencies was sampled through lengths of 4.75 mm I.D. copper tubing, while that for the two lower

Table 2.1 Supplementary data for the spectra presented in Figures 2.3 - 2.6

Run	Date (1968)	Time (EST)	Ht of corn (cm)	Length of sample tube (cm)	Frequency range	No of sweeps in ave.	Total sample time per sweep (sec)	No of data points per sweep	Mean wind (cm/sec) cups	Mean wind (cm/sec) Hastings
1	June 11	10:33-10:36	10	20	0.0976-100.	8	10.24	2048	253	394
2	June 11	11:15-11:19	10	40	0.0122-12.5	5	81.92	2048	243	265
3	June 11	12:51-13:11	10	320	0.00305-1.56	3	327.68	1024	298	---
4	June 11	15:46-19:15	10	2560	0.000122-.125	2	8192.	2048	360	181
5	---	---	--	--	---	-	---	----	---	---
6	June 12	02:10-02:14	10	40	0.0122-12.5	5	81.92	2048	339	565
7	June 12	01:02-01:20	10	320	0.00305-1.56	3	327.68	1024	227	---
8	June 11	20:01-23:26	10	2560	0.000122-.125	2	8192.	2048	301	148
9	July 31	13:48-13:51	200	20	0.0976-100.	8	10.24	2048	377	272
10	July 31	13:27-13:30	200	40	0.0122-12.5	3	81.92	2048	469	501
11	July 31	12:37-12:57	200	320	0.00305-1.56	4	327.68	1024	450	333
12	July 31	08:20-11:01	200	2560	0.000122-.125	1	8192.	2048	384	193

Table 2.1 (cont.)

13	July 30	20:53-20:57	200	20	0.0976-100.	8	10.24	2048	---	77
14	July 30	21:14-21:18	200	40	0.0122-12.5	5	81.92	2048	---	115
15	July 30	22:17-22:40	200	320	0.00305-1.56	5	327.68	1024	143	107
16	July 31	01:02-04:17	200	2560	0.000122-.125	1	8192.	2048	127	60

frequency runs was sampled through lengths of 4.75 mm I.D. polyethylene tubing. The polyethylene tubing was buried 5 cm below the soil surface to prevent spurious signals from arising due to a mechanical disturbance caused by the wind blowing directly on the tubing. The sampling ends of all the tubes were bent to form a gooseneck so that the sampling port pointed vertically downward at a point just below (<1mm) the soil surface. The lengths of tubing used for runs from each frequency range are included in Table 2.1. Following the analysis of Iberall (1950), the lengths were chosen to be short enough so that there was minimal attenuation of frequencies over the ranges used and narrow enough so that there was damping of resonant frequencies. Some of the lengths were long because the frequency spectra were obtained as part of a larger experiment to measure space-time spectra using differential pressure transducers. The larger experiment failed because there simply were not enough sensors available to represent adequately the space dimensions.

Between June 20 and July 25, pressure data for the frequency range from 0.00195 to 2.0 cycles/sec were obtained under the variety of atmospheric conditions and crop heights listed in Table 2.2. A 120 cm long, 4.75 mm I.D. copper tube with its end bent in a gooseneck and pointed downward just below the soil surface was used for all of the runs in Table 2.2.

An IBM 1800 computer which was equipped to digitize analog signals was used for computations. Use of a program named LOGR permitted digitized signal values to be logged into disk storage. A second program named SPEC was written to compute and plot spectra either from data logged on the disk by LOGR or read into the computer from cards. SPEC used Fortran subroutines called RFORT and FORT to compute fast Fourier

Table 2.2 Supplementary data for the spectra presented in Figures 2.8 - 2.10

Run	Date (1968)	Starting time EST	Mean wind (cm/sec)	Anemometer ht (cm)	Corn ht (cm)	Wind direction	Sky
Day:							
17	June 20	13:00	552	50	20		Few scattered clouds
18	July 14	12:38	206	150	90	SSW	Clear, but hazy
19	July 16	13:22	232	475	100	WNW	Scattered clouds
20	July 17	16:06	68	475	100	N	Partly cloudy
21	July 18	13:53	287	475	105	SW	Partly cloudy
22	July 21	15:06	254	475	115		Clear
23	July 22	11:12	349	475	120	S	Clear
24	July 25	12:55	363	475	160	NNW	Partly cloudy
Night:							
25	July 13	04:47	17	50	85		Clear
26	July 14	04:49	102	150	90		Clear
27	July 17	05:06	99	475	100		Clear, light fog
28	July 18	04:58	80	475	100		Clear
29	July 19	05:10	146	475	105	SSW	Clear

transforms of data points by the algorithm of Cooley and Tukey (1965). The algorithm, explained well by Brigham and Morrow (1967), computes the complex Fourier coefficients from the equation

$$S(f_n) = \Delta t \sum_{k=0}^{N-1} p(t_k)\exp(-i2\pi f_n t_k) \qquad 2.1$$

where

$S(f_n)$ = complex Fourier coefficient for nth frequency, f_n

Δt = sample interval (sec)

N = number of data points, chosen to be an integer power of 2

$p(t_k)$ = pressure at the kth time, t_k

The spectral density values were then computed from

$$s(f_n) = \frac{2|S(f_n)|^2}{\Delta f} \qquad 2.2$$

where $s(f_n)$ is the spectral density at the nth frequency and Δf equals the frequency increment (or 1/total sampling time). Various aspects of spectral analysis are described in detail in the Appendix. The amplitude of a pressure wave is taken as $S(f_n)$ or as $|S(f_n)|$ when using Equation 2.2 in reverse to compute amplitudes from spectral density.

Before any Fourier transform was computed, the data was always corrected for the presence of a trend by the method of least squares. After computation and before plotting, the spectra were smoothed four times using the weights shown in Equation 2.3.

$$s'(f_n) = 0.25s(f_{n-1}) + 0.5s(f_n) + 0.25s(f_{n+1}) \qquad 2.3$$

The end points were smoothed by an ordinary averaging with their adjacent points.

The June 11 and July 30 data for the three highest frequency ranges were recorded on magnetic tape by an analog tape recorder and later played back into the 1800 computer for computation of spectra. To prevent aliasing, a low pass, RC filter was used, which had a cut-off frequency of either 1, 10, or 100 cycle/sec depending on the corresponding frequency range.

The June 11 and July 30 data for the lowest frequency range were recorded on digital magnetic tape by a data logger at a 1 sec sampling interval, and then they were read from the digital tape on an IBM 360 computer. No special precautions were taken against aliasing, but electrical noise was no particular problem with the data logger compared to the analog recorder. Moreover, overlapping portions of the resulting spectra from different ranges agree closely, so neglect of aliasing apparently was not important. To reduce the number of points, the data were smoothed, using a 49 weight, low-pass, digital filter which had a sharp cut-off from 0.26 to 0.32 cycle/sec; then, every four points were average together. The four point average was punched on cards for later computation of spectra on the 1800.

The data for the runs obtained between June 20 and July 25 were printed on paper tape by the data logger at a 0.25 sec sampling interval for a 512 sec sampling period. They were then punched onto cards by hand before computation of spectra on the 1800.

Results and Discussion

To obtain spectra which were as representative as possible of the time periods listed in Table 2.1, the spectra for several replicate or sweeps were computed and then averaged from subintervals of the magnetic tape record for the particular time period. The number of sweeps which contributed to each averaged spectrum is also listed in Table 2.1. To illustrate what a typical spectrum looked like before any hand work was done, the computer-drawn average spectrum for Run 15 is presented on the left in Figure 2.2 for the air pressure at the ground surface. It was obtained using the absolute pressure transducer as discussed previously. The other two graphs are pressure spectra from two other points in the field and were obtained as part of the space-time experiment. The curve from the absolute pressure transducer is quite linear and fairly smooth with a slope of about -5.6/3 on the log-log plot, except at the low frequency end. Here the decrease in steepness is undoubtedly due, not to any natural phenomena, but to the fact that an equally weighted average with the second point was used to smooth the end points. A better procedure probably would have been to weight the end point by 0.75 and its adjacent point by 0.25.

In Figures 2.3, 2.4, 2.5, and 2.6, the spectra of air pressure and wind from Runs 1 - 16 are plotted, covering four ranges of pressure for day and night conditions with and without a crop canopy. The spectra were obtained by hand tracing from the computer-drawn curve of Figure 2.2 and its counterparts.

Figure 2.2 Spectra of air pressure plotted directly by computer before there was any smoothing by hand work. The units on the spectral density axis are μbar^2/cycle/sec and the units on the frequency axis are cycles/sec.

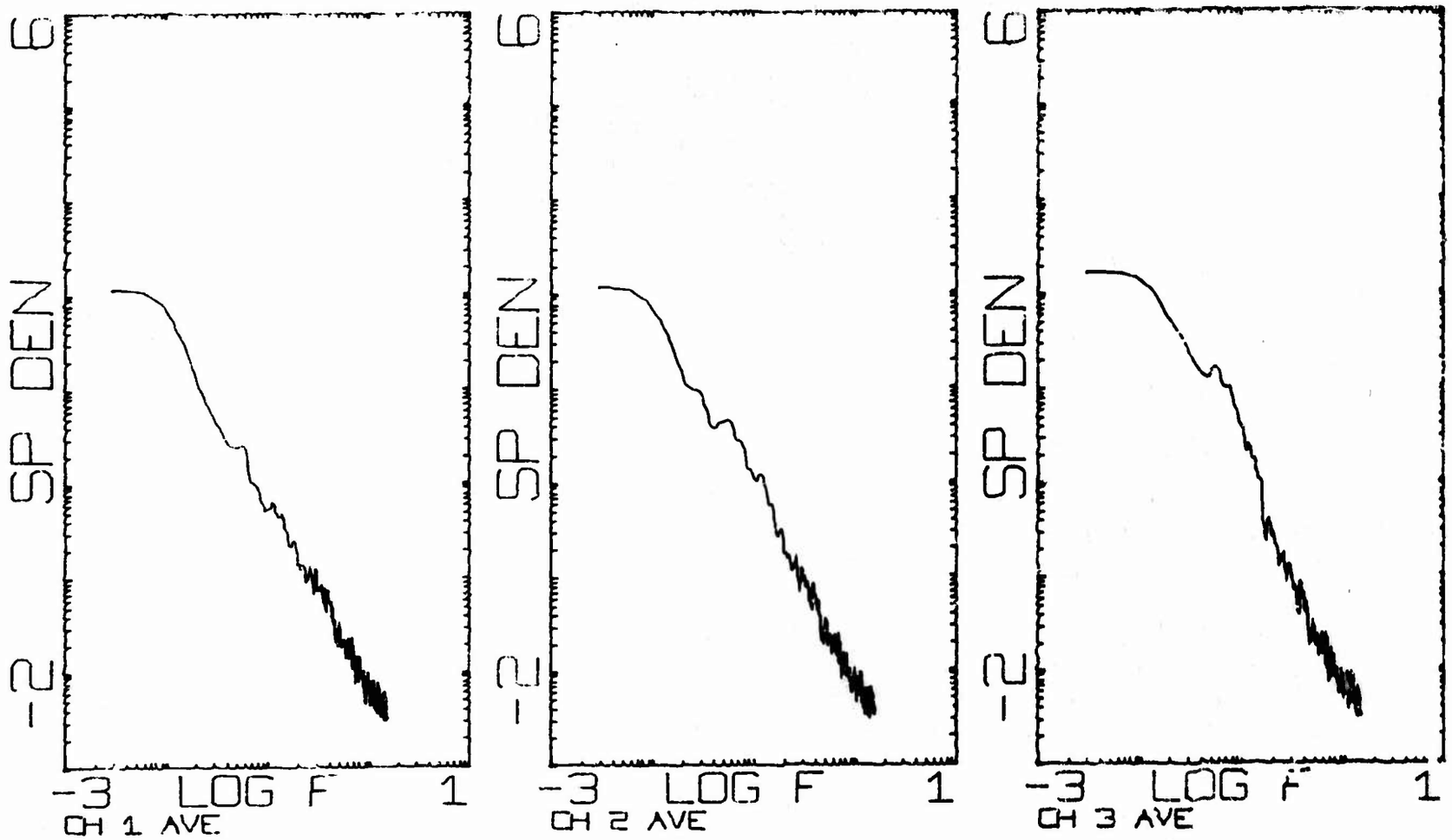
6
SP DEN
-2
-3
LOG F
1
CH 1 AVE
6
SP DEN
-2
-3
LOG F
1
CH 2 AVE
6
SP DEN
-2
-3
LOG F
1
CH 3 AVE

Figure 2.3 Spectra of air pressure and wind for the day of June 11, 1968, near Ithaca, New York, when no crop was present. The numbers on the curves refer to the run numbers in Table 2.1.

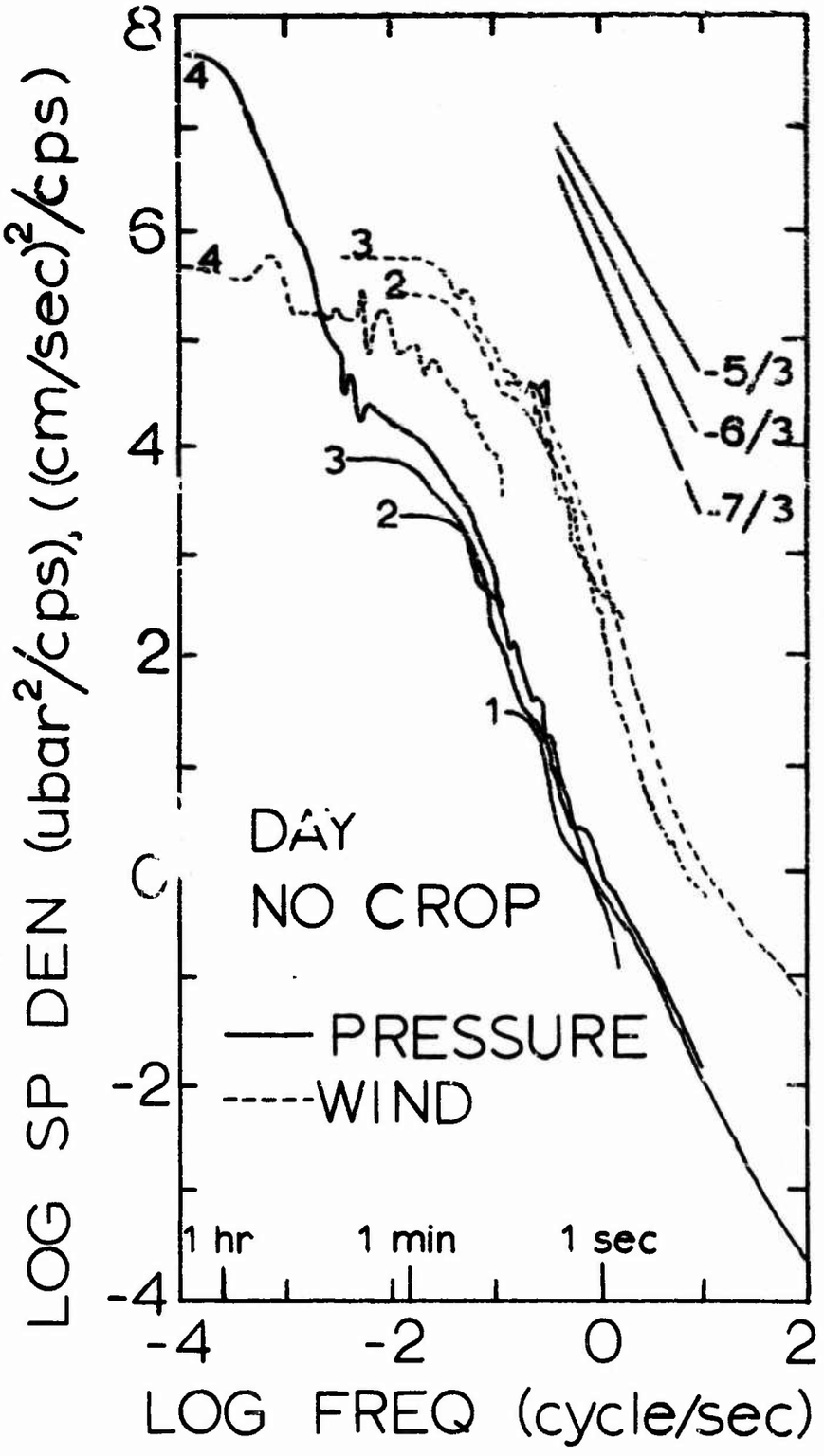
LOG SP DEN (ubar²/cps), ((cm/sec)²/cps)
8
6
4
2
0
-2
-4
4
4
3
2
3
2
1
-5/3
-6/3
-7/3
DAY
NO CROP
PRESSURE
WIND
1 hr
1 min
1 sec
-4
-2
0
2
LOG FREQ (cycle/sec)

Figure 2.4 Spectra of air pressure and wind for the night of June 11, 1968, near Ithaca, New York, when no crop was present. The run numbers on the curves refer to the run numbers in Table 2.1.

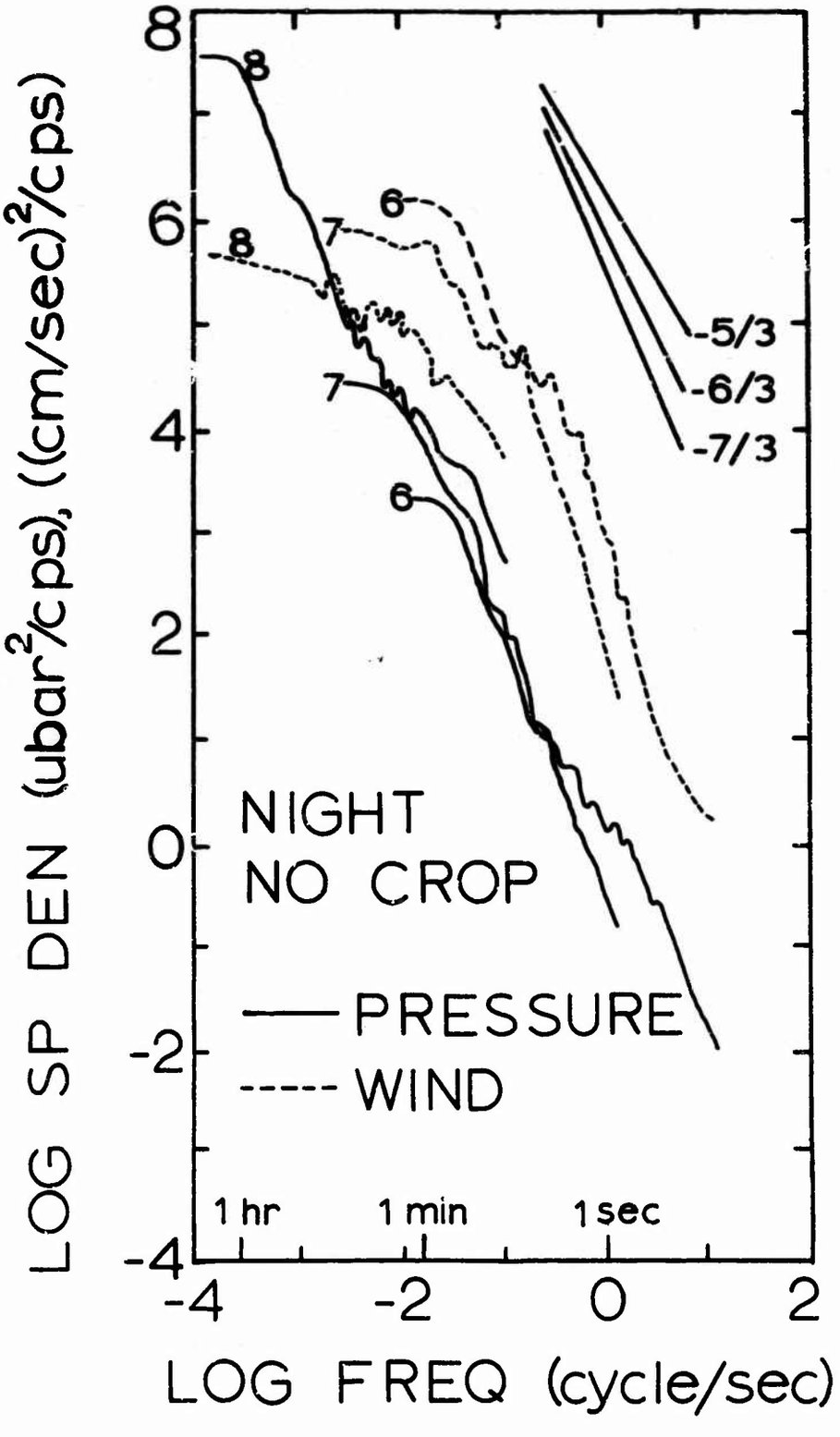
LOG SP DEN (ubar²/cps), ((cm/sec)²/cps)
LOG FREQ (cycle/sec)
8
6
4
2
0
-2
-4
-4
-2
0
2
1 hr
1 min
1 sec
-5/3
-6/3
-7/3
NIGHT
NO CROP
PRESSURE
WIND

Figure 2.5 Spectra of air pressure and wind for the day of July 31, 1968, near Ithaca, New York, when a 200 cm corn crop was present. The numbers on the curves refer to the run numbers in Table 2.1.

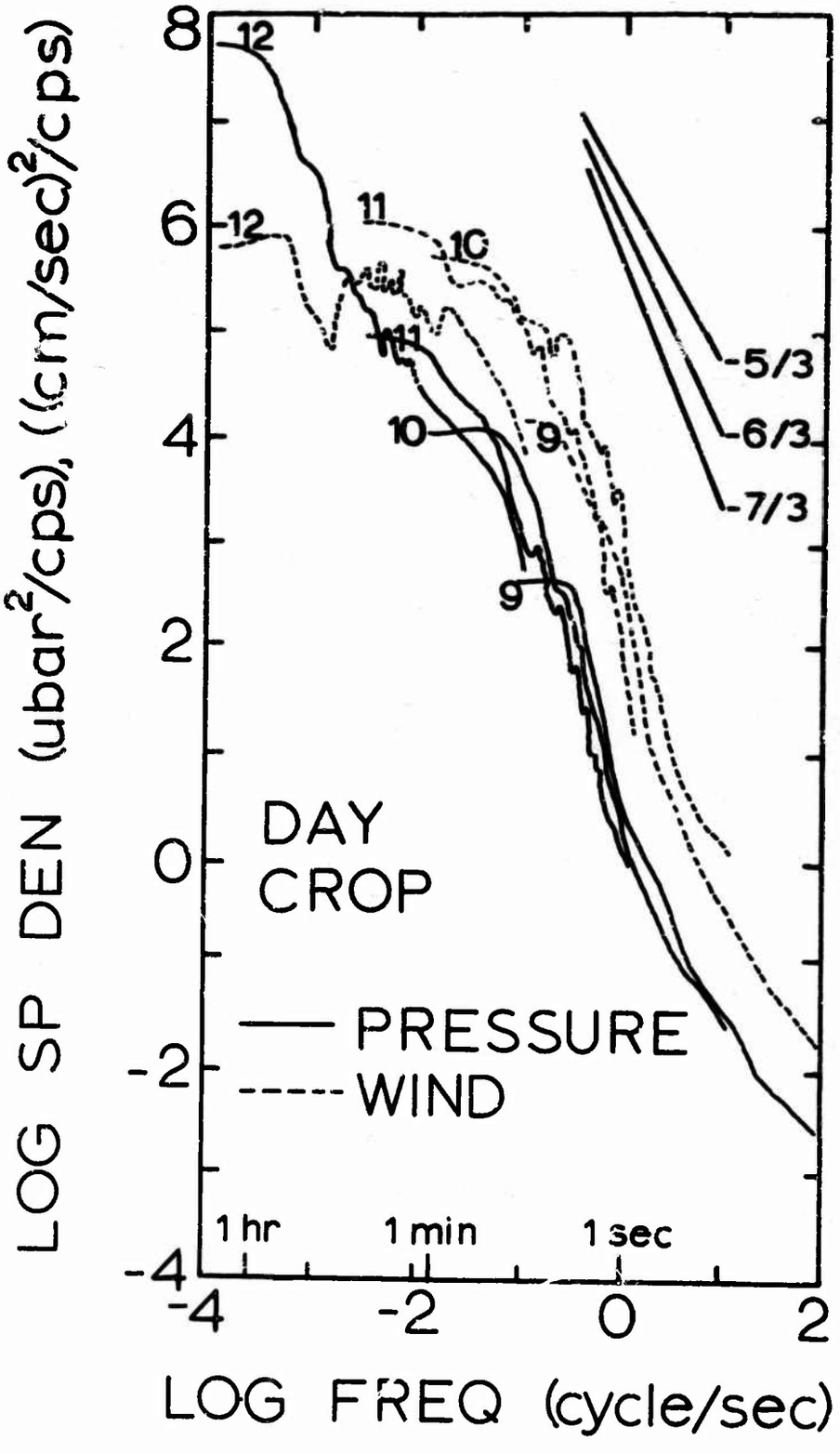
LOG SP DEN (ubar²/cps), ((cm/sec)²/cps)
LOG FREQ (cycle/sec)
8
6
4
2
0
-2
-4
-4
-2
0
2
1 hr
1 min
1 sec
12
12
11
11
10
10
9
9
-5/3
-6/3
-7/3
DAY
CROP
PRESSURE
WIND

Figure 2.6 Spectra of air pressure and wind for the night of July 30, 1968, near Ithaca, New York, when a 200 cm corn crop was present. The numbers refer to the run numbers in Table 2.1.

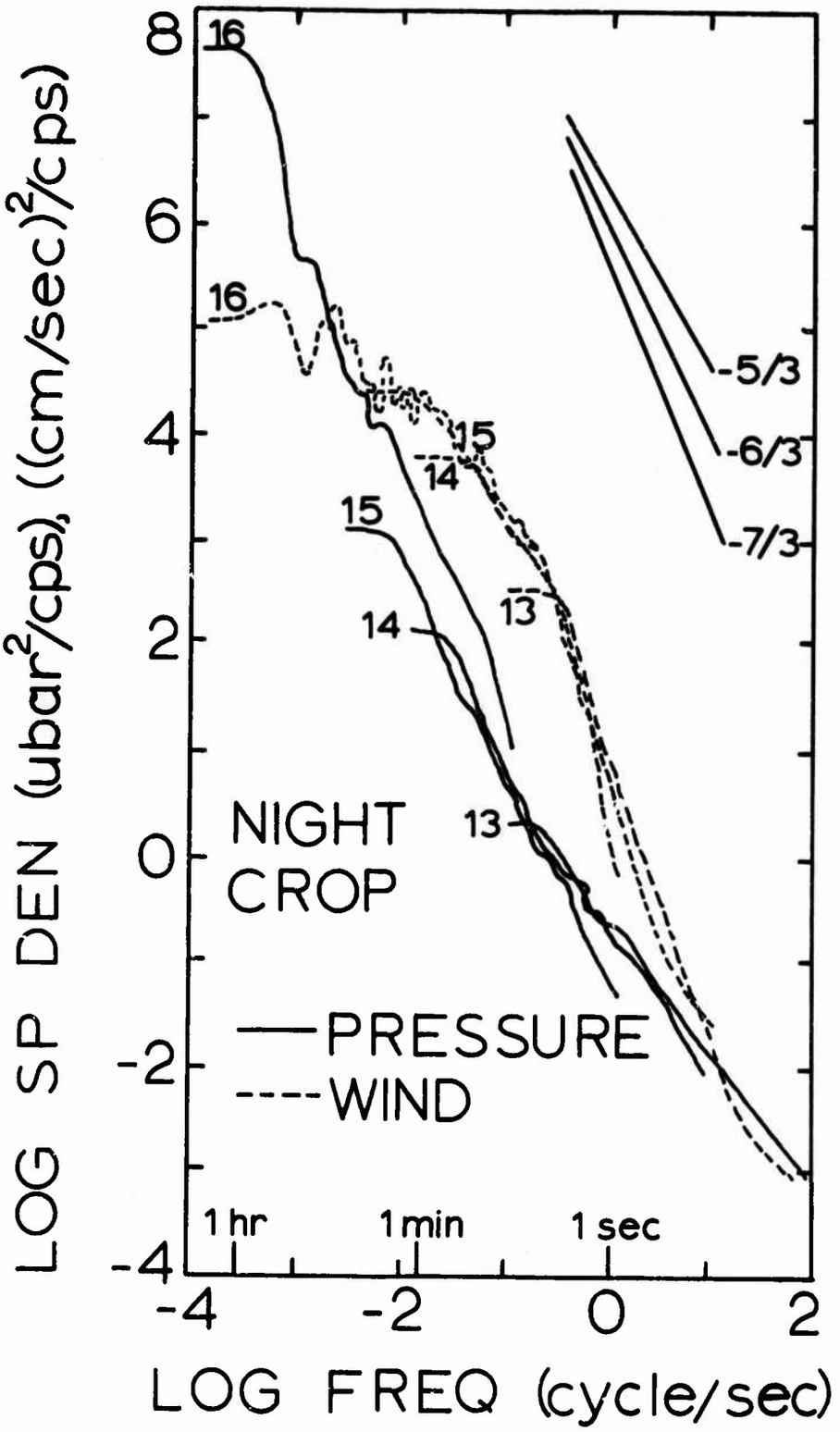
LOG SP DEN (ubar²/cps), ((cm/sec)²/cps)
LOG FREQ (cycle/sec)
8
6
4
2
0
-2
-4
-4
-2
0
2
16
16
15
14
15
14
13
13
-5/3
-6/3
-7/3
NIGHT
CROP
PRESSURE
WIND
1 hr
1 min
1 sec

The overlapping portions of the spectra from the various runs are almost identical. It is apparent that the pressure spectra form roughly a straight line with a slope of about -6/3 on a log-log plot over the entire frequency range covered in this study. Furthermore, they are very similar to the pressure spectra in Fig. 2.7 which have been redrawn from Gossard (1960) and Priestly (1966). The spectra of Gossard and Priestly were obtained by different methods under different conditions from the methods and conditions used in this study. One concludes, therefore, that air pressure spectra which have slopes of about -6/3 over wide frequency ranges are quite general phenomena.

The overlapping portions of the wind spectra from different runs also tend to agree fairly well. On the log-log plots, the spectral density appears roughly constant for frequencies to about 0.1 cycle/sec and then tends to drop sharply to form a steep straight line with increasing frequency.

These air pressure spectra which are straight lines over the whole frequency range covered in these experiments probably do not indicate that the same physical phenomena are operative over the entire range as pointed out by Lumley and Panofsky (1964). The portion for frequencies greater than about 0.1 cycle/sec where the wind spectra also have a steep slope probably indicates an inertial subrange in which there is transfer of energy to smaller and smaller eddies but no production or dissipation. In such a subrange the predicted slope for the pressure spectrum is -7/3 and for the wind spectrum is -5/3 which is not greatly different from the slopes of about -6/3 for both type of spectra in Fig. 2.3-2.6. At frequencies from about $10^{-3.5}$ down to about 10^{-6} cycle/sec, (which

Figure 2.7 Spectra of air pressure redrawn from Gossard (1960) and Priestly (1966).

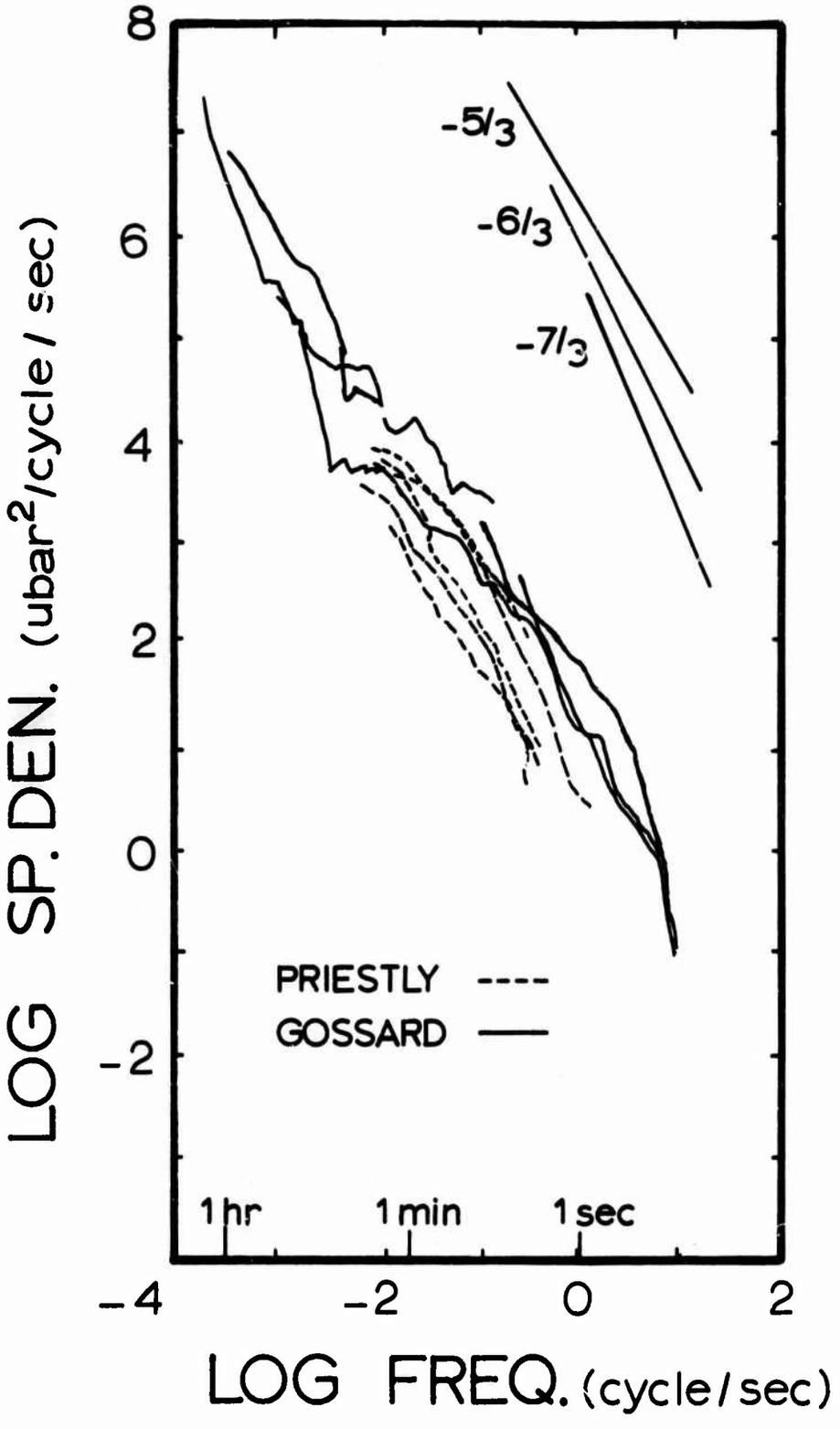
8
6
4
2
0
-2
-4
-2
0
2
-5/3
-6/3
-7/3
PRIESTLY ----
GOSSARD ——
1 hr
1 min
1 sec
LOG SP. DEN. (ubar²/cycle / sec)
LOG FREQ. (cycle/sec)

is below the range of the figures shown here) the spectra are dominated by weather-map phenomena. In this range Gossard found that the pressure spectrum reached a maximum of $10^{11.7}$ μbar^2/cycle/sec at a frequency of $10^{-5.6}$ cycle/sec, which corresponded to a maximum in the wind spectrum previously found by Van der Hoven (1957). As frequency increases from $10^{-5.6}$, the pressure spectrum of Gossard decreases with a slope of -6/3 except for two sharp peaks corresponding to periods of 12 and 24 hours. Lumley and Panofsky mention that on the weather-map scale, the wind speed varies with pressure gradient so the wind spectrum should be proportional to the pressure spectrum times frequency on a log-log plot, and such is roughly the case between the pressure spectrum of Gossard and the wind spectrum of Van der Hoven.

Presumably, the entire pressure spectrum below the maximum would more or less indicate an inertial subrange-type behavior were it not for the input of convective energy at higher frequencies which makes the spectral curve higher and decreases its slope. The convective energy input seems to occur mostly in the frequency range from about $10^{-3.5}$ to about $10^{-1.0}$ cycle/sec as evidenced by the largest differences in the height of the pressure spectra in this range in Fig. 2.3 - 2.7 and by the wind spectra reaching a maxima here. The height of the spectra in Fig. 2.3 - 2.7 in the mid-frequency range varies with wind speed and, at least occasionally, can also be influenced by gravity waves, which presumably caused a rather prominent peak at about $10^{-2.8}$ cycle/sec in two spectra obtained by Gossard. An indication of the amount of influence of wind speed on the mid-frequency spectrum can be obtained from Fig. 2.3 - 2.7 and also from the spectra presented in Fig. 2.8 - 2.10. The wind

Figure 2.8 Spectra of air pressure for daytime hours near Ithaca, New York. The numbers on the curves refer to the run numbers in Table 2.2.

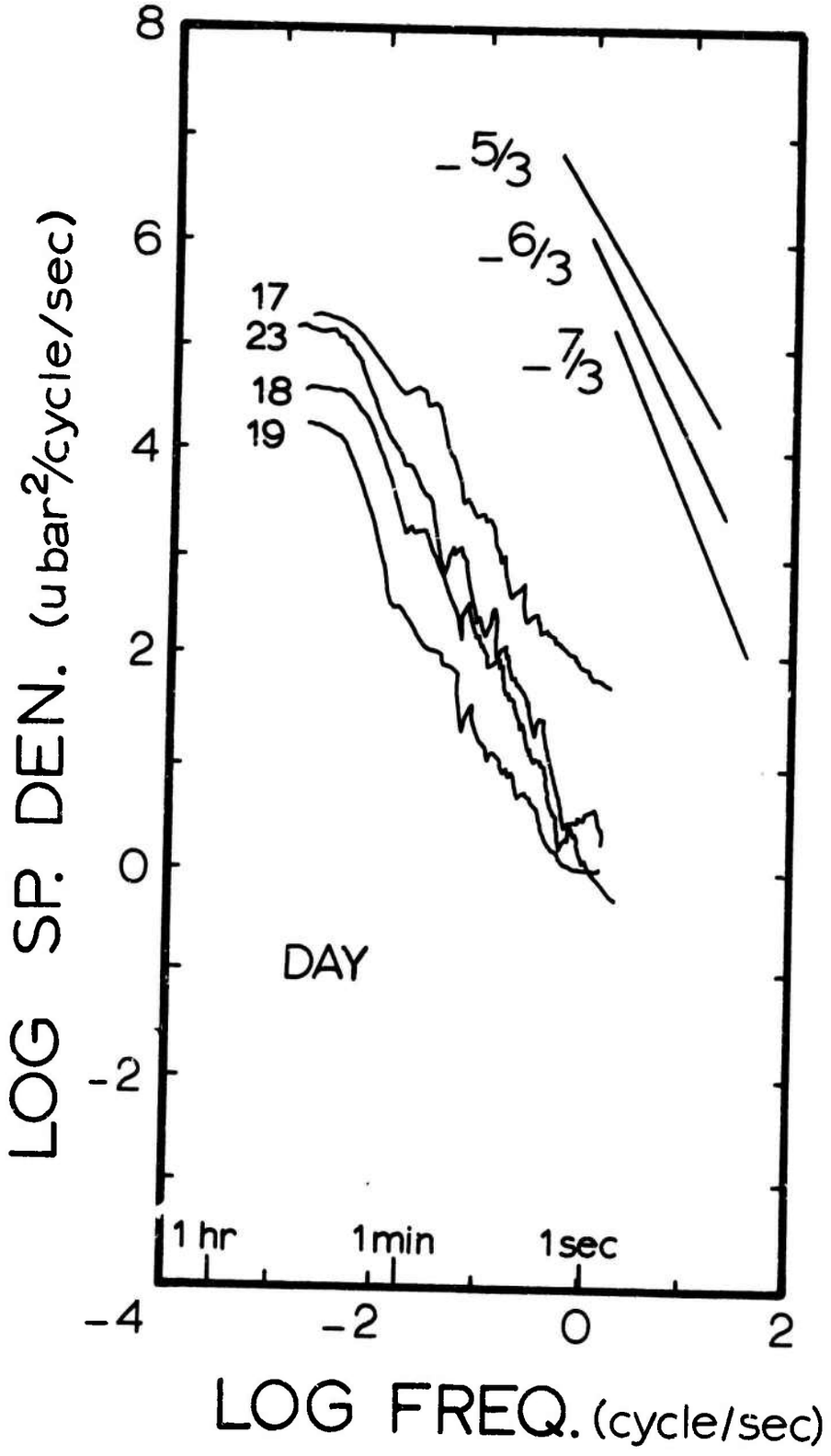
8
6
4
2
0
-2
-4
-2
0
2
-5/3
-6/3
-7/3
17
23
18
19
DAY
1 hr
1min
1sec
LOG SP. DEN. (u bar²/cycle/sec)
LOG FREQ. (cycle/sec)

Figure 2.9 Spectra of air pressure for daytime hours near Ithaca, New York. The numbers on the curvers refer to the run numbers in Table 2.2.

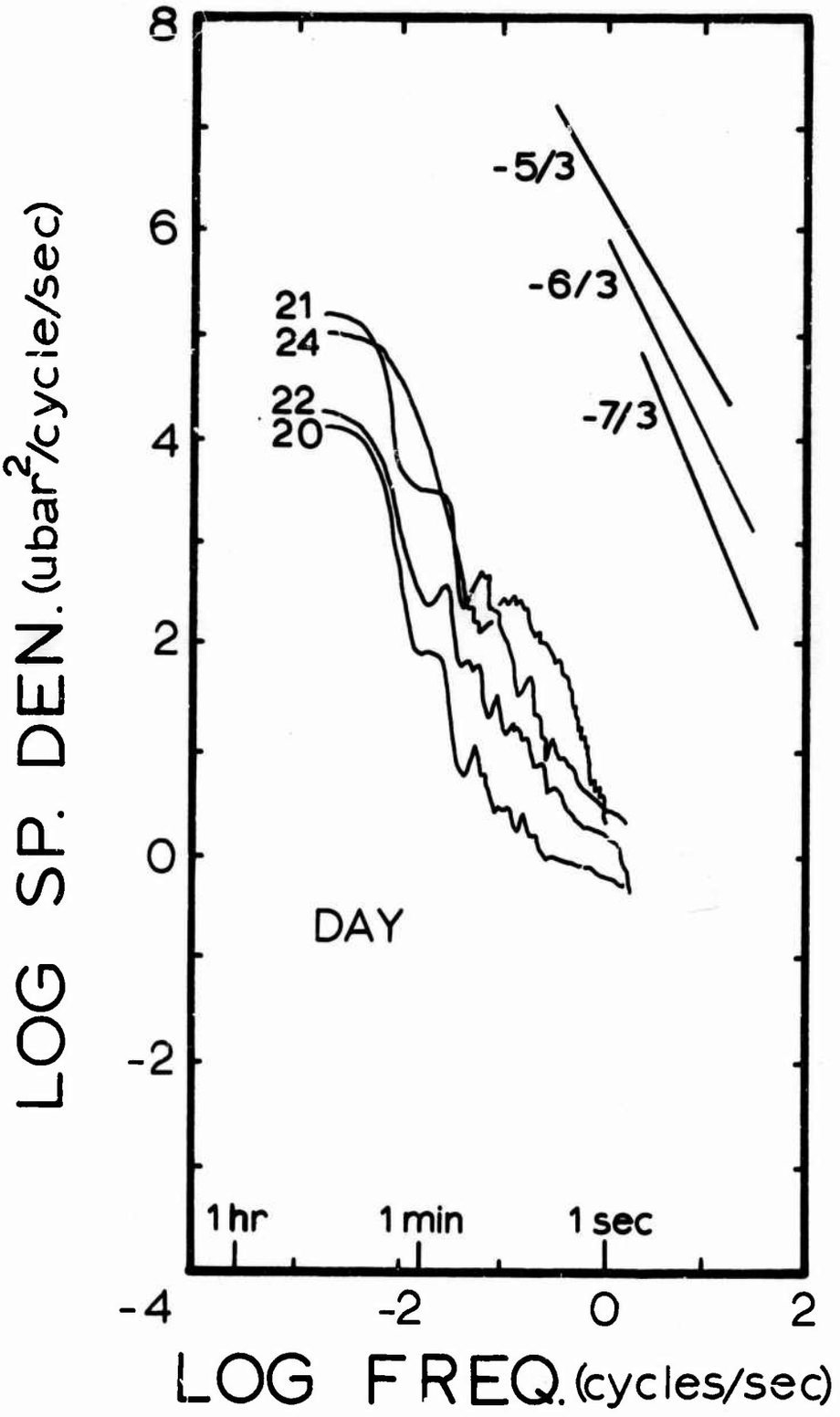
8
6
4
2
0
-2
-4
-5/3
-6/3
-7/3
21
24
22
20
DAY
1 hr
1 min
1 sec
-2
0
2
LOG SP. DEN. (ubar²/cycle/sec)
LOG FREQ. (cycles/sec)

Figure 2.10 Spectra of air pressure for nighttime hours near Ithaca, New York. The numbers on the curves refer to the run numbers in Table 2.2.

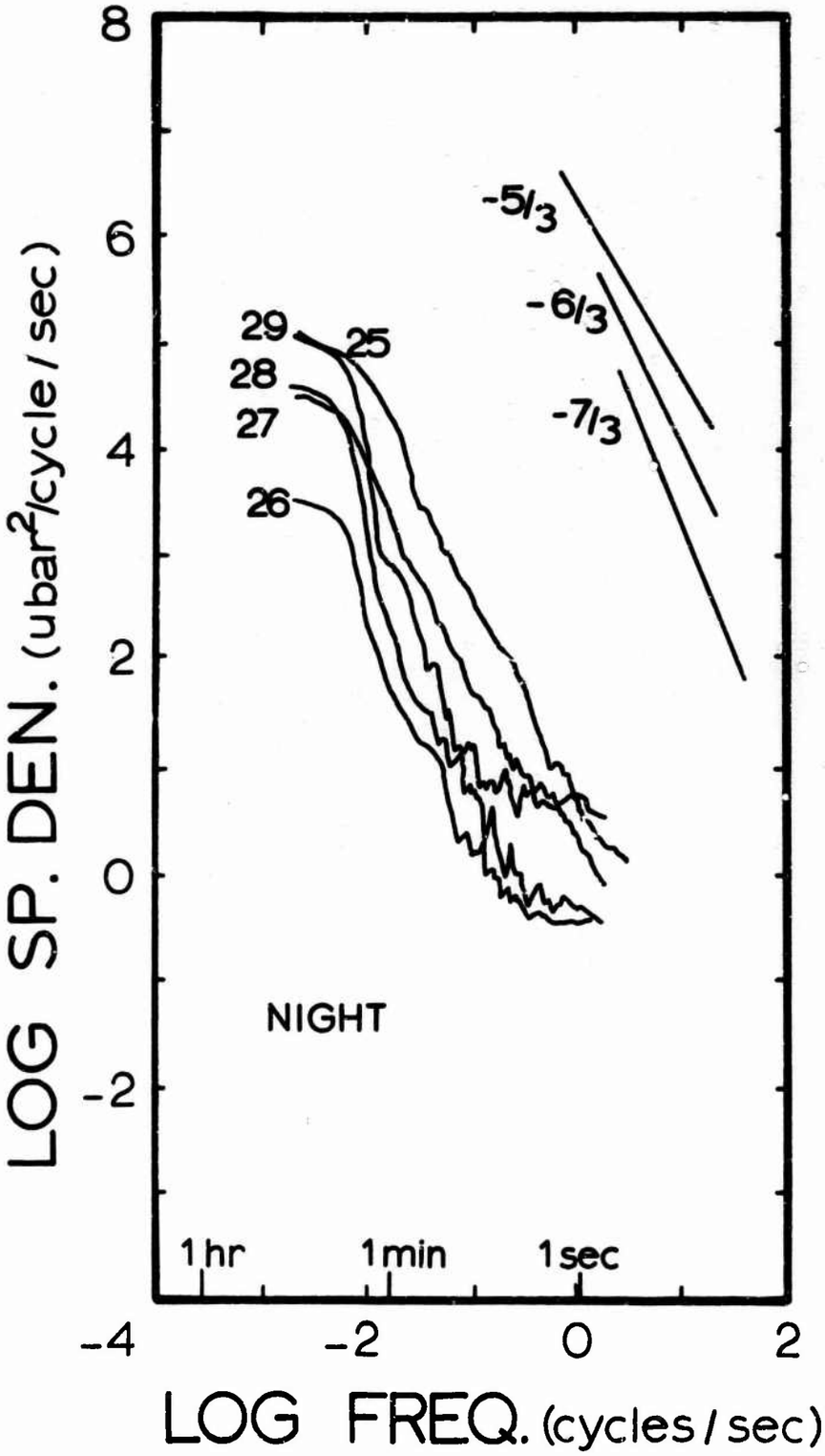
8
6
4
2
0
-2
-4
-2
0
2
LOG SP. DEN. (ubar²/cycle / sec)
LOG FREQ. (cycles / sec)
-5/3
-6/3
-7/3
29
25
28
27
26
NIGHT
1 hr
1 min
1 sec

speeds present for the various runs are given in Tables 2.1 and 2.2. The most striking differences are probably between the spectra obtained during the day and those at rather low wind speeds at night. The spectral density for pressure was 100 times greater during the day of July 31 than it had been the previous night at a frequency of 0.1 cycle/sec. The night spectra in Figure 2.10 are also noticeably smoother than the daytime spectra in Fig. 2.8 and 2.9. The differences between days is large too, however, as evidenced by a 500-fold difference in spectral density at a frequency of $10^{-1.7}$ cycle/sec, between Run 17 in Fig. 2.8, when the wind speed was 552 cm/sec at 50 cm and Run 20 in Fig. 2.9 when the wind speed was 68 cm/sec at 475 cm.

The theories of soil gas movement presented by Farrel et al. (1966) and by the author in Chapter III indicate that, in addition to amplitude, the wave length or eddy size of pressure waves is important. The wave length of a particular wave can be obtained by dividing the frequency of the wave by the wind speed. This method works if the wind speed is available, and if one assumes that the pressure moves along in a frozen pattern of turbulence at the speed of the mean wind. That this is not an unrealistic assumption is indicated by a wave number-frequency spectrum of pressure calculated from pressure correlation measurements made by Priestly (1966). Priestly found that the longitudinal correlation coefficient for a narrow frequency band between points parallel to the wind across a field of short grass could be described by

$$R(f,\delta) = e^{-\alpha\delta}\cos\beta\delta \qquad 2.4$$

where

f = the particular frequency

δ = the spacing between observation points

$R(f,\delta)$ = the longitudinal correlation coefficient for air pressure between points separated by a spacing of δ at a frequency of f.

α,β = empirical constants determined by least squares fit to the data for a narrow frequency band. α indicates the magnitude of the decay of correlation of pressure with increasing spacing between observation points, and β indicates the frequency of the oscillation of the correlation coefficient with spacing. Both are functions of the narrow band frequency at which the pressure measurements were made.

Using Equation 2.4, the wave number-frequency spectrum can be obtained from the Fourier transform of $R(f,\delta)$ according to

$$s(f,k) = 2\int_0^\infty R(f,\delta)\cos 2\pi k\delta\, d\delta$$

$$= \frac{\alpha(f)}{[\alpha(f)]^2 + [\beta(f) + 2\pi k]^2} + \frac{\alpha(f)}{[\alpha(f)]^2 + [\beta(f) - 2\pi k]^2} \qquad 2.5$$

where

k = wave number = 1/wave length

$s(f,k)$ = spectral density at a frequency of f and wave number of k

Using values of α and β given for 16 different frequencies by Priestly and choosing values of k in the range covered by him, the plot of spectral density presented in Fig. 2.11 was obtained using Equation 2.5. The curves are contour lines of constant spectral density plotted against wave

Figure 2.11 Frequency-wave number spectrum for air pressure computed from the data of Priestly (1966). The curves are contour lines of constant spectral density. The numbers on the curves are the values of the spectral density on the contour line in units of $\mu bar^2/[(cycle/sec)(cycle/cm)]$. The dashed diagonal lines represent the frequency-wave number combinations corresponding to eddies moving at 300 cm/sec and 600 cm/sec.

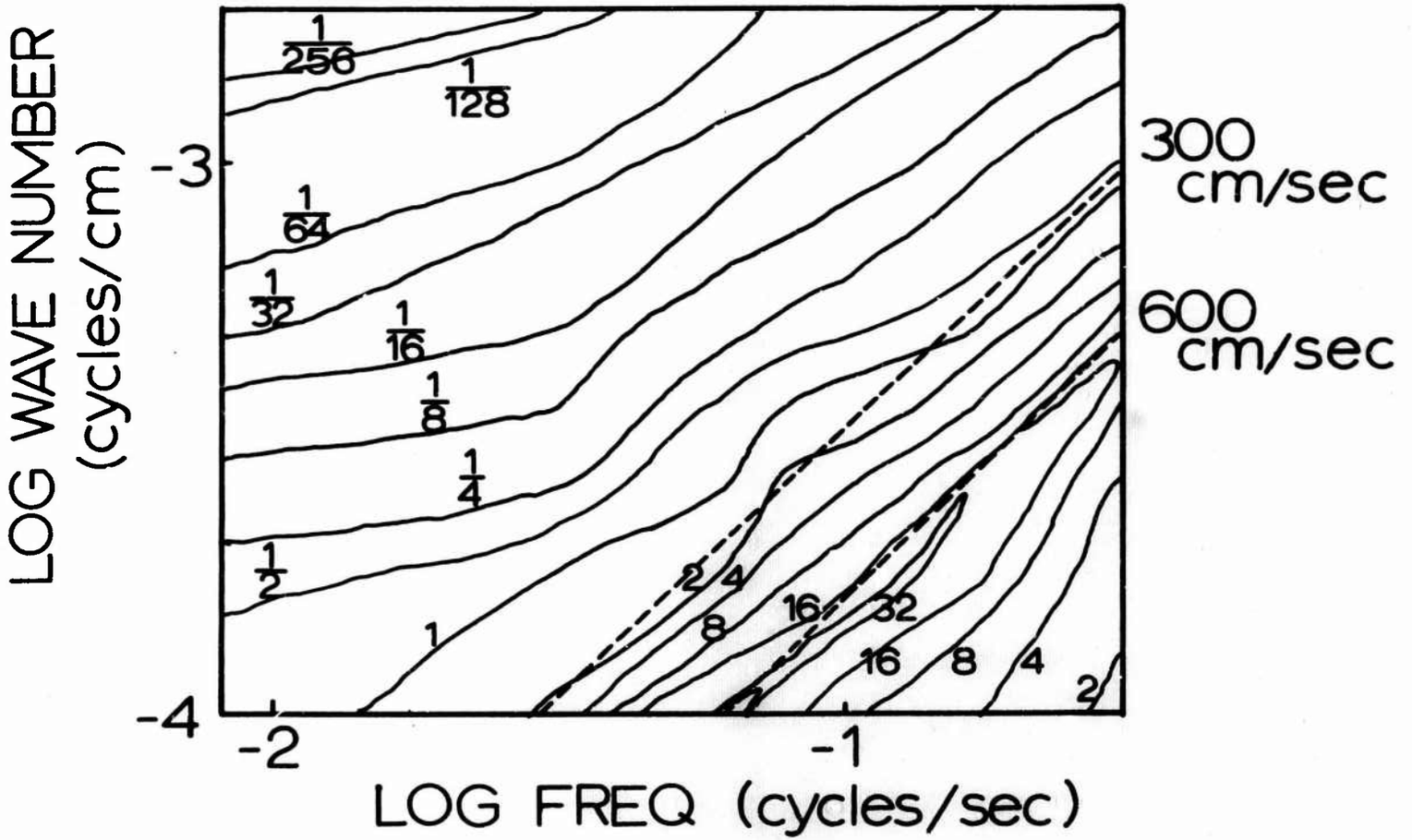
LOG WAVE NUMBER
(cycles/cm)
-3
-4
-2
-1
LOG FREQ (cycles/sec)
1/256
1/128
1/64
1/32
1/16
1/8
1/4
1/2
1
2
4
8
16
32
16
8
4
2
300
cm/sec
600
cm/sec

number and frequency. One of the dotted lines represents the combination of wave number and frequency corresponding to eddies moving at the speed of 600 cm/sec, and it is apparent that the spectral density decreased from both sides of a ridge slightly to the right of this line. The wind speed observed by Priestly at a height of 427 cm was 600 cm per sec, so the eddies were moving at or just slightly faster than the mean wind speed at 427 cm. If the smaller eddies close to the ground surface move more slowly due to surface drag than do the larger, higher eddies, then the ridge in Fig. 2.11 should bend upward with increasing frequency to lie closer to the second dotted line which indicates a 300 cm/sec wind speed. No such bending is apparent, so, at least over the limited range of wave number and frequency covered in Fig. 2.11, the pressure moved with the mean wind in a frozen pattern of turbulence. Thus, it probably is not too unrealistic to obtain the wave length of an eddy from its frequency and the mean wind. However, the anemometer used to measure the mean wind must be mounted at a fairly large height above the ground or crop surface. Priestly's anemometer was at a height of 427 cm, and apparently, the eddies were moving at a speed even slightly faster than the mean wind at this height. The errors of measurement probably are as large as the apparent velocity difference, however.

Summary

To determine the amplitude of air pressure fluctuations at the ground surface, spectra of air pressure and wind were obtained which cover a frequency range from 10^{-4} to 10^{2} cycle/sec during both day and night conditions with and without a corn crop. The pressure spectra were very similar to the spectra obtained by previous workers using different methods under different conditions. The spectral density for pressure decreased in a roughly linear manner with a slope of about -6/3 on a log-log plot for all conditions from about 10^{8} to 10^{-3} μbar^2/cycle/sec over the frequency range. The greatest variability in shape and height of the spectra occurred in the mid-frequency range from about 10^{-3} to 10^{-1} cycle/sec. The variability was associated with the wind speed, and a 500-fold increase was observed between one run when the wind speed was 68 cm/sec and another when the wind was 552 cm/sec.

A wave-number frequency spectrum of air pressure was computed from data obtained from the literature. Over the limited range of wave number and frequency covered by the spectrum, the pressure field moved with the mean wind in a frozen pattern of turbulence. It is suggested, therefore, that the wave length associated with each frequency may realistically be computed from the mean wind.

Literature Cited

Brigham, E. O. and Morrow, R. E. 1967. The fast Fourier transform. IEEE Spectrum 4(3):63-70.

Cooley, J. W. and Tukey, J. W. 1965. An algorithm for the machine calculation of complex Fourier series. Math. Comput. 19:297-301.

Farrel, D. A., Greacen, E. L., and Gurr, C. G. 1966. Vapor transfer in soil due to air turbulence. Soil Sci. 102:305-313.

Gossard, E. E. 1960. Spectra of atmospheric scalars. J. Geophys. Research 65:3339-3351.

Iberall, A. S. 1950. Attenuation of oscillatory pressures in instrument lines. Research paper RP2115. J. of Res. of the National Bureau of Standards. 45:85-108.

Lumley, J. L. and Panofsky, H. A. 1964. The Structure of Atmospheric Turbulence. John Wiley and Sons, Inc., New York, N. Y., 239 pp.

Priestly, J. T. 1966. Correlation studies of pressure fluctuations on the ground beneath a turbulent boundary layer. National Bureau of Standards Reports No. 8942.

Rolston, D. E., Kirkham, D. and Nielsen, D. R. 1969. Miscible displacement of gases through soil columns. Soil Sci. Soc. Amer. Proc. 33:488-492.

Scotter, D. R. and Raats, P. A. C. 1968. Dispersion in porous systems due to oscillating flow. Water Resources Research 4:1201-1206.

Van der Hoven, I. 1957. Power spectrum of horizontal wind speed in the frequency range from 0.0007 to 900 cycles per hour. J. Meteorol. 14:160-164.

Chapter III

THEORY OF MASS FLOW OF GAS IN POROUS MEDIA DUE TO AIR TURBULENCE

The experimental work described in Chapter I showed that the rate of heptane evaporation through a porous medium increased with wind speed or root mean square pressure fluctuation under certain field conditions. These results indicate that air turbulence can cause an increase in the apparent diffusion coefficient of vapor in porous media. To explain the increase on a theoretical basis, mathematical equations are needed to relate the apparent diffusion coefficient to parameters which describe the air turbulence and the porous medium.

The apparent diffusion or "dispersion" of a vapor through porous media was found by Scotter, Thurtell, and Raats (1967) to increase with the velocity and the displacement amplitude of an oscillatory mass flow of bulk gas through the porous medium. The displacement amplitude is half the maximum distance a particle of air would move during one period of oscillation. Scotter and Raats (1968) then developed a theory based on scaled velocities and displacement amplitudes which predicts the rate of dispersion in one medium from measurements made in another, at least for classes of similar media. It may be possible, therefore, to use an adaptation of their theory and their laboratory measurements to predict vapor transfer under field conditions if the velocities and the displacement amplitudes which exist under field conditions can be adequately predicted and properly scaled.

To attempt to calculate the velocity of mass flow of gas in porous media under field conditions, Farrel, Greacen, and Gurr (1966) derived

an equation which used a sinusoidal, one-space dimensional traveling pressure wave for a model of air turbulence. Using a differential pressure transducer, they also attempted to measure the pressure waves found under field conditions. However, natural air pressure does not resemble a pure sinusoid. It more nearly resembles and can be described by a superposition of many pressure waves to form a spectrum as shown by Gossard (1960), Priestly (1966), and the author in Chapter II. Therefore, to calculate mass flow velocity and displacement amplitudes resulting from air turbulence, new equations have been derived which model air turbulence as a whole spectrum of superimposed, traveling pressure waves.

Derivations

Using Darcy's law in the form

$$\bar{v} = -\frac{K}{\mu} \nabla p \qquad 3.1$$

where $\bar{v}$ is the vector velocity of gas flow (cm/sec), K is the air permeability of the porous media (cm^2), μ is the viscosity of gas (poises), and p is the pressure excess above a large mean barometric pressure (μbar), Kirkham (1946) has shown that the air pressure at any point in the soil must satisfy

$$\frac{\partial p}{\partial t} = \frac{KP_o}{\mu\varepsilon} \left(\frac{\partial^2 p}{\partial x^2} + \frac{\partial^2 p}{\partial y^2} + \frac{\partial^2 p}{\partial y^2} \right) \qquad 3.2$$

where t is time (sec), ε is air porosity, P_o is the mean barometric pressure, and x, y, and z are space variables (cm). The soil is assumed to be homogeneous down to some barrier impermeable to gas flow at depth h so one boundary condition is

$$\frac{\partial p}{\partial z} = 0, \quad z = h \qquad 3.3$$

At the soil surface, the two-dimensional pressure field composed of many superimposed two-dimensional pressure waves traveling parallel to the mean wind in the positive X direction is described mathematically by

$$p = \sum_{n=1}^{N} \sum_{m=1}^{M} \left[\frac{a_{nm}}{2} \cos\left(\frac{2\pi t}{T_n} - \frac{2\pi x}{X_m} - \phi_{xm} - \frac{2\pi y}{Y_m} - \phi_{ym} \right) \right.$$

$$\left. + \frac{a_{nm}}{2} \cos\left(\frac{2\pi t}{T_n} - \frac{2\pi x}{X_m} - \phi_{xm} + \frac{2\pi y}{Y_m} + \phi_{ym} \right) \right] \qquad 3.4$$

where M is the number of distinct periods (T_m) present, N is the number of distinct wave lengths in the X direction (X_m) and in the Y direction (Y_m), a_{nm} is the amplitude of the wave with n^{th} period and m^{th} wave length, ϕ_{xm} is the m^{th} phase angle in the X direction and ϕ_{ym} is the m^{th} phase angle in the Y direction.

To make calculated results from the solution of 3.2 more universal, it is useful to introduce appropriate scaling factors to make the variables dimensionless. The obvious factor used for scaling lengths is the soil depth, h, and the one used for scaling pressures is the barometric pressure, P_o. However, the choice of the appropriate factor for scaling time is not so obvious because no unique period of oscillation exists, as it did for the systems examined by Farrel et al. and Scotter and Raats. The time constant chosen is

$$\tau = \frac{h^2 \mu \varepsilon}{K P_o} \qquad 3.5$$

which is the length of time required for the pressure at the bottom of a soil column to change by a factor of 1/e when a step change of pressure is introduced at the surface. The analogous case for heat flow is discussed in Gebhart (1961, p. 52). Pressure is transmitted rather rapidly through soil, so τ is typically on the order of milliseconds. Thus, introducing

$$x' = x/h \qquad 3.6$$

$$y' = y/h \qquad 3.7$$

$$z' = z/h \qquad 3.8$$

$$t' = t/\tau \qquad 3.9$$

$$p' = p/P_o \qquad 3.10$$

$$a'_{nm} = a_{nm}/P_o \qquad 3.11$$

$$T'_n = T_n/\tau \qquad 3.12$$

$$X'_m = X_m/h \tag{3.13}$$

$$Y'_m = Y_m/h \ , \tag{3.14}$$

Equations 3.2, 3.3, and 3.4 become respectively

$$\frac{\partial p'}{\partial t'} = \left(\frac{\partial^2 p'}{\partial x'^2} + \frac{\partial^2 p'}{\partial y'^2} + \frac{\partial^2 p'}{\partial z'^2}\right) \tag{3.15}$$

$$\frac{\partial p'}{\partial z'} = 0, \ z' = 1 \tag{3.16}$$

$$p' = \sum_{n=1}^{N} \sum_{m=1}^{M} \frac{a'_{nm}}{2} \cos\left(\frac{2\pi t'}{T'_n} - \frac{2\pi x'}{X'_m} - \phi_{xm} - \frac{2\pi y'}{Y'_m} - \phi_{ym}\right)$$

$$+ \frac{a'_{nm}}{2} \cos\left(\frac{2\pi t'}{T'_n} - \frac{2\pi x'}{X'_m} - \phi_{xm} + \frac{2\pi y'}{Y'_m} + \phi_{ym}\right) \tag{3.17}$$

Equation 3.15 is satisfied by a general solution of the form

$$p' = \sum_n \sum_m \left[a^*_{nm} \exp(b_n t' + c_m x' + d_m y' + e_{nm} z' + f_m)\right.$$

$$\left. + g^*_{nm} \exp(h_n t' + i_m x' + j_m y' + k_{nm} z' + l_m)\right] \tag{3.18a}$$

where

$$b_n = c_m^2 + d_m^2 + e_{nm}^2 \tag{3.18b}$$

and

$$h_n = i_m^2 + j_m^2 + k_{nm}^2 \tag{3.18c}$$

If one sets

$$a^*_{nm} = g^*_{nm} = a'_{nm}/2$$

$$b_n = h_n = i2\pi/T'_n$$

$$c_m = i_m = -i2\pi/X'_m$$

$$d_m = -j_m = -i2\pi/Y'_m$$

$$f_m = -i\phi_{xm} - i\phi_{ym}$$

and $\quad \ell_m = -i\phi_{xm} + i\phi_{ym}$

where $i = \sqrt{-1}$, the real part of Equation 3.18a satisfies the upper boundary condition given by Equation 3.17. From Equations 3.18b and 3.18c, e_{nm} and k_{nm} are also uniquely defined as

$$e_{nm} = k_{nm} = \pm\sqrt{\left(\frac{2\pi}{X'_m}\right)^2 + \left(\frac{2\pi}{Y'_m}\right)^2 + i\,\frac{2\pi}{T'_n}} \qquad 3.19$$

Using Dwight (1961, eqns. 58.1, 2), e_{nm} can be broken into real and imaginary parts defined as

$$e_{nm} = \pm(\lambda_{nm} + i\gamma_{nm}) \qquad 3.20$$

where

$$\lambda_{nm} = \left[\frac{\left[\left(\frac{4\pi^2}{X'^2_m} + \frac{4\pi^2}{Y'^2_m}\right)^2 + \left(\frac{2\pi}{T'_n}\right)^2\right]^{1/2} + \left(\frac{4\pi^2}{X'^2_m} + \frac{4\pi^2}{Y'^2_m}\right)}{2}\right]^{1/2} \qquad 3.21$$

$$\gamma_{nm} = \left[\frac{\left[\left(\frac{4\pi^2}{X'^2_m} + \frac{4\pi^2}{Y'^2_m}\right)^2 + \left(\frac{2\pi}{T'_n}\right)^2\right]^{1/2} - \left(\frac{4\pi^2}{X'^2_m} + \frac{4\pi^2}{Y'^2_m}\right)}{2}\right]^{1/2} \qquad 3.22$$

The solution which satisfies Equations 3.15 and 3.17 is now

$$\begin{aligned} p' = \sum_{n=1}^{N}\sum_{m=1}^{M} \Bigg[& \frac{a'_{nm}}{2}\exp(-\lambda_{nm}z')\cos\left(\frac{2\pi t'}{T'_n} - \frac{2\pi x'}{X'_m} - \phi_{xm} - \frac{2\pi y'}{Y'_m} - \phi_{ym} - \gamma_{nm}z'\right) \\ & + \frac{a'_{nm}}{2}\exp(-\lambda_{nm}z')\cos\left(\frac{2\pi t'}{T'_n} - \frac{2\pi x'}{X'_m} - \phi_{xm} + \frac{2\pi y'}{Y'_m} + \phi_{ym} - \gamma_{nm}z'\right) \\ & + \frac{a'_{nm}}{2}\exp(+\lambda_{nm}z')\cos\left(\frac{2\pi t'}{T'_n} - \frac{2\pi x'}{X'_m} - \phi_{xm} - \frac{2\pi y'}{Y'_m} - \phi_{ym} + \gamma_{nm}z'\right) \\ & + \frac{a'_{nm}}{2}\exp(+\lambda_{nm}z')\cos\left(\frac{2\pi t'}{T'_n} - \frac{2\pi x'}{X'_m} - \phi_{xm} + \frac{2\pi y'}{Y'_m} + \phi_{ym} + \gamma_{nm}z'\right)\Bigg] \end{aligned} \qquad 3.23$$

To satisfy Equation 3.16, an additional series feature is needed. It can be incorporated by multiplying the terms in the first set of brackets by $(-1)^k F(k)$ and the terms in the second set of brackets by $(-1)^k F(k+1)$ and adding all terms from k = 0 to infinity. The solution with the additional series satisfies Equation 3.15, and it will also satisfy Equation 3.17 if F is chosen = 1 for k = 0, because all of the terms of the new series cancel each other out except the first term. Differentiation of Equation 3.23, followed by substitution into Equation 3.16, along with careful inspection, shows that if

$$F = e^{-2k(\lambda_{nm} + i\gamma_{nm})}$$

Equation 3.16 is satisfied. The solution for the air pressure at any point in the soil is

$$p' = \sum_{n=1}^{N} \sum_{m=1}^{M} \sum_{k=0}^{\infty} \{(-1)^k \exp[-\lambda_{nm}(2k + z')] \frac{a'_{nm}}{2}$$

$$\left[\cos\left(\frac{2\pi t'}{T'_n} - \frac{2\pi x'}{X'_m} - \phi_{xm} - \frac{2\pi y'}{Y'_m} - \phi_{ym} - (2k + z')\gamma_{nm}\right)\right.$$

$$\left. + \cos\left(\frac{2\pi t'}{T'_n} - \frac{2\pi x'}{X'_m} - \phi_{xm} + \frac{2\pi y'}{Y'_m} + \phi_{ym} - (2k + z')\gamma_{nm}\right)\right]$$

$$+ (-1)^k \exp[-\lambda_{nm}(2k + 2 - z')] \frac{a'_{nm}}{2}$$

$$\left[\cos\left(\frac{2\pi t'}{T'_n} - \frac{2\pi x'}{X'_n} - \phi_{xm} - \frac{2\pi y'}{Y'_n} - \phi_{ym} - (2k + 2 - z')\gamma_{nm}\right)\right.$$

$$\left. + \cos\left(\frac{2\pi t'}{T'_n} - \frac{2\pi x'}{X'_m} - \phi_{xm} + \frac{2\pi y'}{Y'_m} + \phi_{ym} - (2k + 2 - z')\gamma_{nm}\right)\right]\} \qquad 3.24$$

To calculate the vertical velocity of soil gas, Equation 3.1 is used in the form

$$v'_z = \frac{\partial p'}{\partial z'} \qquad 3.25$$

where

$$v_z' = v_z/(\varepsilon h/\tau).$$

Since p is oscillatory, v_z' is also oscillatory and the average for a long period of time is, of course, zero. To calculate an average rate for the vertical movement of the soil air, Farrel et al. defined a mean half period velocity by the average value of the vertical velocity over a half period of the pure sinusoid at the surface. However, since no unique period of wave exists in the boundary conditions specified by Equation 3.4, it appears simpler and more meaningful to define a scaled, root mean square (rms) velocity by

$$v_{rms}' = \left(\frac{1}{t_2 - t_1} \int_{t_1}^{t_2} v_z'^2 \, dt\right)^{1/2} \qquad 3.26$$

where $t_2 - t_1$ is a long period of time with respect to the longest period wave at the surface. The corresponding unscaled rms velocity is given by

$$v_{rms} = v_{rms}' \, (\varepsilon h/\tau).$$

Now if, in the characterization of the waves at the surface, the T_n' are chosen to be integer divisions of total sampling period $t_2 - t_1$, v_{rms}' is particularly easy to calculate, because the integration in Equation 3.26 is over whole periods of orthogonal functions so that most terms are zero. Choosing the T_n' to be integral divisions of the total sampling interval is a reasonable procedure if enough terms are chosen to represent all of the statistical variance of p, such as is done in the spectral analysis technique described in the Appendix.

To calculate v_{rms}', therefore, one first isolates the time dependent factors in Equation 3.26, using trigonometric formulas to obtain

$$v'_{rms} = \{ \frac{1}{t_2 - t_1} \int_{t_1}^{t_2} [\sum_{n=1}^{N} \sum_{m=1}^{M} \sum_{k=0}^{\infty} \cos \frac{2\pi t'}{T'_n}$$

$$(A_{nmk}\cos E_{nmk} + A_{nmk}\cos F_{nmk} - B_{nmk}\sin E_{nmk} - B_{nmk}\sin F_{nmk}$$

$$+ C_{nmk}\cos G_{nmk} + C_{nmk}\cos H_{nmk} - D_{nmk}\sin G_{nmk} - D_{nmk}\sin H_{nmk})$$

$$+(A_{nmk}\sin E_{nmk} + A_{nmk}\sin F_{nmk} + B_{nmk}\cos E_{nmk} + B_{nmk}\cos F_{nmk}$$

$$C_{nmk}\sin G_{nmk} + C_{nmk}\sin H_{nmk} + D_{nmk}\cos G_{nmk} + D_{nmk}\cos H_{nmk})$$

$$\frac{\sin 2\pi t'}{T'_n}]^2 \, dt \}^{1/2} \qquad 3.27$$

where

$$A_{nmk} = -\frac{1}{2}(-1)^k a'_{nm}\lambda_{nm}\exp[-\lambda_{nm}(2k + z')]$$

$$B_{nmk} = +\frac{1}{2}(-1)^k a'_{nm}\gamma_{nm}\exp[-\lambda_{nm}(2k + z')]$$

$$C_{nmk} = +\frac{1}{2}(-1)^k a'_{nm}\lambda_{nm}\exp[-\lambda_{nm}(2k + 2 - z')]$$

$$D_{nmk} = -\frac{1}{2}(-1)^k a'_{nm}\gamma_{nm}\exp[-\lambda_{nm}(2k + 2 - z')]$$

$$E_{nmk} = \frac{2\pi x'}{X'_m} + \phi_{xm} + \frac{2\pi y'}{Y'_m} + \phi_{ym} + (2k + z')\gamma_{nm}$$

$$F_{nmk} = \frac{2\pi x'}{X'_m} + \phi_{xm} - \frac{2\pi y'}{Y'_m} - \phi_{ym} + (2k + z')\gamma_{nm}$$

$$G_{nmk} = \frac{2\pi x'}{X'_m} + \phi_{xm} + \frac{2\pi y'}{Y'_m} + \phi_{ym} + (2k + 2 - z')\gamma_{nm}$$

$$H_{nmk} = \frac{2\pi x'}{X'_m} + \phi_{xm} - \frac{2\pi y'}{Y'_m} - \phi_{ym} + (2k + 2 - z')\gamma_{nm}$$

Then, since all the T'_n are integer divisions of $t_2 - t_1$, one notes that only terms containing $\cos^2(\frac{2\pi t'}{T'_n})$ or $\sin^2(\frac{2\pi t'}{T'_n})$ after squaring will be

unequal to zero after the integration so that Equation 3.27 becomes

$$v'_{rms} = \{\frac{1}{2} \sum_{n=1}^{N} \sum_{m=1}^{M} \sum_{k=0}^{\infty}$$

$$[(A_{nmk}\cos E_{nmk} + A_{nmk}\cos F_{nmk} - B_{nmk}\sin E_{nmk} - B_{nmk}\sin F_{nmk}$$

$$+ C_{nmk}\cos G_{nmk} + C_{nmk}\cos H_{nmk} - D_{nmk}\sin G_{nmk} - D_{nmk}\sin H_{nmk})^2$$

$$+(A_{nmk}\sin E_{nmk} + A_{nmk}\sin F_{nmk} + B_{nmk}\cos E_{nmk} + B_{nmk}\cos F_{nmk}$$

$$+ C_{nmk}\sin G_{nmk} + C_{nmk}\sin H_{nmk} + D_{nmk}\cos G_{nmk} + D_{nmk}\cos H_{nmk})^2]\}^{1/2} \qquad 3.28$$

After squaring the quantities in parentheses, applying trigonometric identities, and substituting for A, B, C, D, E, F, G, and H, Equation 3.28 can be simplified to

$$v'_{rms} = 1/2 \{ \sum_{n=1}^{N} \sum_{m=1}^{M} a'^2_{nm} (\lambda_{nm}^2 + \gamma_{nm}^2)[1 + \cos(\frac{4\pi y'}{Y'_m} + 2\phi_{ym})]$$

$$\sum_{k=0}^{\infty} [\exp(-2\lambda_{nm}(2k + z')) + \exp(-2\lambda_{nm}(2k + 2 - z'))$$

$$-2\exp(-2\lambda_{nm}(2k + 1)) \cos 2\gamma_{nm}(z' - 1)]\}^{1/2} \qquad 3.29$$

Equation 3.29 predicts the scaled root mean square vertical velocity at any depth z' in the porous media.

The displacement amplitude can also be computed from Equation 3.24. Since displacement is the integral of velocity over time, as indicated in Equation 3.30

$$D = \int v \, dt \qquad 3.30$$

Equations 3.24 and 3.25 can be used to derive equations to calculate displacement amplitude.

Since v is oscillatory, D is also oscillatory, and, therefore, an average D in the vertical direction is probably the most meaningful parameter which can be defined. Analogous to the root mean square velocity, the average D in the vertical direction is taken as the root mean square displacement in the vertical direction. The displacement amplitude is then defined as $\sqrt{2}$ times the rms displacement.

If D is scaled with respect to the soil depth so that

$$D' = \frac{D}{eh} \tag{3.31}$$

then, using Equation 3.25, the rms displacement is defined by

$$D'_{rms} = \{\frac{1}{t_2 - t_1} \int_{t_1}^{t_2} [\int \frac{\partial p'}{\partial z'} dt']^2 dt\}^{1/2} \tag{3.32}$$

After substituting Equation 3.24 for p' in Equation 3.32 and integrating, one has an equation exactly analogous to Equation 3.26 for velocity. Then, if steps similar to the ones used to go from Equation 3.26 to 3.29 are taken, one obtains

$$D'_{rms} = 1/2\{\sum_{n=1}^{N}\sum_{m=1}^{M} a'_{nm}{}^2 (\frac{T\dot{h}}{2\pi})^2 (\lambda_{nm}{}^2 + \gamma_{nm}{}^2) [1 + \cos(\frac{4\pi y'}{Y'_m} + 2\phi_{ym})]$$

$$\sum_{k=0}^{\infty} [\exp(-2\lambda_{nm}(2k + z')) + \exp(-2\lambda_{nm}(2k + 2 - z'))$$

$$-2\exp(-2\lambda_{nm}(2k + 1))\cos 2\gamma_{nm}(z' - 1)]\}^{1/2} \tag{3.33}$$

Results and Discussion

Equations 3.29 and 3.33 for the rms velocity and displacement have several interesting features. First, neither v'_{rms} nor D'_{rms} has any x dependence, so both are uniform in the downwind direction. The y dependence changes with the phase relationships between all the various waves in the cross-wind directions. Presumably, these angles are rather random in a turbulent flow, and calculations of v' using sets of random numbers for ϕ_{ym} showed deviations of only a few per cent on either side of the value for v' obtained by setting all $\phi_{ym} = 0$. The effect of wave superposition can also be seen. The total v'_{rms} or D'_{rms} equals the square root of the sum of squares of the velocities or displacements for the individual waves.

For single waves, velocities computed from Equation 3.29 (with $Y_m = \infty$, $\phi_{ym} = 0$, $y' = 0$) are equivalent to velocities computed from the equation of Farrel et al. multiplied by $\pi/2\sqrt{2}$. One notes in Equations 3.29 and 3.33 that for a single pressure wave v' and D' vary linearly with the amplitude. The dependency on period and wave length for a single wave is more complicated. In Figure 3.1 are plotted lines of constant v'_{rms} for $z' = 0$ against the scaled period and scaled X-wave length of single waves of scaled amplitude 10^{-6}. The curves in Figure 3.1 and all of the other figures are for the arbitrary point $y' = 0$ and for y direction phase angles assumed equal to zero. The curves were computed using

$$Y_m = X_m, \qquad X_m \leq 50 \text{ cm}$$

$$Y_m = (84.)\left(\frac{X_m}{100.}\right)^{0.74}, \qquad X_m > 50 \text{ cm} \qquad 3.34$$

Figure 3.1 Contour lines of constant scaled soil air velocity at zero depth plotted against the log of scaled period and X-wave length of pressure wave at the soil surface. The vertical lines in the upper left indicate no change of velocity with period. The horizontal lines in the lower right indicate no change of velocity with X-wave length. The four diagonal lines show a wind velocity of 100 cm/sec scaled to the four soils in Table 3.1, and, for most soils, they indicate that the winds found in nature fall into the region of the curve where there is no change of soil air velocity with the period of associated pressure waves.

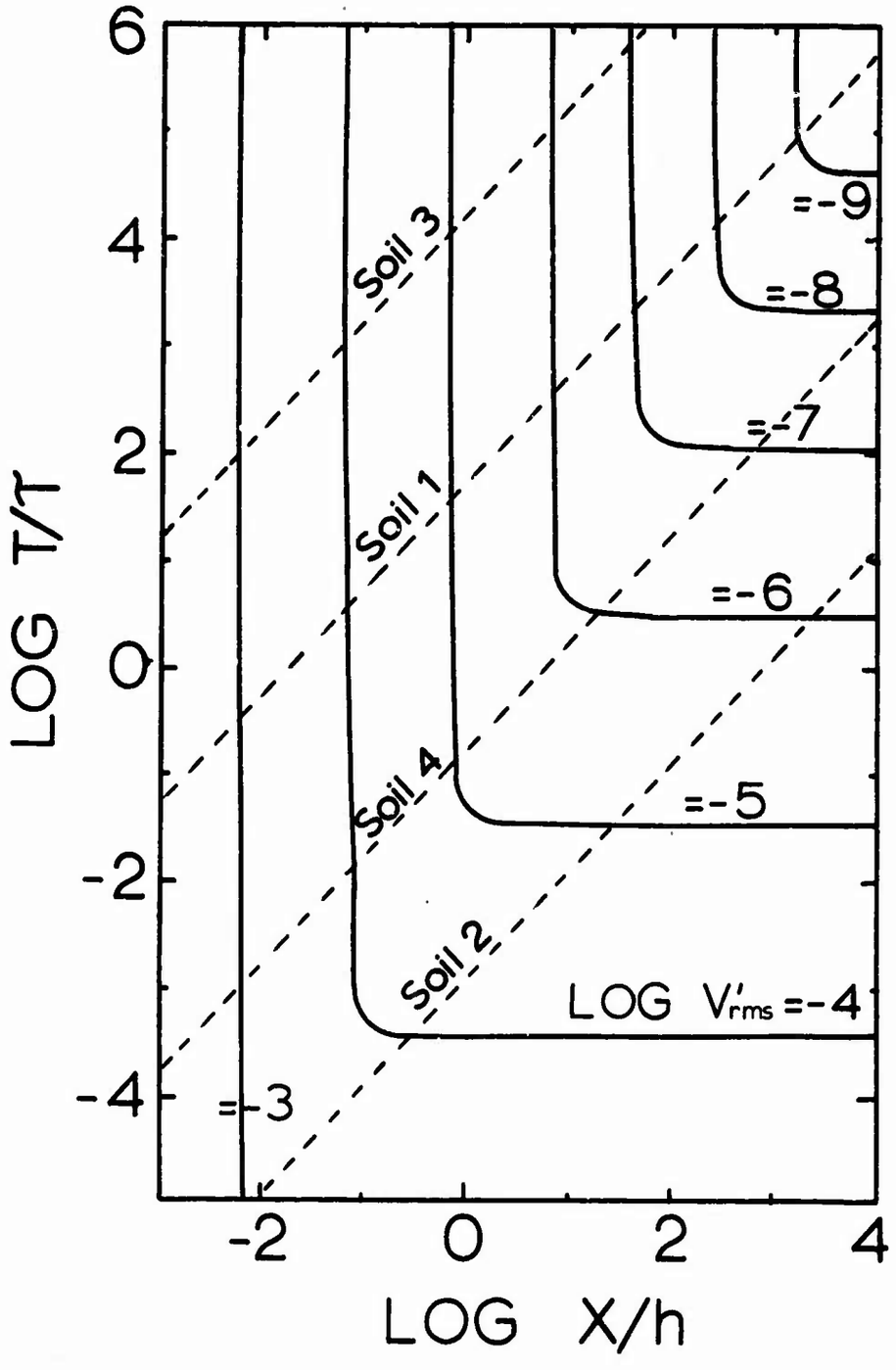
6
4
2
0
-2
-4
LOG T/τ
-2
0
2
4
LOG X/h
Soil 3
Soil 1
Soil 4
Soil 2
=-9
=-8
=-7
=-6
=-5
=-3
LOG V'rms =-4

which is a relation found by Priestly (1966) for pressure fluctuations over short grass. Since the wave lengths in Equation 3.34 are not scaled, Figure 3.1 strictly applies only to a medium which has the same properties as Soil I in the Table 3.1. However, one can see that, when the log of the scaled period is greater than twice the log of the scaled X-wave length -2, the velocity does not change with period but does decrease linearly with increasing wave length up to a scaled wave length of 1.0, and then it decreases somewhat faster than linearly. When the log of the scaled period is less than twice the log of the scaled X-wave length - 2, the velocity does not change with X-wave length but does decrease with the square root of increasing period up to a scaled period of 1.0, and then it decreases somewhat faster than with the square root. The lines corresponding to a wind of 100 cm/sec are scaled and plotted for each of the four soils listed in Table 3.1. For the shallow soils, I and III, an eddy size of 2.5 cm is at log X/h = 0, so a wind of 100 cm/sec is found to be mostly in the region where soil air velocity does not change with period but does change with X-wave length. Thus, the physical size of the eddies, and not their period, determines how much they influence soil air velocity. For the deep soils, II and IV, an eddy size of 2.5 cm is at log X/h = -4, so, also in the deep soils, eddy size and not period is important over a large range.

The attenuation with depth of single waves whose scaled amplitude is 10^{-6} is shown in Fig. 3.2. The left side shows that waves which have a period which is long compared to τ cause a low soil air velocity at the surface, and this velocity is attenuated about linearly with depth. On

Table 3.1 Properties of four soils
(The properties correspond to the Main Sand and 10 mm gravel studied by Farrel et al. (1966))

Property	Soil I	Soil II	Soil III	Soil IV
Depth (cm)	2.5	2.50×10^{5}	2.5	2.50×10^{5}
Permeability (cm^2)	1.15×10^{-6}	1.15×10^{-6}	3.45×10^{-4}	3.45×10^{-4}
Time constant* (sec)	3.97×10^{-4}	3.97×10^{6}	1.32×10^{-6}	1.32×10^{4}
Particle size (cm)	0.04	0.04	1.0	1.0

*Assume porosity of 0.4, barometric pressure of 10^6 μbar, and viscosity of 1.83×10^{-4} poise

Figure 3.2 Scaled soil air rms velocity plotted against scaled depth. On the left the X-wave length of the pressure wave at the surface is held constant while the period is shortened. For waves of long period, the velocity at zero depth is rather low, but there is little attenuation with depth. Short period waves yield high velocities at zero depth, but they rapidly attenuate with depth. On the right the same effect is seen as one shortens the X-wave length while holding period constant.

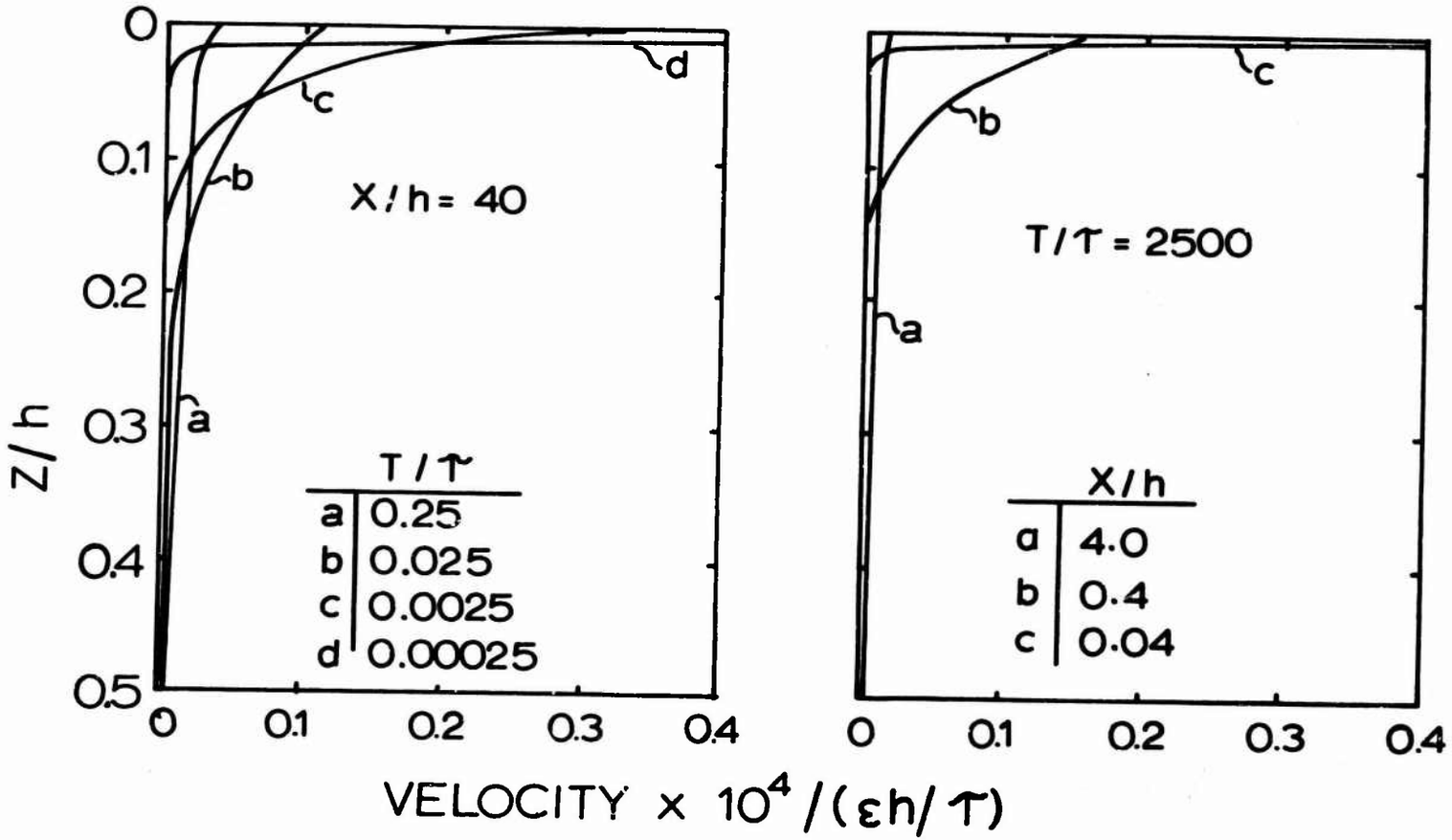
0
0.1
0.2
0.3
0.4
0.5
Z/h
X/h = 40
T/τ
a 0.25
b 0.025
c 0.0025
d 0.00025
T/τ = 2500
X/h
a 4.0
b 0.4
c 0.04
0
0.1
0.2
0.3
0.4
VELOCITY x 10^4 /(εh/τ)

the other hand, waves which have periods short compared to τ cause a high soil air velocity at the surface, but this velocity is rapidly attenuated with depth.

In Chapter II, several spectra were presented for the air pressure at the soil surface. The spectral density was found to decrease in a roughly linear manner with a slope of about -2.0 over the entire frequency range covered. There was some change in the height or altitude of the curve with wind velocity. The curve can be described empirically by

$$s(f) = Af^{-2} \qquad 3.35$$

where

$s(f)$ = spectral density

f = frequency

A = altitude of curve = spectral density at f = 1 cycle/sec.

By breaking a curve into frequency increments, a procedure which is the opposite of obtaining a spectrum (see Appendix), the amplitude of n^{th} wave can be obtained from

$$a_n = \sqrt{\frac{s(f_n)\Delta f}{2}} \qquad 3.36$$

where

a_n = amplitude of wave with n^{th} frequency and m^{th} wave length

Δf = frequency increment

f_n = n^{th} frequency

Thus, from the spectra in Chapter II, the amplitudes of a series of pressure waves at the soil surface are known for each of a broad range of frequencies. A two-dimensional spectrum, also presented in Chapter II, shows that, over a limited range of frequency and wave number, air pressure

tends to move in a frozen pattern of turbulence. Thus, one can obtain the wave length of each wave from its frequency and a supplementary measurement of mean wind, so that

$$X_m = W/f_n \qquad 3.37$$

Using Equations 3.34, 3.35, 3.36, and 3.37, computations of soil air rms velocity and displacement have been made from Equations 3.29 and 3.33 with $y' = \phi_{ym} = 0$. The frequency increment was taken as 0.1 on a log scale so that, as one moved toward higher frequencies, a wider and wider frequency band was taken to represent a single wave. A trial run using $\Delta f = 0.05$ on a log scale increased the calculated velocities only a few per cent, so presumably the frequency increment was small enough (and the corresponding number of waves large enough) to adequately represent the spectra. The computations were made using a value of 3.14 for the altitude, A. Using Equations 3.36 and 3.35, the velocities and displacement amplitudes from Equations 3.29 and 3.33 are seen to vary with the square root of the altitude. Consequently, rms velocities or displacements may easily be obtained for spectra with an altitude other than 3.14 from

$$\frac{v_{rms}}{v_{rms(3.14)}} = \frac{D_{rms}}{D_{rms(3.14)}} = \sqrt{\frac{A}{3.14}} \qquad 3.38$$

Early trial runs showed that the frequency range covered by the spectra in Chapter II was not adequate because, for shallow depths, velocities were still increasing with frequency at a frequency of 100 cycle/sec. Therefore, the computations have been made covering a range from 10^{-6} (which is lower than the point where Gossard (1960) found the spectral density to reach a maximum) to 10^{4} cycle/sec.

The results of the computations for the four soils in Table 3.1 are presented in Figures 3.3-3.8. In Fig. 3.3, the log of soil air rms velocity at several depths is plotted against the log of frequency for a wind speed of 100 cm/sec. It can be seen that increasing permeability, going from Soils I and II in the left graph to Soils III and IV in the right, caused a porportional increase in velocity for all frequencies. The deep soils (II and IV) have higher velocities than the shallow soils (I and III) at low frequencies, but, at higher frequencies, the curves become identical. In the shallow soils, the velocity caused by high frequency waves is several orders of magnitude higher than the velocity caused by low frequency waves. Greater attenuation with depth of the velocities due to higher frequencies is apparent for all four soils.

In Figure 3.4, the log of soil air rms displacement at several depths is plotted against the log of frequency for a wind speed of 100 cm/sec. The low frequencies make the largest contribution to displacement at all depths in all the soils. Since the rms displacement increases all the way to the low frequency edge of the graph, Equation 3.35 may inadequately represent the spectrum of air pressure. However, the summations to obtain the total rms displacement, soon to be presented, started at 10^{-6} cycle/sec, so the maximum spectral density found by Gossard at $10^{-5.5}$ cycle/sec was covered. Increasing permeability causes a nearly proportional increase in displacement over the whole frequency range. The rms displacement for the deep soils is always greater than it is for the shallow soils, starting with a difference of ten at the lowest frequency and increasing to 1000 at the highest frequency. The contributions of the higher frequencies attenuate rapidly with depth for all the soils.

Figure 3.3 Log of soil air rms velocity at various depths for four soils plotted against the log of frequency of the pressure wave at the soil surface which has caused the velocity. The numbers on the curves give the depth in cm. The velocity was computed from a spectrum of air pressure at the soil surface similar to those presented in Chapter II for a wind speed of 100 cm/sec. Before computation, the spectrum was split into frequency bands 0.1 log units wide, and the velocity shown here is the velocity which would be caused by the various bands if each were present all alone. The frequencies higher than 1 cycle/sec are seen to cause the highest soil air velocities, and the effects of the high frequencies are seen to attenuate most rapidly with increasing depth. Soils I and II have low permeability while III and IV have high permeability; soils II and IV are deep while I and III are shallow.

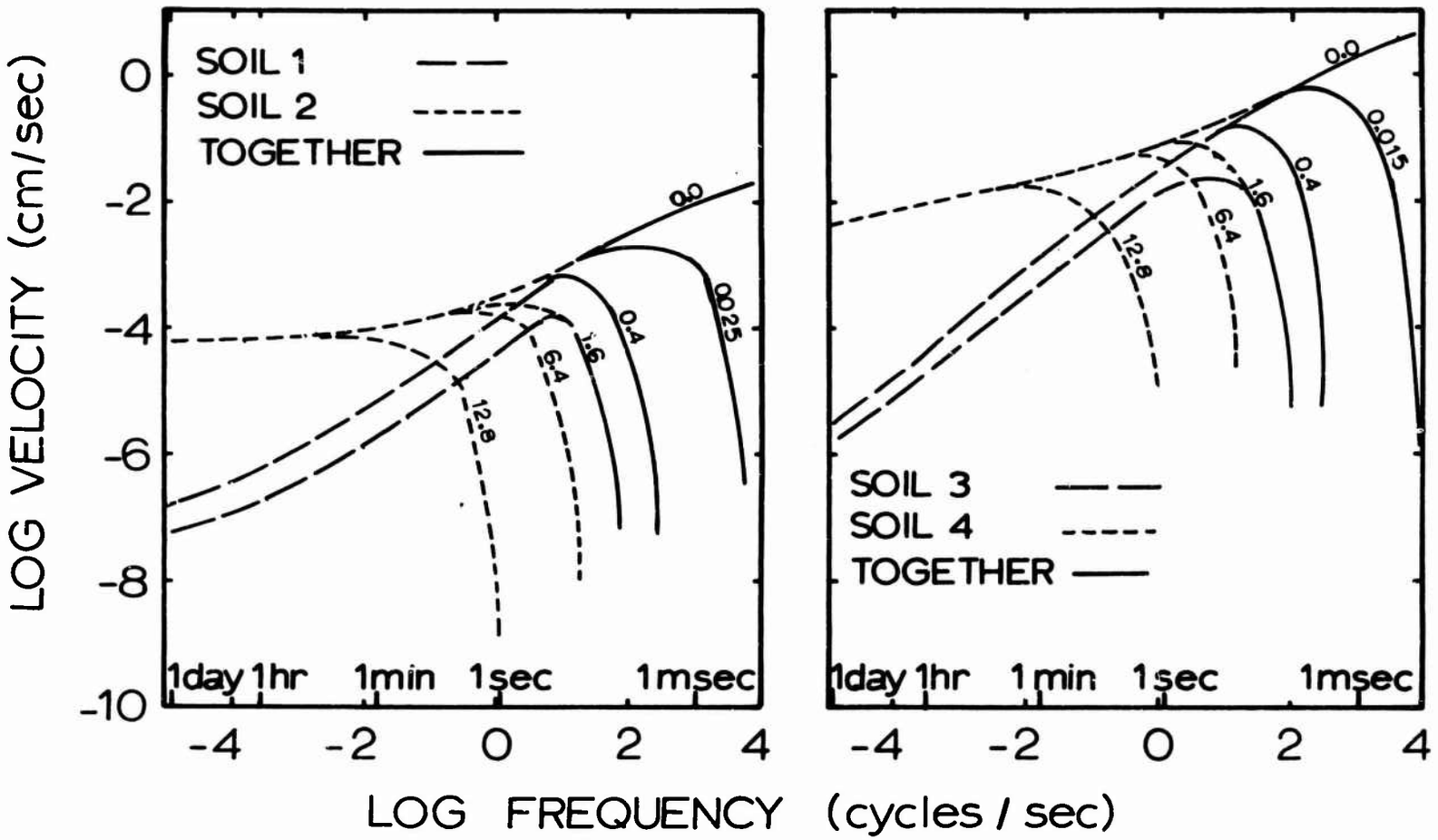
LOG VELOCITY (cm/sec)
0
-2
-4
-6
-8
-10
SOIL 1
SOIL 2
TOGETHER
0.9
0.025
0.4
1.6
6.4
12.8
1day 1hr 1min 1sec 1msec
-4 -2 0 2 4
SOIL 3
SOIL 4
TOGETHER
0.9
0.015
0.4
1.6
6.4
12.8
1day 1hr 1min 1sec 1msec
-4 -2 0 2 4
LOG FREQUENCY (cycles / sec)

Figure 3.4 Log of soil air rms displacement at various depths for four soils plotted against the log of the frequency of the pressure wave at the soil surface which has caused the displacement. The numbers on the curves give the depth in cm. The displacement was computed from a spectrum of air pressure at the soil surface similar to those presented in Chapter II for a wind speed of 100 cm/sec. Before computation, the spectrum was split into frequency bands 0.1 log units wide, and the displacement shown here is the displacement which would be caused by the various bands if each were present all alone. The lowest frequencies are seen to cause the greatest soil air displacement, and the effects of high frequencies are seen to attenuate most rapidly with increasing depth. Soils I and II have low permeability while III and IV have high permeability; soils II and IV are deep while I and III are shallow.

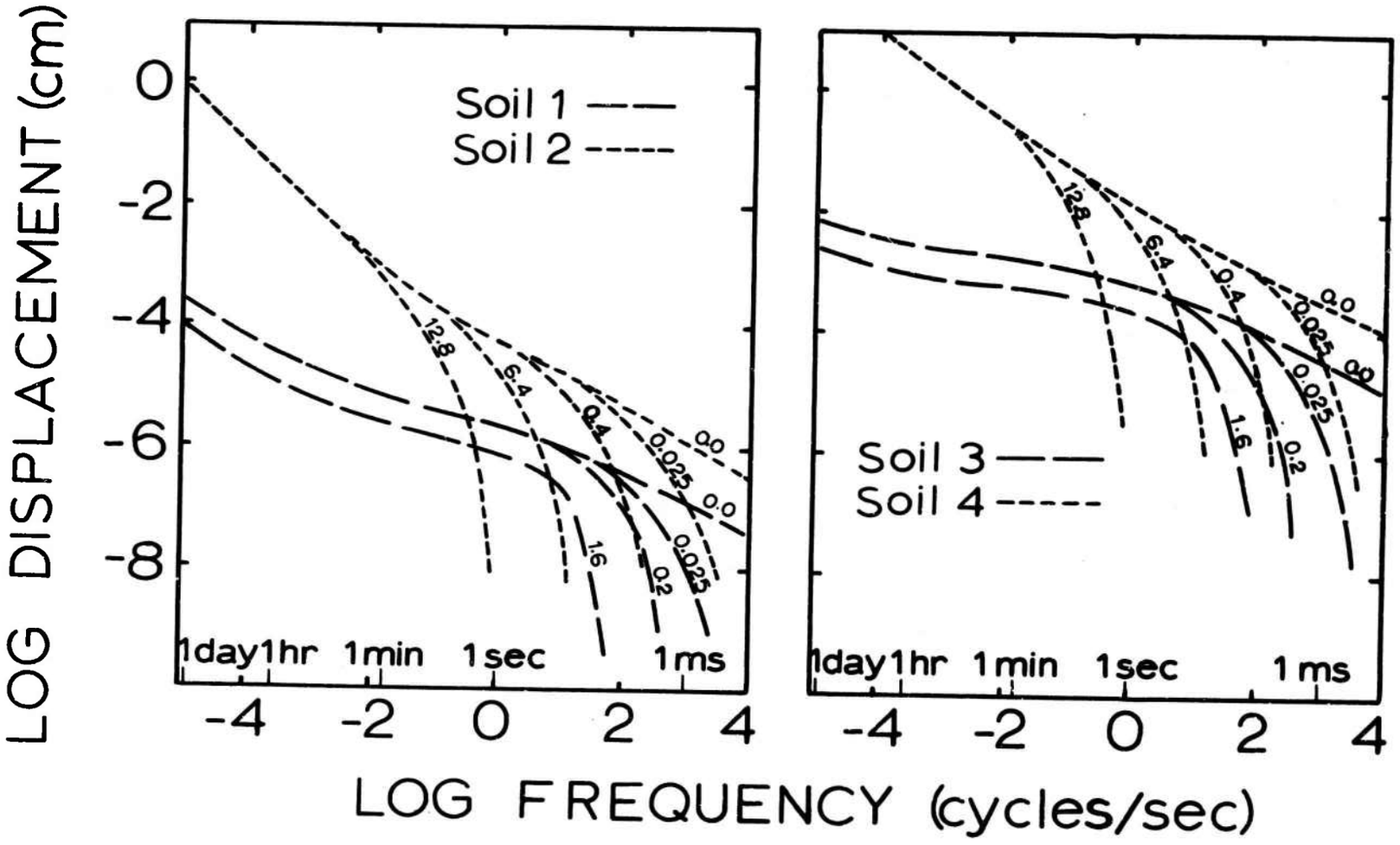
LOG DISPLACEMENT (cm)
0
-2
-4
-6
-8
Soil 1
Soil 2
Soil 3
Soil 4
12.8
6.4
0.4
0.0
0.025
1.6
0.2
1day
1hr
1min
1sec
1ms
-4
-2
0
2
4
LOG FREQUENCY (cycles/sec)

Figure 3.5 Log of soil air rms velocity at a depth of 0.025 cm at three wind speeds plotted against the log of the frequency of the pressure wave at the soil surface which has caused the velocity. The numbers on the curves give the wind speed in cm/sec. The velocity was computed from a spectrum of air pressure at the soil surface similar to those in Chapter II but with constant altitude of the spectral density curve. The soil air velocity is seen to decrease with increasing wind speed at the surface. This effect is due to a consequent lengthening of wave lengths without changing amplitude. Soils I and II have low permeability while III and IV have high permeability; soils II and IV are deep while I and III are shallow.

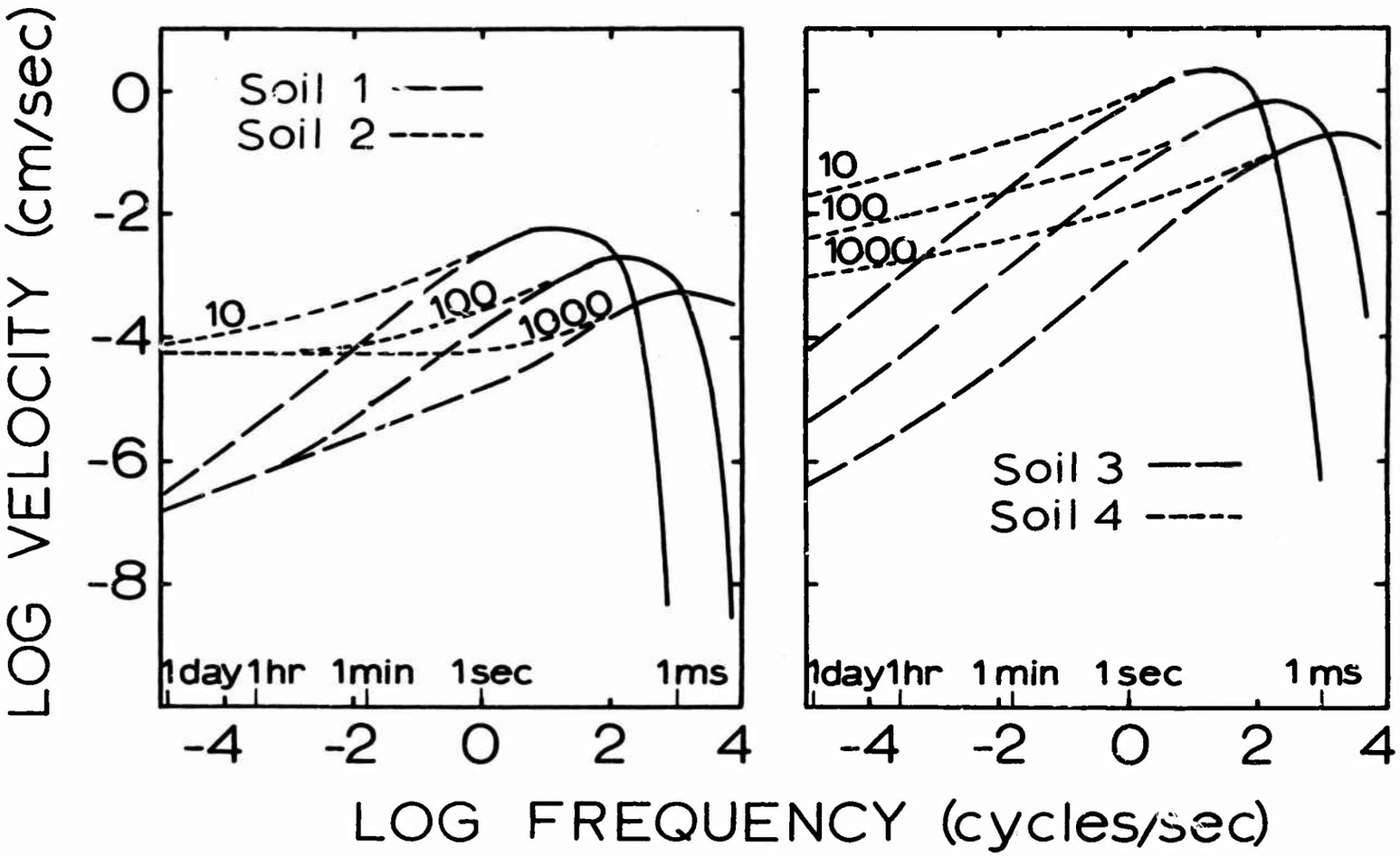
LOG VELOCITY (cm/sec)
0
-2
-4
-6
-8
Soil 1
Soil 2
10
100
1000
Soil 3
Soil 4
1day 1hr 1min 1sec 1ms
-4 -2 0 2 4
LOG FREQUENCY (cycles/sec)

Figure 3.6 Log of soil air rms displacement at a depth of 0.025 cm at three wind speeds plotted against the log of the frequency of the pressure wave at the soil surface which has caused the displacement. The numbers on the curves give the wind speed in cm/sec. The displacement was computed from a spectrum of air pressure at the altitude of the spectral density curve. The soil air displacement is seen to decrease with increasing wind speed at the surface. This effect is due to a consequent lengthening of wave lengths without changing amplitudes. Soils I and II have low permeability while III and IV have high permeability; soils II and IV are deep while I and III are shallow.

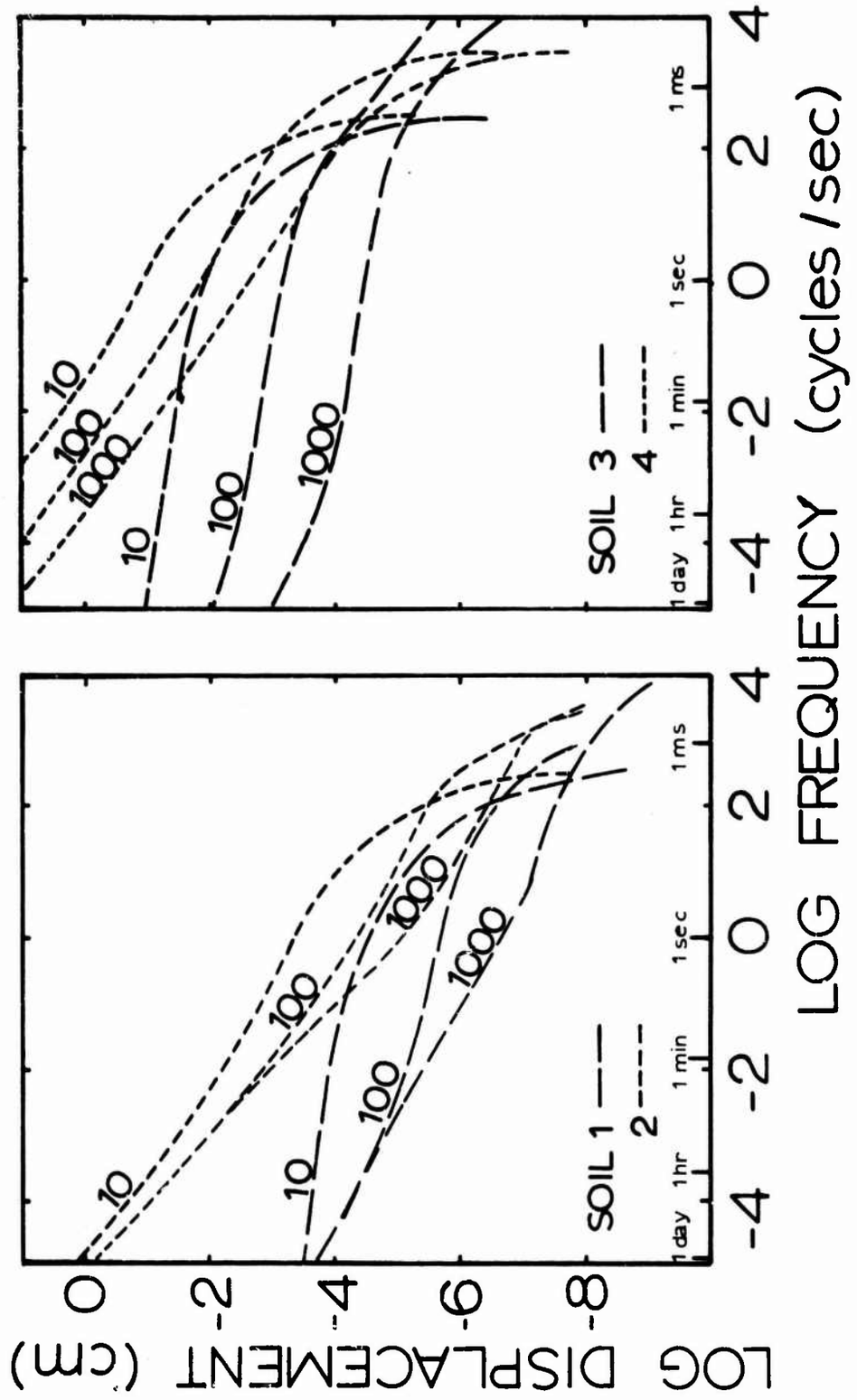
LOG DISPLACEMENT (cm)
0
-2
-4
-6
-8
-4
-2
0
2
4
LOG FREQUENCY (cycles / sec)
1 day
1 hr
1 min
1 sec
1 ms
SOIL 1
2
SOIL 3
4
10
100
1000

In Figure 3.5, the log of soil air rms velocity at a depth of 0.025 cm is plotted against the log of frequency for three wind speeds. The features of the changes of velocity with frequency and permeability are the same as for Figure 3.3. The effect of increasing the wind speed is to decrease the soil air velocity at all frequencies and both permeabilities, except that there is little change at both low frequency and low permeability. While a decrease in soil air velocity with an increase in wind at the soil surface may be surprising and seem backward at first, the explanation is rather simple. These soil air velocities have been calculated using a constant altitude of 3.14 for the air pressure spectrum. Thus, the amplitude of the pressure waves was held constant, while the wave lengths calculated from Equation 3.37 were increased. As illustrated in Fig. 3.1, an increase in wave length causes a proportional decrease in soil air velocity for most soils over a wide range of wave lengths found in nature. An increase in wind velocity causes an increase in soil air velocity by increasing the altitude of the pressure spectrum. The increase is not as great as one might expect, however, because of the accompanying increase in wave lengths.

In Figure 3.6, the soil air rms displacement at a depth of 0.025 cm is plotted against frequency for three wind speeds. The changes in the displacement amplitude with frequency and permeability are similar to those illustrated in Fig. 3.4. The effect of increasing wind speed is to decrease the displacement. As with the soil air velocity in Fig. 3.5, the reason for this decrease with increasing wind is that the altitude of the air pressure spectrum was held constant. Therefore, the only effect of the wind is to increase the wave lengths which, in turn, cause a decrease in rms displacement.

The total rms soil air velocity which one obtains from Equation 3.29 is the square root of the sum of squares of all the velocities for all the frequencies plotted in Fig. 3.3 and 3.5. In Fig. 3.7, the log of this total rms velocity is plotted against the log of depth for four soils and three wind velocities. As can be seen, the velocity ranges from infinitesimal to several cm/sec near the surface of the soil with higher permeability. The values at 0.025 depth are surprisingly close to velocities calculated for zero depth by Farrel et al. (1966) from their equation for the single pressure waves they measured with a differential pressure transducer.

There is a roughly proportional increase of velocity with permeability at all depths in going from soils I and II to III and IV. The nearly straight, now vertical lines at the top of the graph for all soils show the exponential decrease of soil air velocity with depth at shallow depths. The effect of increasing wind velocity is to decrease the soil air velocity, but, as discussed previously, the decrease comes from increasing the wave lengths while holding altitude constant.

The total soil air rms displacement one obtains from Equation 3.33 is the square root of the sum of squares of all the displacements for all the frequencies plotted in Fig. 3.4 and 3.6. The rms displacement is seen to increase by a factor of about 10^4 when the depth increased by a factor of 10^5. Increasing permeability also caused the displacement to increase, but the amount of increase is influenced by the wind speed. The wind speed is seen to have a large influence at the high permeability in Soils III and IV and very little influence in the low permeability soils, I and II.

Figure 3.7 Log of soil air rms velocity for four soils and three wind speeds plotted against the log of soil depth. The numbers on the curves are wind speed in cm/sec. The velocity has been computed from a spectrum of air pressure at the soil surface similar to those presented in Chapter II. Soils I and II have low permeability while III and IV have high permeability.

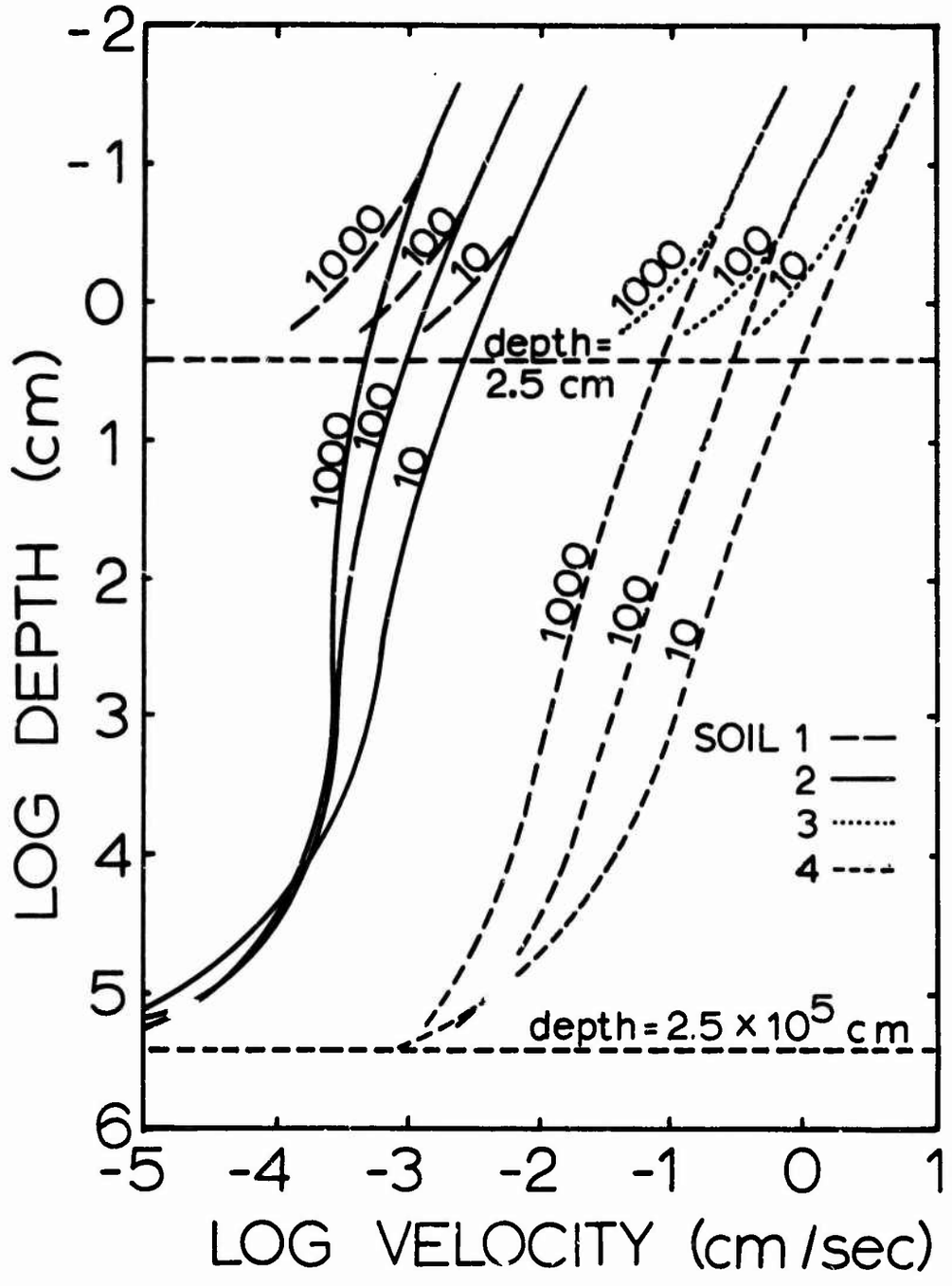
LOG DEPTH (cm)
LOG VELOCITY (cm/sec)
depth= 2.5 cm
depth = 2.5 x 10^5 cm
1000
100
10
SOIL 1
2
3
4

The soil air rms velocity and rms displacement have been calculated from Equation 3.29 and 3.33 for the spectra in Chapter II for a variety of conditions. The significance of their contribution to soil gas exchange, however, can only be assessed by evaluating their effect upon the mixing of the soil air for the various conditions. Scotter and Raats (1968) have developed a method for evaluating the increase in effective diffusion coefficient or "dispersivity" of the soil air, when there is an oscillating flow velocity. Figure 3.9, which was obtained by them, shows the increase of dispersivity with increase in scaled velocity and scaled displacement amplitude. By scaling flow velocities and displacement amplitudes to particle size and diffusion coefficient, the dispersivity may be obtained for another system from their measurements if the medium is similar to their glass spheres and the flow is similar to their purely oscillatory flow. The dashed line in the upper graph in Figure 3.9 represents the dispersivity as a function of a steady flow velocity from an equation derived by Saffman (1960), as discussed by Scotter and Raats. It represents roughly the upper limit for the other curves.

If one assumes, for the sake of illustration, that soil particles are similar to glass spheres, one can use Figure 3.9 directly to obtain dispersivities for field media. If one further assumes that root mean square parameters for somewhat random flows are similar to rms parameters for purely oscillatory flows, one can use Figure 3.9 to obtain dispersivities for field flows. This can be accomplished because Figure 3.9 can be converted to rms parameters by multiplying the velocity scales by $\pi/2\sqrt{2}$ and the displacement scales by $1/\sqrt{2}$. Equations 3.29 and 3.33 can then be used to obtain rms velocities and displacements for field flows.

Figure 3.8 Log of soil air displacement for four soils and three wind speeds plotted against the log of soil depth. The numbers on the curves indicate wind speed in cm/sec. The displacement has been computed from a spectrum of air pressure at the soil surface similar to those presented in Chapter II. Soils I and II have low permeability while III and IV have high permeability.

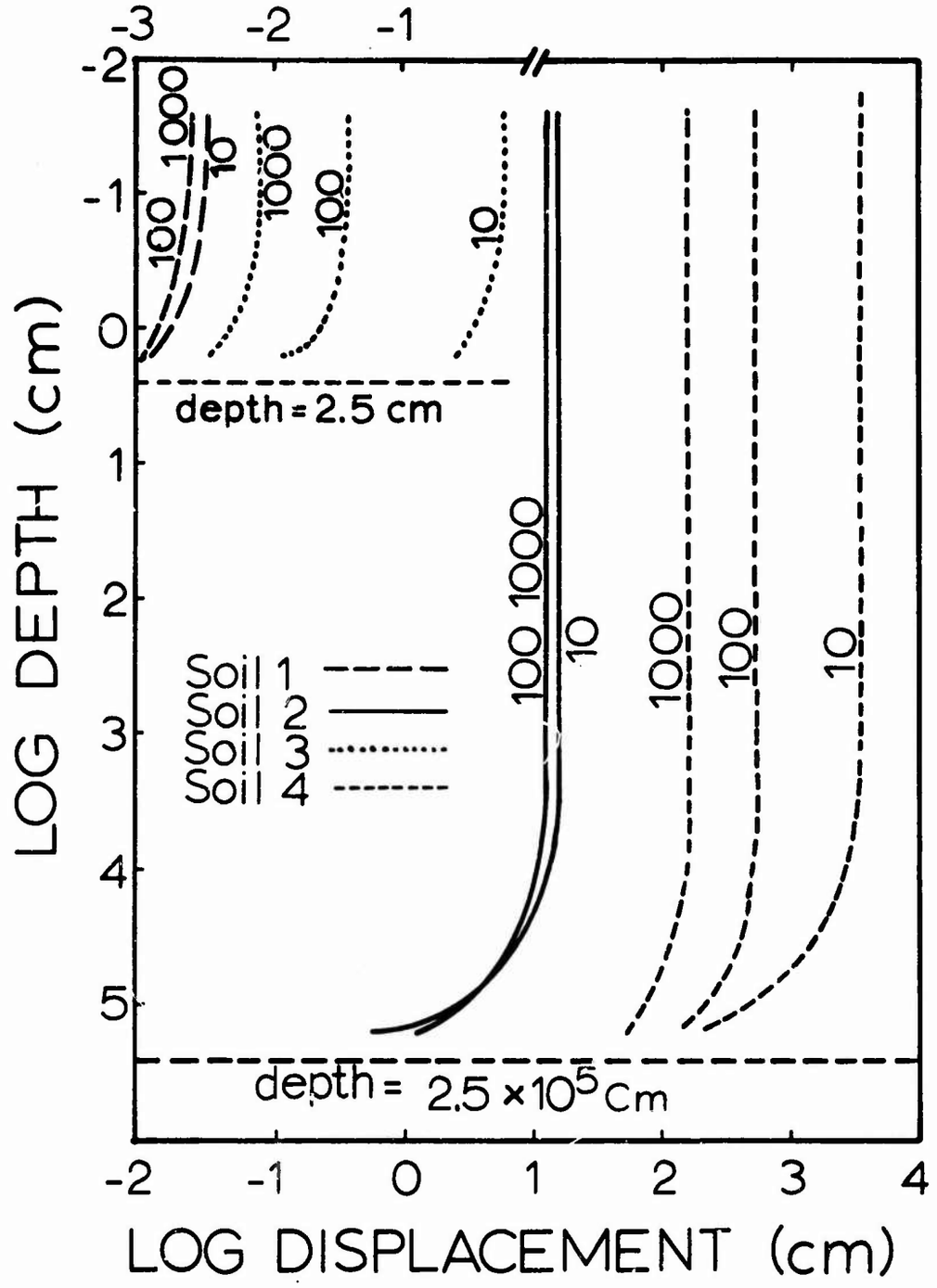
-3
-2
-1
-2
-1
0
1
2
3
4
5
LOG DEPTH (cm)
depth = 2.5 cm
depth = 2.5 x 10^5 Cm
Soil 1
Soil 2
Soil 3
Soil 4
100
1000
10
1000
100
10
100
1000
10
1000
100
10
-2
-1
0
1
2
3
4
LOG DISPLACEMENT (cm)

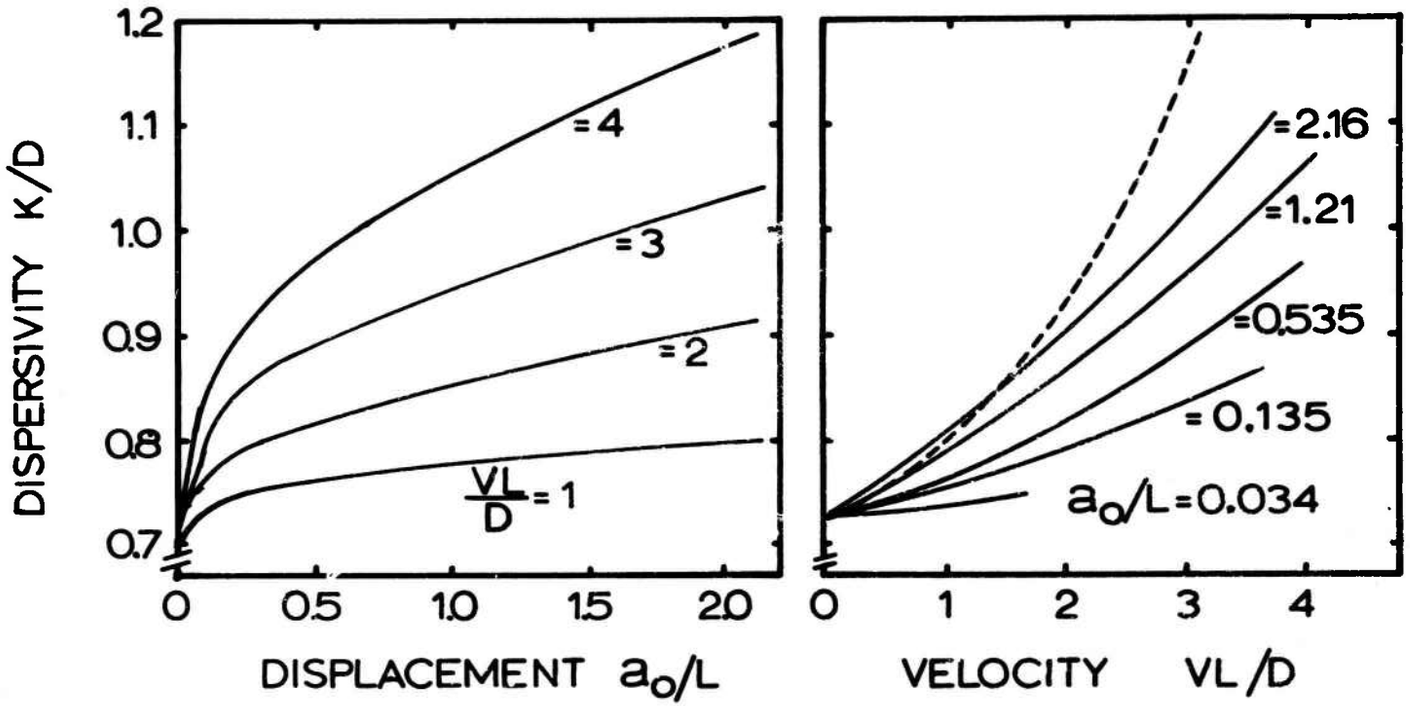

Figure 3.9 Scaled soil air dispersion coefficient plotted against scaled soil air velocity and displacement amplitude from Scotter and Raats (1968). The dashed line in the left graph is a limiting theoretical curve for steady flow they computed from Saffman (1960). The L is the diameter of the soil particles, and the D is the diffusion coefficient for air.

Scotter and Raats (1969) developed an equation to calculate the ratio of the flux of a gas when there is a non-zero soil velocity to the diffusive flux when there is zero velocity. The equation is

$$\frac{F}{F_o} = \frac{d}{s \int_o^d \frac{dz}{f(z)}}$$

where

F = the flux of gas

F_o = the flux due to pure diffusion

d = the depth in the soil at which the concentration of the gas is held constant. The concentration is assumed to be zero at the soil surface.

s = tortuosity of the soil = 0.71 for the glass spheres of Scotter and Raats

f(z) = K*/D = ratio of dispersivity, K*, to diffusion coefficient

The integral can be evaluated numerically by using the modified Figure 3.9 to obtain values of K*/D from the rms velocity and rms displacement at each depth. Thus, using Figures 3.4 and 3.8 to obtain rms velocities and rms displacements, values of F/F_o were computed for the four soils of Table 3.1 for d = 2.5 and s = 0.71. The results of the calculation are presented in Table 3.2 for four combinations of air pressure spectrum altitude and wind speed. For the soils with low permeability, I and II, the soil air velocities and displacements are low, and no increase of flux beyond pure diffusion is predicted. In Soil III, a slight increase in flux is predicted for the highest wind speed condition. For Soil IV, the scaled displacements are in the hundreds, which is completely off the graph of Fig. 3.9. Therefore, the limiting curve shown in the

Table 3.2 Values of F/F_o calculated from Equation 3.39 using four wind conditions for the four soils in Table 3.1

Altitude of pressure spectrum	Wind (cm/sec)	Soil			
		Low Permeability		High Permeability	
		Shallow	Deep	Shallow	Deep
		I	II	III	IV
3.14	100	1.00	1.00	1.00	1.37
3.14	30	1.00	1.00	1.00	1.98
0.314	30	1.00	1.00	1.04	1.30
314.	1000	1.00	1.00	1.23	2.72

figure from Saffman (1960) was used. The values for Soil IV are all somewhat larger than one, so for this particular soil an increase in soil gas exchange is predicted for all of the wind conditions at the surface.

The predicted values of F/F_o in Table 3.2 are much smaller than the actual values of F/F_o which can be obtained from the data in Chapter I for the evaporation of heptane from a depth of 2 cm. However, the fine gravel, for instance, had a particle size about the same as Soil IV and a permeability twenty times as great. Such an increase in permeability gives scaled velocity values completely off Fig. 3.9, so the K^*/D is presumably large. However, it is difficult to extrapolate exactly how large the value is. A large K^*/D could give an F/F_o value compatible with the data for fine gravel in Chapter I. The sands, on the other hand, had permeabilities about the same as Soil IV, but they had much smaller particle diameters. Smaller particle diameters give lower scaled rms velocities and larger scaled rms displacements than Soil IV. As was done for Soil IV, a K^*/D can be obtained from the limiting curve of Saffman. It would be lower than for Soil IV, and, hence, so would the F/F_o value. A lower F/F_o value does not agree with the results in Chapter I. The Chenango silt loam in Chapter I had a somewhat larger permeability and much smaller particle size than the sands. It represents yet a more extreme disagreement between predicted and observed values of F/F_o than do the sands.

There are three reasons why one would expect the F/F_o values calculated from Equation 3.39 to be smaller than measured values when Figure 3.9 and Equations 3.29 and 3.33 are used to obtain values for K^*/D. First, the media used to obtain the measured data are much rougher

and not as homogeneous as the beads or glass spheres which were used to obtain the curves in Figure 3.9. Scotter et al. (1967) found that dispersion coefficients for Paar silt loam were about the same magnitude as the dispersion coefficient for 4 mm glass beads with the same flow velocity and displacement amplitude. Furthermore, the dispersion coefficient for the 2.0-4.7 mm aggregate portion of the silt loam was of the same magnitude as the dispersion coefficient for the 0-4.7 mm aggregate portion. Thus, dispersion coefficients for silt loam which are predicted from measurements of dispersion coefficients using scaled flows in glass beads will grossly underestimate the amount of mixing. Also one would expect a low estimate for sand but that the agreement should be closer than with silt loam. Plots of K^*/D like the ones in Figure 3.9 should be obtained using some porous media other than glass beads so that a better estimate of the increase in mixing due to heterogeneity of the media can be obtained.

A second possible reason why the calculated F/F_o values are smaller than the observation in Chapter I is that the dispersion coefficient in Figure 3.9 which was obtained using an oscillatory flow may not apply to a natural flow which is as random as it is oscillatory. In the oscillatory flow, mixing of soil gases proceeds at a steady rate (when looking at time scales long compared to the period of oscillation), which is somewhat larger than pure diffusion. In the natural case, however, the mixing probably is not steady. A gust of wind could cause the flow velocities to increase with an accompanying increase in mixing of the soil gases. Yet, during every lull in the wind mixing proceeds at least as fast as diffusion. In other words, the average (rms) velocities and displacements one can calculate from Equations 3.29 and 3.33 cannot be

used to obtain accurate values of K*/D from Figure 3.9, because K*/L does not respond linearly to changes in flow velocity and displacement amplitude. New equations are needed from which integrated values of K*/D can be obtained. Laboratory experiments, similar to the one conducted by Scotter and Raats in obtaining Figure 3.9, need to be conducted to determine how K*/D is affected by several, superimposed oscillations in the flow. By gradually increasing the number of oscillations, one may be able to determine how K*/D is affected by the whole spectrum of superimposed waves which exists in natural conditions.

There is a third reason why predicted values of F/F_o obtained using Equations 3.29 and 3.33 may underestimate soil gas exchange under natural conditions. Equations 3.29 and 3.33 predict an average velocity and displacement in the vertical direction only; no account has been taken of velocities and displacements in the horizontal direction. Using previous work with steady flow as a basis for argument, Scotter and Raats (1969) speculate that horizontal velocities and displacement do not contribute significantly to the mixing of soil air in oscillatory flow, but experimental verification is needed.

There is still another possible reason for discrepancy between the predicted values of F/F_o and the experimental observations. One notes from Fig. 3.3 and 3.4 that high frequencies make the largest contribution to velocity, but low frequencies make the largest contribution to displacement. Therefore, it is not completely reasonable to use the average velocity from Equation 3.29 with the average displacement from Equation 3.33. As noted previously, the scaled values calculated for Soil IV from Equation 3.33 are very large. The rms displacements for the frequencies at which the rms velocities are a maximum are very small. Should they be used instead? Again, some laboratory studies of the

dispersion resulting from several superimposed waves of differing amplitude, frequency, and wave length are required in order to understand the natural system.

Summary

An equation has been derived which permits calculation of the air pressure at any point in the soil from the spectrum of air pressure at the soil surface. From the equation, two additional equations have also been derived. The first permits calculation of the root mean square vertical velocity and the second permits calculation of the root mean square displacement of the soil air from the air pressure spectrum at the surface. Using the velocity equation, calculations with single pressure waves indicate that the physical size or wave length of eddies is more important than their periods for normal wind speeds. Additional calculations, using the latter two equations and an empirical equation to describe spectra obtained from field measurements, showed that frequencies higher than 1 cycle/sec made the largest contribution to soil air velocity. Similar calculations showed that low frequencies below 1 cycle/day made the largest contributions to the displacement. The contributions of high frequencies to both velocity and displacement were found to attenuate rapidly with depth. Increasing permeability caused a roughly proportional increase in velocity and displacement for most of the conditions studied. The total rms velocity at the surface for all frequencies in the air pressure spectrum was surprisingly close to values computed by other workers for single pressure waves.

An attempt was made to compare measured to predicted increases of soil gas exchange over diffusion from the computed rms velocities and displacements. A method developed by previous workers was used to compute the predicted increases in soil gas exchange from the rms velocities and displacements. The computed increases were much lower than the measured values. Several reasons for the discrepancy clearly indicate fruitful avenues for further research.

Literature Cited

Dwight, Herbert Bristol. 1961. Tables of Integrals and Other Mathematical Data. The Macmillan Company. New York, N. Y., 336 pp.

Farrel, D. A., Greacen, E. L., and Gurr, C. G. 1966. Vapor transfer in soil due to air turbulence. Soil Sci. 102:305-313.

Gebhart, Benjamin. 1961. Heat Transfer. McGraw-Hill Book Company, Inc., New York, N. Y., 454 pp.

Gossard, E. E. 1960. Spectra of atmospheric scalars. J. Geophys. Research. 65:3339-3351.

Kirkham, Don. 1946. Field method for determination of air permeability of soil in its undisturbed state. Soil Sci. Soc. Amer. Proc. 11:92-99.

Priestly, J. T. 1966. Correlation studies of pressure fluctuations on the ground beneath a turbulent boundary layer. National Bureau of Standards Reports No. 8942.

Saffman, P. G. 1960. Dispersion due to molecular diffusion and macroscopic mixing in flow through a network of capillaries. J. Fluid Mech. 7:194-208.

Scotter, D. R. and Raats, P. A. C. 1968. Dispersion in porous systems due to oscillating flow. Water Resources Research. 4:1201-1206

Scotter, D. R. and Raats, P. A. C. 1969. Dispersion of water vapor in soil due to air turbulence. Soil Sci. 108:170-176.

Scotter, D. R., Thurtell, G. W., and Raats, P. A. C. 1967. Dispersion resulting from sinusoidal gas flow in porous materials. Soil Sci. 104:306-308.

SUMMARY AND CONCLUSIONS

The effects of air turbulence upon soil gas exchange have been investigated. In Chapter I, field measurements are described of the evaporation of heptane from beneath surface coverings of straw, coarse gravel, fine gravel, very coarse sand, medium sand, and Chenango silt loam. They were obtained using a vapor exchange meter (VEM) which could be buried beneath the soil surface. Air turbulence was evaluated by measurements of the root mean square fluctuation of air pressure and by measurements of the mean wind velocity.

Regression analysis revealed that air turbulence significantly affected heptane evaporation from beneath straw and coarse sand. The regression coefficients on wind ranged from 0.0712 for a 2 cm surface layer of coarse gravel to 0.00688 ($\mu gm/cm^2/sec$)/(cm/sec) for a 2 cm surface layer of Chenango silt loam. Increasing the surface layer depth from 1 to 8 cm caused a decrease of 0.00627 to 0.00058 ($\mu gm/cm^2/sec$)/(cm/sec) in coarse sand. One can conclude that the transport of water vapor through coarse mulches or shallow depths of soil can be greatly affected by the air turbulence. On the other hand, it seems likely that in a soil which has enough water to support plant growth, the pore size is small enough so that gaseous exchange is primarily a diffusive process. However, the heptane flux values are quite scattered and are larger than predicted by diffusion theory at zero wind speed. Arguments are presented which indicate that neither the density gradient effects of heavy heptane vapor nor of thermal gradients caused the discrepancy. The reason why the flux values are larger than predicted remains unexplained.

In Chapter II, spectra of the air pressure fluctuations at the soil surface during both day and night with and without a corn crop are presented. They were calculated from air pressure measurements obtained at a field site near Ithaca, New York, using an absolute pressure transducer. The spectral density decreased in a roughly linear manner with a slope of about -6/3 on a log-log plot from 10^{8} to 10^{-3} μbar^2/cycle/sec over a frequency range from 10^{-4} to 10^{2} cycle/sec for all conditions. The spectra are very similar to the spectra obtained by previous workers using different methods under different conditions. The greatest variability between spectra was in the height of the curves in the mid-frequency range from 10^{-3} to 10^{-1} cycle/sec. The height changed with wind speed; a 500-fold increase was observed between one run when the wind velocity was 68 cm/sec and another when the wind velocity was 552 cm/sec.

In Chapter III, an attempt is made to predict theoretically the influence of air turbulence upon soil gas exchange. Two new equations are derived from which average root mean square soil air velocities and displacements are calculated using the spectra of air pressure fluctuations presented in Chapter II. The contributions to the rms velocity and displacement of each frequency over the whole frequency range of the spectra are shown for four soils. The frequencies higher than 1 cycle/sec made the largest contribution to soil air velocity while the very lowest frequencies made the largest contributions to displacement. The contributions of high frequencies to both velocity and displacement are shown to attenuate rapidly with depth. Increasing permeability caused a roughly proportional increase in velocity and displacement for the cases considered.

A method developed by previous workers was used to evaluate the amount of increase in soil gas exchange which the calculated velocities and displacements could cause. The calculated increases were found to be far smaller than the field measurements presented in Chapter I. Several reasons for the difference are discussed; they indicate areas for future research.

UNCLASSIFIED
Security Classification

DOCUMENT CONTROL DATA · R & D

(Security classification of title, body of abstract and indexing annotation must be entered when the overall report is classified)

1. ORIGINATING ACTIVITY (Corporate author)

Microclimate Investigations, SWC-ARS-USDA
Bradfield Hall; Cornell University
Ithaca, New York 14850

2a. REPORT SECURITY CLASSIFICATION

UNCLASSIFIED

2b. GROUP

3. REPORT TITLE

EFFECTS OF AIR TURBULENCE UPON GAS EXCHANGE FROM SOIL
with appendix
BASIC CONCEPTS OF SPECTRAL ANALYSIS BY DIGITAL MEANS

4. DESCRIPTIVE NOTES (Type of report and inclusive dates)

Interim Report

5. AUTHOR(S) (First name, middle initial, last name)

F. A. Kimball and E. R. Lemon

6. REPORT DATE	7a. TOTAL NO. OF PAGES	7b. NO. OF REFS
November 1969	188	50

8a. CONTRACT OR GRANT NO.	9a. ORIGINATOR'S REPORT NUMBER(S)
Cross-service Order 2-63	USDA-ARS-SWC No. 405 [redacted]
b. PROJECT NO.	C.U.Research Report No. 870 and 870A
c. DA Task 1T0-61102-B53A-17	9b. OTHER REPORT NO(S) (Any other numbers that may be assigned this report)
d.	ECOM 2-68I-4 and ECOM 2-68I-5

10. DISTRIBUTION STATEMENT

Distribution of this document is unlimited

11. SUPPLEMENTARY NOTES	12. SPONSORING MILITARY ACTIVITY
	U. S. Army Electronics Command Atmospheric Sciences Laboratory Fort Huachuca, Arizona

13. ABSTRACT

An instrument to measure the rate of gas movement from beneath the surface of soil or other porous media was constructed. Subsequent measured rates of gas movement from beneath surface coverings of coarse and fine gravel, very coarse and medium sand, Chenango silt loam and straw were correlated against concurrent measurements of wind and air pressure fluctuations. At a depth of 2 cm gas movement in silt loam was not significantly affected by air turbulence but in coarse gravel was increased 10-fold by wind velocities of 400 cm/sec. Intermediate effects were observed for media of intermediated pore sizes.

Mathematical equations for calculation of soil air mass flow are derived. They are based upon the spectrum of air pressure fluctuations at the ground surface. Air pressure in the field was measured during both day and night with and without a corn crop. The spectra of air pressure were calculated and all were roughly straight lines with a slope of about -6/3 on a log-log plot. Spectral density decreased from 10^{8} to 10^{-1} μbar^2/cycle/sec over a frequency range from 10^{-4} to 10^{2} cycle/sec. Soil air mass flow was calculated from the spectra for several soils. Using previous work, an attempt was made to evaluate the increase of soil gas movement beyond diffusion from the soil air mass flow. The predicted increases in soil gas movement were lower than the observed increases; several reasons for the discrepancy are discussed.

Spectral density, Fourier transformation, auto-covariance, cross spectral density, cross-covariance, and other concepts of spectral analysis are discussed at an elementary level in the appendix.

DD FORM 1 NOV 68 1473 REPLACES DD FORM 1473, 1 JAN 64, WHICH IS OBSOLETE FOR ARMY USE.

UNCLASSIFIED
Security Classification

14. KEY WORDS	LINK A		LINK B		LINK C	
	ROLE	WT	ROLE	WT	ROLE	WT
Soil - Mass flow						
Soil - Diffusion						
Soil - Dispersion						
Porous Media - Mass flow						
Porous Media - Diffusion						
Porous Media - Dispersion						
Air Pressure - Fluctuations						
Air Pressure - Spectrum						
Spectral Analysis - Methods						
Spectral Analysis - Concepts						
Spectral Analysis - Air Pressure						